การสร้างอนุภาคจากสารสกัดพอลิฟีนอลจากชาสำหรับฤทธิ์ต้านมะเร็ง

นายพุฒิกร พุกฝึกดี

วิทยานิพนธ์นี้เป็นส่วนหนึ่งของการศึกษาตามหลักสูตรปริญญาวิทยาศาสตรมหาบัณฑิต
สาขาวิชาเคมี ภาควิชาเคมี
คณะวิทยาศาสตร์ จุฬาลงกรณ์มหาวิทยาลัย
ปีการศึกษา 2559

FABRICATION OF PARTICLES FROM TEA POLYPHENOL EXTRACT FOR ANTICANCER ACTIVITY

Mr. Puttikorn Pukfukdee

A Thesis Submitted in Partial Fulfillment of the Requirements
for the Degree of Master of Science Program in Chemistry
Department of Chemistry
Faculty of Science
Chulalongkorn University
Academic Year 2016

Thesis Title	FABRICATION OF PARTICLES FROM TEA POLYPHENOL EXTRACT FOR ANTICANCER ACTIVITY
By	Mr. Puttikorn Pukfukdee
Field of Study	Chemistry
Thesis Advisor	Professor Supason Wanichwecharungruang, Ph.D.

Accepted by the Faculty of Science, Chulalongkorn University in Partial Fulfillment of the Requirements for the Master's Degree

.....Dean of the Faculty of Science
(Associate Professor Polkit Sangvanich, Ph.D.)

THESIS COMMITTEE

.....Chairman
(Associate Professor Vudhichai Parasuk, Ph.D.)

.....Thesis Advisor
(Professor Supason Wanichwecharungruang, Ph.D.)

.....Examiner
(Associate Professor Voravee Hoven, Ph.D.)

.....External Examiner
(Kriengsak Lirdprapamongkol, Ph.D.)

พุฒิกร พุกฝึกดี : การสร้างอนุภาคจากสารสกัดพอลิฟีนอลจากชาสำหรับฤทธิ์ต้านมะเร็ง (FABRICATION OF PARTICLES FROM TEA POLYPHENOL EXTRACT FOR ANTICANCER ACTIVITY) อ.ที่ปรึกษาวิทยานิพนธ์หลัก: ศ. ดร.ศุภศร วนิชเวชารุ่งเรือง, 94 หน้า.

สารพอลิฟีนอลจากชาเป็นกลุ่มสารที่พบมากในใบชามีชื่อทางวิทยาศาสตร์ว่า Camellia sinensis สารพอลิฟีนอลจากชามีสมบัติที่ดีคือมีฤทธิ์ต้านอนุมูลอิสระและต้านมะเร็งสูง อย่างไรก็ตามผลของสารพอลิฟีนอลในชาต่อความเป็นพิษของเซลล์มะเร็งที่แรงขึ้นแต่ปลอดภัยสำหรับเซลล์ปกตินั้นเป็นสิ่งจำเป็นต่อประสิทธิภาพในการรักษาโรคมะเร็ง ดังนั้นในงานวิจัยนี้ผู้วิจัยได้สังเคราะห์อนุภาคพอลิเมอไรซ์พอลิฟีนอลจากสารสกัดพอลิฟีนอลจากชาอู่หลง อนุภาคพอลิเมอไรซ์พอลิฟีนอลที่สังเคราะห์ได้สามารถกระจายตัวได้ดีในน้ำและสามารถกักเก็บยาที่ไม่ละลายน้ำได้ ยกตัวอย่างเช่น พาคลิแทกเซลและแซนโทน อนุภาคพอลิเมอไรซ์พอลิฟีนอลมีลักษณะเป็นทรงกลมขนาด 250±5 นาโนเมตร พาคลิแทกเซลและแซนโทนสามารถถูกกักเก็บในอนุภาคได้ที่ความจุเท่ากับร้อยละ 30 และ 27 โดยน้ำหนักตามลำดับ พาคลิแทกเซลที่ถูกกักเก็บในอนุภาคกระจายตัวได้ดีในน้ำและสามารถยับยั้งการเจริญเติบโตของเซลล์มะเร็งปอด (A549 เซลล์ไลน์) ได้ดีกว่าการใช้พาคลิแทกเซลที่ไม่ได้ถูกกักเก็บโดยมีค่าความเข้มข้นที่สามารถยับยั้งเซลล์มะเร็งปอดได้ 50% (IC_{50}) น้อยกว่า 0.02 ไมโครกรัมต่อลิตร ส่วนพาคลิแทกเซลที่ไม่ได้ถูกกักเก็บในอนุภาคในตัวทำละลาย DMSO มีค่า IC_{50} เท่ากับ 0.18 ไมโครกรัมต่อลิตร

ภาควิชา เคมี ลายมือชื่อนิสิต .....

สาขาวิชา เคมี ลายมือชื่อ อ.ที่ปรึกษาหลัก .....

ปีการศึกษา 2559

5772089823 : MAJOR CHEMISTRY

KEYWORDS: OOLONG TEA POLYMERIZED POLYPHENOL / OOLONG TEA POLYPHENOL / PACLITAXEL-LOADED PARTICLE / XANTHONE-LOADED PARTICLE / DISPERSE WELL IN WATER

PUTTIKORN PUKFUKDEE: FABRICATION OF PARTICLES FROM TEA POLYPHENOL EXTRACT FOR ANTICANCER ACTIVITY. ADVISOR: PROF. SUPASON WANICHWECHARUNGRUANG, Ph.D., 94 pp.

Tea polyphenols, compounds expressed in various tea (*Camellia sinensis*) leaves, possess powerful antioxidant and anti-camcer activities. Nevertheless, more cytotoxicity to cancer cells with safety to normal cells of the tea polyphenols is needed for greater potential in cancer treatment. In this work, we have synthesized the oolong tea polymerized polyphenol (P-OTE) particles from the oolong tea polyphenol extract (OTE). The obtained particles are water dispersible and can entrap hydrophobic drugs such as paclitaxel (PTX) and xanthone. The P-OTE particles are spherical with size of 250±5 nm. PTX and xanthone can be loaded onto the particles at approximately 30% and 27% (w/w) loading content, respectively. The PTX-loaded P-OTE particles disperse well in water. The PTX-loaded P-OTE particles show excellently improved anticancer activity against lung cancer (A549) cell line as compared to the unencapsulated PTX, i.e., the IC_{50} value of < 0.02 μg/l for the entrapped PTX as compared with the IC_{50} value of 0.18 μg/l for the unentrapped PTX in DMSO.

Department: Chemistry Student's Signature .....

Field of Study: Chemistry Advisor's Signature .....

Academic Year: 2016

ACKNOWLEDGEMENTS

I would like to express my deepest gratitude to my beloved advisor, Professor Dr. Supason Wanichwecharungruang for her generous assistance and providing me insight and expertise that greatly supported this research. I also gratefully acknowledge the committees, Associate Professor Dr. Vudhichai Parasuk, Associate Professor Dr. Voravee Hoven and Dr. Kriengsak Lirdprapamongkol for their comments, and suggestions on my research work. I gratefully appreciate to Miss Khajeelak Chiableam and Dr. Kriengsak Lirdprapamongkol for kind suggestions, guidance and helps in cytotoxicity test. Also, I thank members of research group and all of my friends for their friendships I have had during my study. I would like to express my gratitude to Department of Chemistry, Faculty of Science, Chulalongkorn University. Last but not the least, I would like to thank my family for their support thoughtout the course of my graduate study.

CONTENTS

Page

Page

Page

Page

LIST OF TABLE

Table Page

LIST OF FIGURE

Figure Page

CHAPTER I

INTRODUCTION

1.1 Cancer and Treatment

Cancer is a major public health problem in the world which is the second leading cause of death in the United States [1]. Cancer begins when cells in a part of the body start to grow out of control. There are many kinds of cancer, but they all start because of out-of-control growth of abnormal cells. There are different types of cancer treatment including surgery, radiotherapy, and chemotherapy [2, 3] . Chemotherapy differs from surgery or radiation in that it treats the whole body. Chemotherapy is the use of anti-cancer drugs to treat cancer. It can stop the growth of a cancer and kill cancer cells that have spread to other parts of the body. An application of anti-cancer drugs is characterized by poor water solubility, limited effectiveness, and lack of selectivity [4]. Limitation of anticancer drugs are not selective to cancer cells and affect the normal cells as well leading to severe side effects. As well as the skin and hair, areas of the body that chemotherapy may affect include the mouth, the lining of the digestive system, and the bone marrow, which makes new blood cells [5, 6]. The paclitaxel (PTX) and xanthone were used as a model drugs in this study.

1.2 PTX and Xanthone and Its Limitations

PTX is one of the most widely used and effective broad-spectrum chemotherapeutic agents in the treatment of cancers. It was first discovered derived from natural sources in the bark of Western (*Taxus brevifolia*) [7] and its chemical structure is shown in Figure 1.1a. PTX has a broad range of anticancer activity such as lung, ovarian, and breast cancers [8]. However, its clinical application has been limited by their chemical formulation due to its very poor aqueous solubility and low

therapeutic index. The solubility of PTX is enhanced with a mixture of 1:1 Cremophor EL® (CrEL, organic solvent of poly-oxyethylated castor oil and ethanol as Taxol® [9]. However, CrEL is known is associated with dose-limiting toxicities and side effects such as hypersensitivity reactions and neurotoxicity [10]. Therefore, a need for the development of alternative drug delivery systems of PTX formulation to enhance its solubility and will increase its therapeutic effects and reduce its side effects.

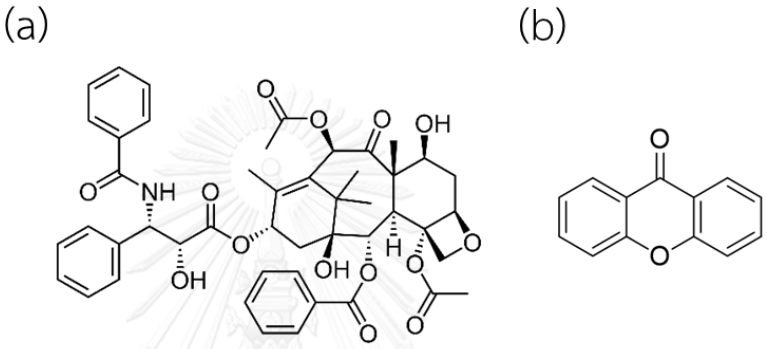

Figure1.1 Chemical Structure of PTX (a) and Xanthone (b)

A new strategies for cancer treatment is chemoprevention, which is defined as the use of natural to prevent or reduce of carcinogenic progression and cancer risk with low toxicity that are able to arrest, suppress, or delay the process of carcinogenesis to invasive cancer [11]. Mangosteen (*Garcinia mangostana* Linn), is indigenous to South East Asia. Phytochemical studies have shown that they contains phytochemical compounds such as oxygenated and prenylated xanthone more than other plant [12]. Recent studies revealed that it also contains considerable amounts of biologically active compounds called xanthone (Figure1.1b), which is a flavonoid and polyphenol compound such as alpha and beta mangostin [13]. Xanthone exhibits a multi-targeting pharmacological activities containing anti-oxidant [14], anti-allergic [15], anti-inflammatory [16], anti-bacterial [17], and anti-cancer effect such **α**-mangosteen and **γ**-mangosteen [18]. The anticancer activities of xanthone include cell

cycle arrest, tumor growth suppression, completely inhibits induction of apoptosis and differentiation, potent cytotoxicity, reduction of inflammation, and inhibition of adhesion, cell invasion and clonogenicity, cell migration, and tumor metastasis [19]. However, applications of xanthone are limited by hydrophobic and poorly soluble in water. They frequently display low oral bioavailability their therapeutic application, poor systemic delivery, and low efficacy [20]. To circumvent these problem, we have used to prepare a novel approach nanodelivery system to entrap the xanthone and PTX by natural product with more potent cancer drugs and low toxicity as well.

1.3 Nanoparticles Drug Delivery Systems for Cancer Therapies

In recent years, the developments of nanotechnology have shown that nanoparticles (1-100 nm in at least one dimension) have a great potential as drug carriers [21], especially for cancer therapies. The advantages of nanoparticle have enhancing aqueous solubility of hydrophobic drugs, such as PTX, improved biopharmaceutics effects, and reduced in toxicity that make them a favorable material for biomedical applications [22]. The various type of nanocarrier used for drug delivery (Figure 1.2) are biodegradable polymeric nanoparticles [23, 24], liposomes [25], solid lipids nanoparticles [26], silicon or carbon materials [27-29], magnetic nanoparticles [30]. These nanocarriers can deliver various types of cancer drugs, prevent premature degradation, inactivation upon administration, and increase systematic circulation of drug delivered to cancer cell, thereby providing a means to decrease the side effects of cytotoxic drugs [31, 32]. Nanocarriers can preferentially accumulate in the tumor site by virtue of the enhanced permeability and retention (EPR) effect of the vasculature [33].

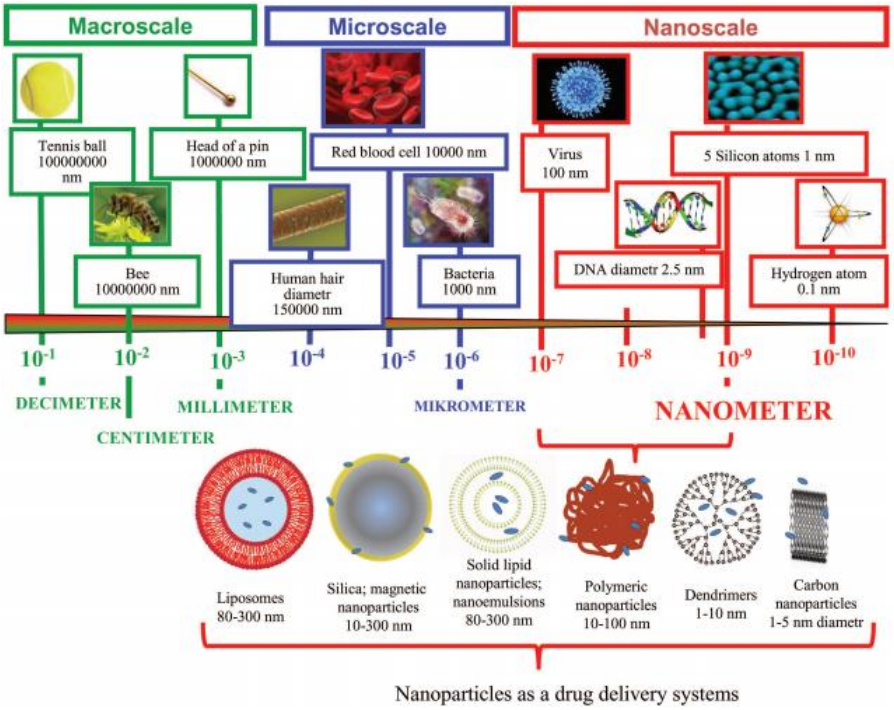

Figure 1.2 Nanoparticle Drug Delivery Systems with relation to other scales [34].

1.4 Natural Product

A natural product is chemical substances produced by a living organism which a term used commonly in reference to chemical substances found in nature that have distinctive pharmacological effects. Natural products are the source of the most complex and fascinating chemical structures. It also represent large biological diversity and natural biological activity, whether as single compounds or as complex mixtures. The advantage of natural product can be an effective bridge from tradition to modern scientific developments, including genetics, molecular biology, biotechnology, and pharmaceutical science. A natural product mainly plant-derived constituents have long been sources of drugs and a large proportion of the pharmaceuticals available in modern medicine is directly or indirectly derived from natural sources. Natural products are also of great interest in the process of drug discovery that remain an important source of new structures, though not the final drug entity [35]. Eventually,

a growing world-wide interest in the use of natural product as complementary or alternative medicine, either for the prevention or treatment of many diseases. Polyphenol in particular are considered to be one of the most important natural products.

1.5 Tea Polyphenol (TP)

Tea (*Camellia sinensis*, family Theaceae) is the most widely consumed beverage in the world [36]. Tea has been extensively studied for its wide range of health benefits, including the prevention of cancer [37] and cardiovascular diseases [38], anti-cancer [39], anti-oxidant [40], anti-inflammatory [41], anti-angiogenic [42], anti-viral [43], neuroprotective [44], anti-arthritic [45], and cholesterol-lowering effects of tea [46]. Effects of tea on cancer chemoprevention have been attributed to its anti-oxidant activities [47, 48]. The difference between of green tea, black tea and oolong tea, regardless of degree of fermentation [49, 50], is depended on their contents of free amino acids, mainly L-theanine and several natural amino acids including glutamic acid, asparagine, serine, alanine, leucine, and isoleucine [51]. Green tea (unfermented) produced from fresh tea leaves, while partially crushed leaves oxidized in a moist environment for short time produce oolong tea (partially-fermented), while longer oxidation results in black tea (fully fermented). Many potential health promotion properties associated with these three types of tea consumption have been reported [52, 53]. Green tea is composed of polyphenols, including phenolic acids and catechins, alkaloids (caffeine, theophylline, and theobromine), amino acids, carbohydrates, proteins, chlorophyll, volatile organic compounds, fluoride, aluminum, minerals, and trace elements [54]. The health-promoting effects of tea are mainly attributed to its polyphenol content [55], particularly flavanols and flavonols, which is characterized by being rich 30% of fresh leaf dry weight [56]. Polyphenols can range from simple molecules such as phenolic acids, to large highly polymerized compounds such as

tannins [57]. Green tea contains an infusion of the leaves plant rich in polyphenolic compounds known as catechins, which belong to the family of flavonoids that are powerful antioxidants and free iron scavengers, the most active and abundant in catechins in tea is (-)-EGCG [58], but tea contains as many as twelve catechins [59]. Eight prominent catechins (Figure 1.3) are (-)-epicatechin (EC), (+)-catechin (C), (-)-epigallocatechin (EGC), (-)-gallocatechin (GC), (-)- epicatechingallate (ECG), (-)-catechin gallate (CG), (-)-epigallocatechin gallate (EGCG), and (-)-gallocatechingallate (GCG).

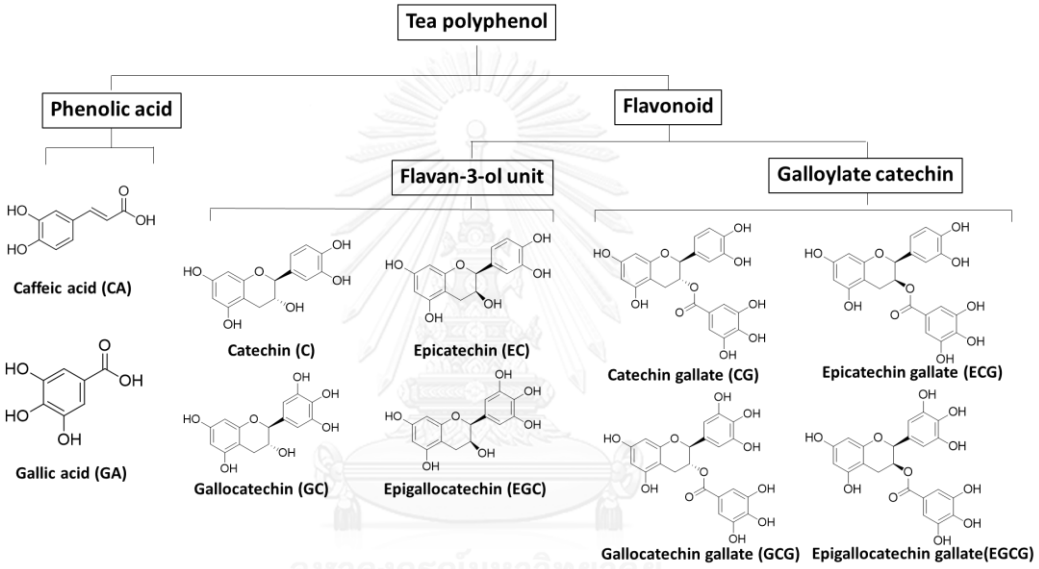

Figure 1.3 Chemical Structures and Classifications of TPs.

Oolong tea and Black tea contains two major groups of oxidized polymeric substances such as theaflavins (TFs) and thearubigins (TRs) [60]. Oolong tea contained much lower concentrations of these catechins than green tea [56]. The extended oxidation of oolong tea increased the concentrations of thearubigins (TRs) and theaflavins (TFs), such that these teas may have different biological activities.

1.6 Literature Review of TPs Anti-Cancer Activity

In 1995, Shim *et al*. [61] studied the cancer chemopreventive effect of TPs among cigarette smokers and found that it can block the cigarette-induced increase in sister chromatid exchange frequency.

In 2001, Jung *et al*. [62] studied the anti-proliferative properties of TPs on intracellular signaling and VEGF induction *in vitro* in colon cancer cells (HT29) and the *in vivo* on the growth of HT29 cells in nude mice. In the *in vitro* studies, at a dose of 30 μM EGCG treatment inhibited Erk-1 and Erk-2 activation in a dose-dependent manner, inhibited the increase of VEGF expression, and promoter activity induced by serum starvation. However, EGC, ECG, EC didn't affect Erk-1 or Erk-2 activation. Moreover, EGCG can inhibit cancer cell growth *in vivo* by inhibiting the formation of new blood vessels.

In 2004, Kim *et al*. [63] studied the anti-invasive effect and MMP-9 induction in gastric cancer cells (AGS) of EGCG. The result showed that EGCG inhibited the phorbol 12-myristate 13-acetate (PMA)-induced cell invasiveness and reduced MMP-9 expression in a dose-dependent manner.

In 2010, Vu *et al.* [64] reported that EGCG-treated pancreatic cancer cells (AsPC-1 and BxPC-3) decreased cell adhesion ability on micro-pattern dots, accompanied by dephosphorylations of both insulin-like growth factor-1 receptor (IGF-1R) and focal adhesion kinase (FAK) whereas retained the activations of mitogen-activated protein kinase and mammalian target of rapamycin. At a dose of 100 μM EGCG treatment suppresses more than 50% of cell proliferation in dose-dependent manner without evidence of apoptosis analyzed.

In 2011, Wang *et al.* [65] studied the anti-cancer activity of EGCG in both human and mouse lung cancer cells in culture. The result showed that EGCG increased the

expression of miR-210, a major miRNA regulated by HIF-1α and reduced cell proliferation rate.

In 2012, Du *et al.* [66] studied the cancer chemopreventive effects of 10 polyphenols on human colorectal cancer cells (HCT-116 and SW-480) using MTS assay. EGCG showed the most potent activities and induced cell cycle arrest in the G1 phase and cell apoptosis.

1.7 Oolong Tea Polyphenol (OTP)

Major contents of oolong tea are illustrated in Table 1.1, which has two categories: monomeric polyphenols (high of EGCG content) and polymeric polyphenol (TFs and TRs) [63]. TFs and TRs have been demonstrated to possess various pharmacological activities such as anti-cancer, anti-oxidant activity by reducing oxidative stress, anti-obesity and strong hepatoprotective activities, anti-diabetes, anti-hypertensive and anti-allergic, preventive effect of atherosclerosis, heart disease, and anti-septic effects [36, 67-74]. This beneficial effect has been attributed to the presence of high amounts of EGCG and polymeric substances. Moreover, it has been reported that polymeric polyphenol are able to exhibit stronger anti-cancer activity than monomeric polyphenol [75-80].

Table1.1 Components of Oolong Tea Beverage [81].

Compounds	Content (mg/100 ml)
Polymerized	33.65
Epigallocatechin gallate	25.75
Caffeine	23.51
Epigallocatechin	16.14
Gallocatechin	6.68
Epicatechin gallate	5.73
Epicatechin	5.08
Gallic acid	2.19
Allocatechin gallate	1.85
Catechin	1.65
Catechin gallate	0.6
Total polyphenol	99.32

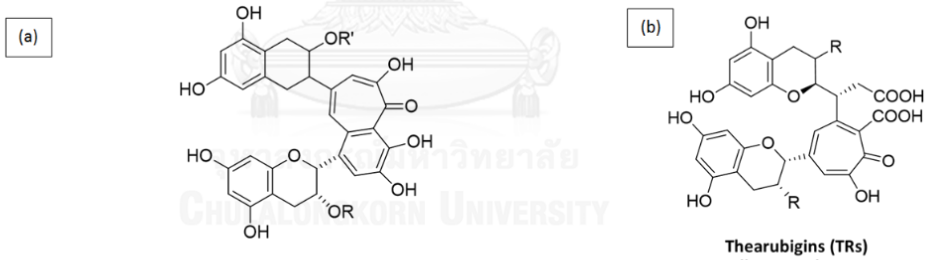

Compound	R	R'
Theaflavin (TF1)	H	H
Theaflavin-3-monogallate (TF2a)	Galloyl	H
Theaflavin-3'-monogallate (TF2b)	H	Galloyl
Theaflavin-3,3'-digallate (TF3)	Galloyl	Galloyl

Figure 1.4 Chemical Structure of (a) TFs, and (b) TRs

1.8 Literature Review Anti-Cancer Activity of Tea Polymerized Polyphenol (TPP)

In 2000, Pan *et al.* [82] studied the growth inhibitory effects of TPPs in human histolytic lymphoma cancer cells (U937). The result showed that TPPs displayed strong growth anti-cancer activity, with estimated IC50 values of 12 μM.

In 2007, Prasad *et al.* [75] studied the mechanism of TPPs on cellular proliferation and cell death in the human prostate cancer cell line PC-3. They found that TFs act as anti-proliferative agents by modulating cell growth regulators in prostate cancer cells.

In 2015, Konarikova *et al.* [83] studied the potential anti-cancerogenic effect of the TPP on different types of carcinoma cell lines (colon carcinoma cell line HT-29, human breast carcinoma cell line MCF-7, human alveolar carcinoma cell line A549 and compared with effects on the healthy cell line NIH-3T3) using MTT assay. In the result of TPP possess high cytotoxic effects and genotoxic properties against all carcinoma cell lines by IC50 lower than the lowest concentration used (0.00078 μg/mL) and no anti-proliferative effect against normal cells.

1.9 Literature Review of TPs as Drug Carrier

In 2013, Chen *et al*. [84] demonstrated a method to fabricate biocompatible functional spheres from TPs in water by oxidative coupling reaction. The TP spheres were self-luminescent, stimuli-responsive including GSH responsive, and acid resistant. Doxorubicin (DOX) were loaded into TP sphere with the high loading efficiency is about 15.4 wt %.

In 2014, Chung *et al.* [85] synthesized a drug carrier by self-assembly of the EGCG derivatives and proteins. The combined anticancer effect of the green tea-based carrier and the protein drug showed greater anticancer effect than the free protein.

1.10. Enzymatic Polyphenol Polymerization using Horseradish Peroxidase (HRP) as Catalyst

Enzymatic polymerization is a natural way for polymer synthesis, and has received particular attention in recent years. Peroxidase such as HRP is typical of oxidoreductase family, which catalyzes various oxidation reactions using hydrogen peroxide (H_2O_2) as the hydrogen receptor. HRP found to have higher activity over wide range of temperature, pH, and contaminant concentrations [86]. It was reported that the enzymatic oxidative polymerization of phenol derivatives produced polymerized polyphenols with a high thermal stability under the mild conditions [87]. However, the enzymatic polymerization of phenol proceeds in buffer medium [88].

The mechanism of catalysis of HRP has been investigated [89] and the catalytic cycle of HPR for phenol substrate are illustrated in Figure 1.4 with ferulic acid as reducing substrate. The first step in the catalytic cycle of HRP in the oxidative of phenol monomers is the reaction between H_2O_2 and the Fe(III) native state of the enzyme to generate compound 1, a high oxidation state intermediate comprising an Fe(IV) oxoferryl group in the active center and a porphyrin in the form of a cation radical. Compound 1 oxidizes the first equivalent of phenol group by oxidoreduction and generates a phenoxy radical. The proton of the phenoxy radical is abstracted by a base to form the compound 2, an Fe(IV) oxoferryl species that is one oxidising equivalent above the native state. The Fe(IV) is reduced back to Fe(III) by another phenol groups, forming another phenoxy radical.

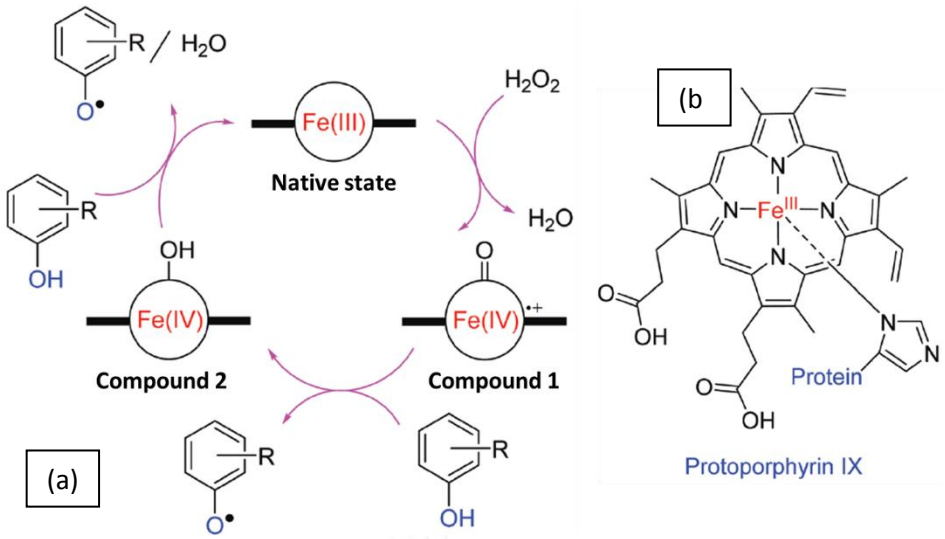

Figure 1.5 (a) The catalytic cycle of HRP for a phenol substrate. (b) Structure of Iron heme group in HRP [90].

1.11 Literature Review of Enzymatic Polyphenol Polymerization using HRP

In 1987, Dordick et al. [91] synthesized the polymerized polyphenol (PP) by enzymatic polymerization in mixture of water and water-miscible solvents. The polymerized polyphenol had much higher melting points, and electrical conductivity than phenol-formaldehyde resins.

In 2001, Mita et al. [92] synthesized the PP with low molecular weight by enzymatic co-polymerization between phenol and 2,4-disubstituted phenol. The PP showed high solubility in high polar organic solvents.

In 2003, Kurisawa et al. [93] synthesized the polymerized catechins by an oxidative enzymatic polymerization using HRP as the catalyst under a mild reaction condition. The poly-(catechin) showed much greater amplified antioxidant activity, and superoxide scavenging, whereas the catechin monomer showed very less inhibition effects.

1.12 Enzymatic Template Polymerization of Phenol in the Presence of Poly(ethylene glycol) (PEG)

The presence of the template have been used for controlling the chemical structure of polymers synthesized by enzymatic polymerization [94], influenced the polymerization rate of the monomer and control molecular weight and molecular weight distribution. Template polymerization leads to formation of polymer–polymer complexes stabilized via non-covalent binding forces like electrostatic interactions, hydrogen bonds, hydrophobic interactions, and stereo-complexation. Template polymerization is classified in to two different mechanisms, zip and pick-up mechanisms [95]. These two types of reaction can be illustrated in Figure 1.6. In the case of zip mechanism, monomer units are connected to the template by strong forces (hydrogen bond, electrostatic bond). Thereafter the polymerization proceeds along the template chain and daughter polymer forms a complex with the template. In the case of pick-up mechanism, the monomer is free at the beginning and polymerization starts outside the template in solution. When the complexes of oligoradical-template is formed in solution, it is strongly connected to the template, then polymerization proceeds on the template.

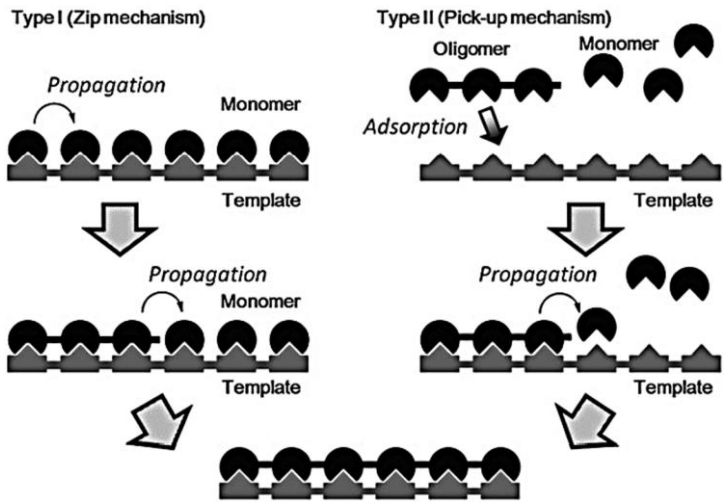

Figure 1.6 The mechanisms on template polymerization [95].

PEG have been reported as templates to control enzymatic polymerizations of phenol in water [96, 97], yielding a complex of the polyphenol and the template polymer (Figure 1.6). When PEG was used as template, the regioselectivity greatly improved to give the polymer mainly consisting of the phenylene units [97].

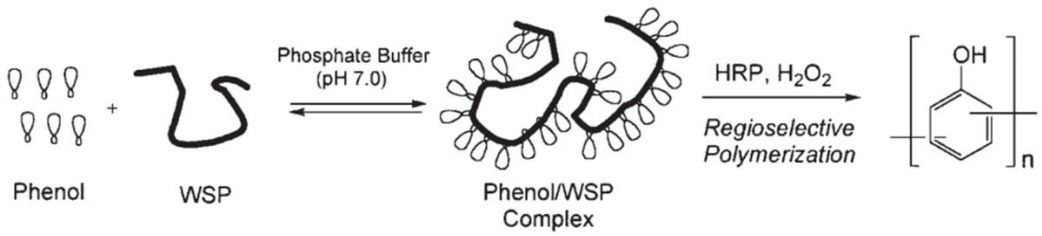

Figure 1.7 Enzymatic Template Polymerization of Phenol in the Presence of PEG [98].

1.13 Literature Review of Enzymatic Template Polymerization

In 1998, Kurioka *et al*. [98] synthesized the monodisperse polyphenol particles in the sub-micron range by dispersion polymerization using HRP as catalyst of phenol using poly(vinyl methyl ether) stabilizer in the mixture of 1,4-dioxane and phosphate buffer (pH 7).

In 2004, Kim *et al*. [99] synthesized the polyphenol by enzymatic polymerization using the PEG, one of water-soluble polymers as template in an aqueous medium. The polyphenol polymer yield was the higher than 90% when using PEG as template. The addition of PEG improved the regioselectivity of polymerization to give the polymer mainly consisting of phenylene units.

1.14 Objective and Scope of Work

Objective

To synthesize oolong tea polymerized polyphenol (P-OTE) particles from oolong tea polyphenol extract (OTE) for drug entrapment and develop entrapment of PTX and xanthone from P-OTE particle with efficient anti-cancer activity into cancer cells.

Scope

The goal of this research can be concluded as follow:

1. Synthesis of P-OTE particles from OTE through methanolic extraction

2. Characterization of OTE and P-OTE particles

3. Evaluation of the loading capacity of anticancer drug-loaded P-OTE particles in A549 cell line.

4. *In vitro* anti-cancer studies of PTX-loaded P-OTE particles and Xanthone-loaded P-OTE particles

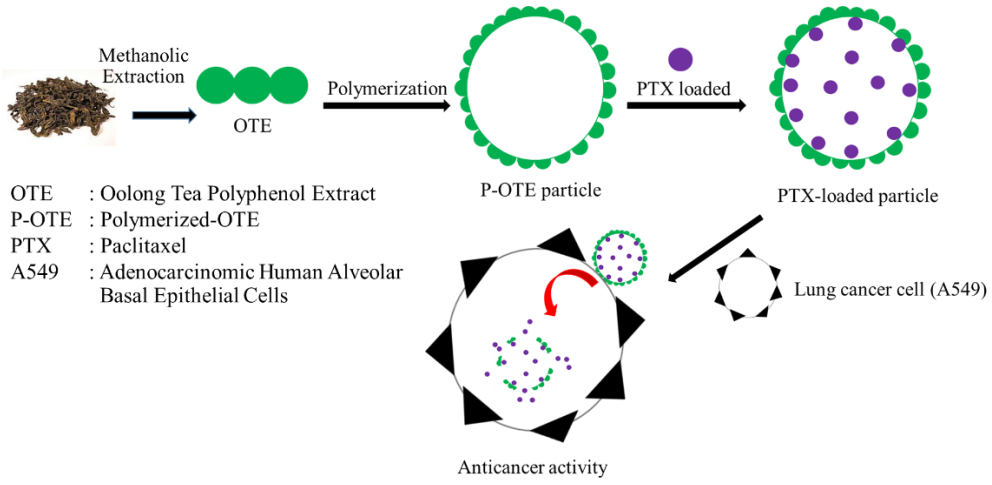

CHAPTER II
EXPERIMENTAL

2.1 Material

Solvent used in oolong tea polyphenol extraction were purchased from RCI Labscan (Bangkok, Thailand). Dried oolong tea leaves were purchased from Boon Rawn Farm, Chiang Rai, Thailand. Horseradish peroxidase were purchased from Suzhou yacoo chemical reagent corporation, China. Polyethylene glycol (PEG, M_W = 35000 Da), Hydrogen peroxide (30.8%) were purchased from Merck, Darmstadt, Germany. Xanthone power (± 95% purity) extract were supplied by Well Teachnology Company (Bangkok, Thailand). Paclitaxel (PTX) were purchased from Sigma-Aldrich ChemieGmbH (Steinheim, Germany). Epigallocatechin-3-gallate (EGCG), Gallic acid (GA), Epicatechin-3-gallate (ECG) were purchased from Chemieliva Pharmaceutical and Chemical Company (Choqqing, China). 2,2-diphenly-1-picrylhydrazyl (DPPH), butylated hydroxytoluene (BHT) were purchased from Sigma, USA

2.2 Instrument and Equipment

2.2.1 Characterization of the physical and chemical properties

2.2.1.1 UV-Visible Spectroscopy, and Fluorescence Spectroscopy

Ultraviolet absorption spectra were obtained with the aids of an HP8453 UV/VIS spectrophotometer (Agilent Technologies, CA USA) using 1 cm-pathlength quartz cell. Fluorescence spectra were obtained from a Varian Cary Eclipse spectrofluorometer, with the excitation and emission monochrometer band pass set at 5 nm and 3 nm, respectively, using 1 cm^3 quart fluorescence cell.

2.2.1.2 Fourier Transform Infrared Spectroscopy (FT-IR)

Attenuated Total Reflectance – Fourier transform infrared (ATR-FTIR) spectra were recorded with 64 scans in the mid-infrared region (4000-650 cm^{-1}) through

Nicolet 6700 FT-IR spectrometer (Thermo Electron Corporation, Madison, WI, USA) connected to a Contiuμm™ infrared microscope equipped with a mercury-cadmium-telluride (MCT) detector and ATR accessory consisting of a slide-on miniature germanium (Ge) as the internal reflection element.

2.2.1.3 Nuclear Magnetic Resonance (NMR)

All ^{1}H-NMR spectra were obtained on a Varian Mercury NMR spectrometer, which operated at 400 MHz for ^{1}H nuclei (Varian Company, CA, USA).

2.2.2 Particle Size Distribution and Surface Charge (Zeta potential)

Dynamic light scattering (DLS) was performed by the Scientific and Technological Research Equipment Center, Chulalongkorn University, Thailand. The particle size distribution was determined by DLS using a Malvern Zetasizer Nano ZS (Zs, Malvern instruments, United Kingdom). Approximately 1 ml of the suspension samples was placed inside the sample holder of the particle size analyzer and then determined directly without dilution. Once the required intensity was reached, an analysis was performed to obtain the mean particle size and polydispersity index. The zeta potential was also measured using the PSS Nicomp 380 ZLS.

2.2.3 Morphological Analysis

2.2.3.1 Scanning Electron Microscopy (SEM) and Energy Dispersive X-ray Spectrometry (EDS)

SEM was performed by the Center of Analytical Service, Faculty of Science, Chulalongkorn University Thailand. SEM photographs were obtained using JEM-6400 Scanning electron microscope (JEOL, Tokyo, Japan). To prepare sample for SEM, a drop of the aqueous product suspension was placed on a glass slide and dried in desiccator overnight. The sample was coated with a gold layer under vacuum at 15 kV for 90 s. The coated sample was then mounted on a SEM stud for visualization. The

accelerating voltage used was 15 kV. The chemical composition of the samples was determined by EDS.

2.2.3.2 Transmission Electron Microscopy (TEM)

TEM was performed by the Scientific and Technological Research Equipment Center, Chulalongkorn University, Thailand. TEM photographs were obtained using JEM-2100 Transmission electron microscopy (JEOL, Tokyo, Japan) with an accelerating voltage of 120 kV in conjunction with selected area electron diffraction (SAED). The samples suspensions were diluted with distilled water, pipetted onto collodion film-coated copper grids with a mesh size of 300, dried using absorbent paper, stained with phosphorus tungsten acid for 4 minutes, and finally dried under ambient conditions.

2.2.3.3 Atomic Force Microscopy (AFM)

AFM was performed by the Scientific and Technological Research Equipment Center, Chulalongkorn University, Thailand. AFM photographs were obtained using a PicoSPM instrument (Molecular Imaging Corp. Tempe, AZ). Imaging was carried out using oxide-sharpened silicon nitride AFM probed with a tip radius of ca. 10 nm (cantilever nominal spring constant = 0.12 $N.m^{-1}$); resonance frequency of approximately 26 Hz; Veeco Probes, Camarillo, CA) in the contact mode. The scanning force constant was 50-80 nN and scan rates were approximately 0.2 Hz. Image areas of 5.0 by 5.0 μM were collected. Samples were prepared by spreading a drop of nanoparticle solution on a degreased glass plate uniformly.

2.2.3.4 Confocal Laser Scanning Microscopy (CLSM)

CLSM used for visualizing hairs was a Nikon Digital Eclipse C1si Confocal Microscope system (Tokyo, Japan), equipped with BD Laser (405 nm), Ar laser (488 nm),

HeNe Laser (543 nm) (Melles Grito, USA), a Nikon TE2000-U microscope (Nikon, Tokyo, Japan) with Nikon EZ-C1 software.

2.2.4 Gel Permeation Chromatographic (GPC) and Mass Spectroscopy (MS) Analysis

2.2.4.1 MS

To confirm the polymerization, its mass was determined on micrOTOF-Q II 10335 MS from Bruker, equipped with Quadrupole time-of-flight (Qq-TOF) as mass analyzer, and an atmospheric pressure ionization source in the nebulizer assisted electrospray in positive ion mode.

2.2.4.2 GPC

GPC was performed by the Petroleum and Petroleum Chemical College, Chulalongkorn University Thailand. The molecular weights of the samples were estimated on a Perkin-Elmer GPC system consisting of the Series 10 pump, the LC-25 RI detector, and the 3600 Data Station. Samples were eluted in tetrahydrofuran through two PL Gel Columns (Polymer Laboratories; 100 A and 1000 A pore sizes) in series at a flow rate of 0.6 mL/min.

2.2.5 Functional Group on the Surface by X-ray Photoelectron Spectroscopy (XPS)

XPS was performed by the Petroleum and Petroleum Chemical College, Chulalongkorn University Thailand. Chemical composition of the surface layer was determined by XPS (AXIS-ULTRA DLD, Shimadzu/Kratos XSAM800 type spectrometer, using $MgK\alpha_{1,2}$ radiation). The resolution at which all spectra were obtained was calculated by taking the center of the peak, at half-height, for a known, unique assignment. The overview spectra were taken between 50 and 1300 eV with an energy

step of 0.5 eV, while the detailed spectra of the peaks of interest (O1s and C1s) were recorded with an energy step of 0.1 eV.

2.2.6 Thermal Analysis

2.2.6.1 Thermal Gravimetric Analysis (TGA)

TGA was performed by the Scientific and Technological Research Equipment Center, Chulalongkorn University, Thailand. Thermogravimetric analysis (TG) was done on STA-449C Jupiter (NETZSCH Corporation, Germany). The experiment temperature ranged from 25 °C to 700 C at a constant heating rate of 10 C min_1 in N_2 atmosphere.

2.2.6.2 Differential scanning calorimetry (DSC)

DSC was performed by Scientific and Technological Research Equipment Center, Chulalongkorn University, Thailand using a Netzsch DSC 204 Phoenix. DSC analysis was used to measure the glass transition behaviors (T_g) of samples. Approximately 10 mg of samples was loaded in the aluminum pans, and then the pans were sealed and heated under nitrogen atmosphere (investigated temperature range: 0– 300 C, heating rate: 10 °C/min).

2.2.7 Powder XRD Analysis

The crystalline phases of samples were analyzed by X-ray diffraction (XRD) using an X-ray diffractometer (Rigaku D/MAX-2200 Ultima-plus, Tokyo, Japan) the measurement conditions were a Cu K α radiation, generated at 40 kV and 30 mA as X-ray source 2–40° (2θ) and step angle 0.01°/s

2.3 Preparation of Oolong Tea Polyphenol Extract (OTE)

OTE were prepared using methanolic extraction method. The dried oolong tea leaves (78 grams) were extracted in a round bottom flask with the methanol (500 ml)

at 70 °C for 3 h. After the mixture was cooled, the extract was filtered through Whatman No.1 filter paper (diam. 125 mm) to remove particles. The methanol extract was concentrated in a rotary evaporator at 50 °C under reduced pressure until the methanol was completely evaporated. Crude extract was partitioned by shaking in separating funnel with dichloromethane: methanol: water (3:1:0.2) (v/v/v) and was repeatedly shaken to attain equilibrium. The methanol layer was evaporated under reduced pressure at 55 °C using rotary evaporator to obtain an OTE. Yield percentage of OTE products were calculated bases on weight of dried OTE to weight of dried oolong tea leaves as shown in Eq. 1 below.

$$\text{Yield (\%)} = \frac{\text{weight of dried OTE}}{\text{weight of dried oolong tea leaves}} \times 100 \quad \text{(Eq. 1)}$$

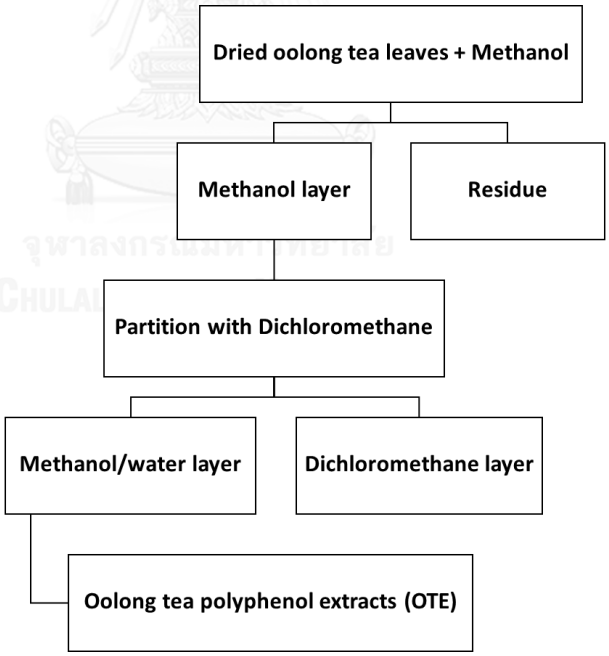

Figure 2.1 Methanolic Extraction of OTE

2.3.1 Determination of the Chemical Composition of OTE by High Performance Liquid Chromatography (HPLC)

OTE was analyzed by reverse phase high performance liquid chromatographic system (Water binary HPLC pump) coupled to a UV-visible light detector (Water 2489). The column of this experiment was C18 reverse phase column (100 X 4.6 mm i.d.) packed with Hypersil C18 (Thermo Fisher Inc, Watham, Massachusetts, USA). The flow rate was set up at 0.7 ml/min and the UV detector was performed at 270 nm. Injection volume was 22 µl. Sample was dissolved in acetonitrile. The mobile phase composed of a solution of formic acid 0.1% in Mili Q water (Solvent A) and acetonitrile (Solvent B). The gradient elution was started with 95% solvent A and 5% solvent B, then the content of solvent B was increased linearly to 15% within 14 min and maintained for 11 min. After that, the percentage of solvent B was increased to 35% within 28 min, and to 85% within 12 min. At the end, the column was re-equilibrated back to solvent B (95%) for 15 min before the next injection. Analysis was carried out in triplicate.

2.3.2 Calibration Curve

The method development was concentrated on establishing the linear calibration curve for four components. The each standard solution containing gallic acid (30-70 µg/ml), caffeine (150-800 µg/ml), epigallocatechin-3-gallate (120-500 µg/ml), and epicatechin-3-gallate (40-120 µg/ml) was prepared in acetonitrile.

2.4 Synthesis of Polymerized Oolong Tea Extract (P-OTE) particle by Enzymatic Template Polymerization

OTE (0.54 g) was first mixed with PEG (0.0342 g), and HRP (10 mg), respectively. Hydrogen peroxide (5% aq. solution, 3.4 mL) was added dropwise to the mixture at room temperature and then a single drop of hydrogen peroxide to the mixture will generate a bubble. 12.5 mL of methanol and 12.5 mL of 0.1 M phosphate buffer (pH 7) were added to the mixture and placed in a 50 mL flask under stirring. After 24 h,

the solution was further purified by dialysis against water (MWCO 50,000) and freeze-dried by Freeze dryer (Freezone 77520, Benchtop, Labconce). After freeze-drying, a brownish powder was obtained. The product was named P-OTE (Polymerized Oolong Tea Extract) particle. Yield percentage of P-OTE particles were calculated bases on weight of dried P-OTE particle to weight of dried OTE as shown in Eq. 2. And the percentage of PEG incorporated into particles were calculated bases on weight of PEG to weight of dried P-OTE particle as shown in Eq. 3, respectively

$$\text{Yield (\%)} = \frac{\text{weight of dried P-OTE}}{\text{weight of OTE}} \times 100 \qquad \text{(Eq. 2)}$$

$$\text{PEG incorporated into particle (\%)} = \frac{\text{weight of dried OTE}}{\text{weight of dried oolong tea leaves}} \times 100 \qquad \text{(Eq. 3)}$$

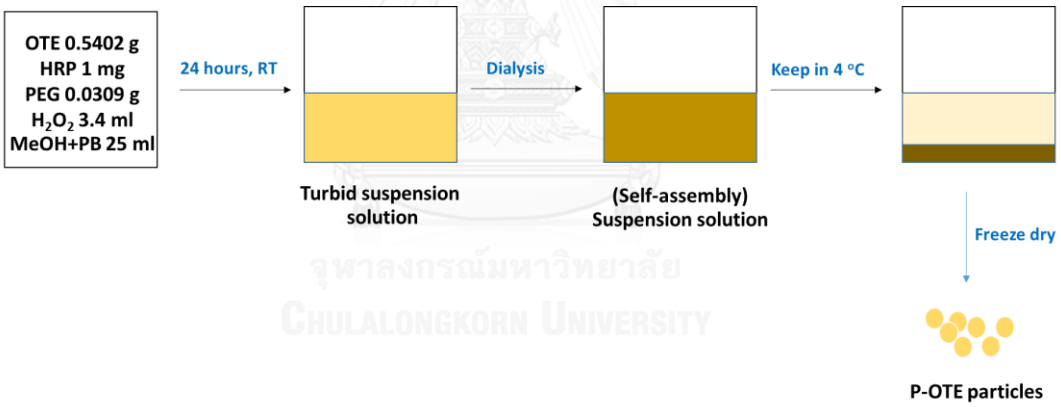

Figure 2.2 Synthesis of P-OTE particles Through Enzymatic Template Polymerization

2.5 DPPH Radical Scavenging Activity

The free radical-scavenging activity of samples assessed according to the method of Chen and Ho [100]. Briefly, 100 µl of samples at the various concentration (50-500 mg/l) was mixed with 200 µl of 0.079 mg/ml DPPH methanol solution and 2.8 ml of methanol. The mixture was shaken for 1 min by vortexing and left in the dark at room temperature for 30 min. After incubation, the absorbance of the mixture was

measured at 517 nm. BHT were used as references. This test was carried out in triplicate and the ability to scavenge DPPH radical was calculated by the following equation:

$$\text{DPPH radical scavenging activity (\%)} = \frac{Abs_{control} - Abs_{sample}}{Abs_{control}} \qquad \text{(Eq. 4)}$$

Where $Abs_{control}$ is the absorbance at 517 nm of 2 mM DPPH radical solution and Abs_{sample} is the absorbance of DPPH radical solution mixed with samples.

2.6 Potentiometric Studies to determine the pKa of P-OTE particle

To start, P-OTE particle (1 g/l) was dissolved in DMSO: water (3:2) (v/v). P-OTE solution was titrated using 1 M NaOH from acidic medium (pH = 1) to alkaline medium (pH = 14). The initial pH is adjusted to pH = 1 by 1 M HCl. The NaOH was added in discrete amounts according to the buffering capacity of the solution. The pH was recorded with a Mettler Toledo pH meter after each step of the titration, which was carried out until the mixture reached pH 14. The pKa values for P-OTE solution are below the titration range modeled in this study.

2.7 Determination of Drug Loading Percentage (%Loading) and Encapsulation Efficiency Percentage (%EE)

The PTX and xanthone as two drugs were selected as the model drug in this experiment. The P-OTE particle (1200 ppm) were mixed with PTX (600 ppm) in ethanol solution and kept in the dark for 24 h at room temperature. After that, the mixture was centrifuged at 13500 rpm for 30 min (Centrifugation was performed on Allegra 64R high speed centrifuge, Beckman Coulter, Inc., Japan) and the concentration of free PTX in the supernatant was quantified by UV-visible measurement (OPTIZEN POP QX model) through the absorbance at a maximum absorption at 227 nm [101, 102], according to the standard curve of drugs. The percent of drug loading and encapsulation efficiency were calculated by the following equations Eqs. (5) and (6),

respectively [103]. Each experiment was carried out in independent triplicate. The xanthone loading into P-OTE particle was carried out similarly to that described in previous paragraph.

$$\%EE = \frac{\text{weight of incoperated paclitaxel}}{\text{weight of starting paclitaxel}} \times 100 \quad \text{(Eq. 5)}$$

$$\%Loading = \frac{\text{weight of incoperated paclitaxel}}{\text{weight of incoperated paclitaxel + particles weight}} \times 100 \quad \text{(Eq. 6)}$$

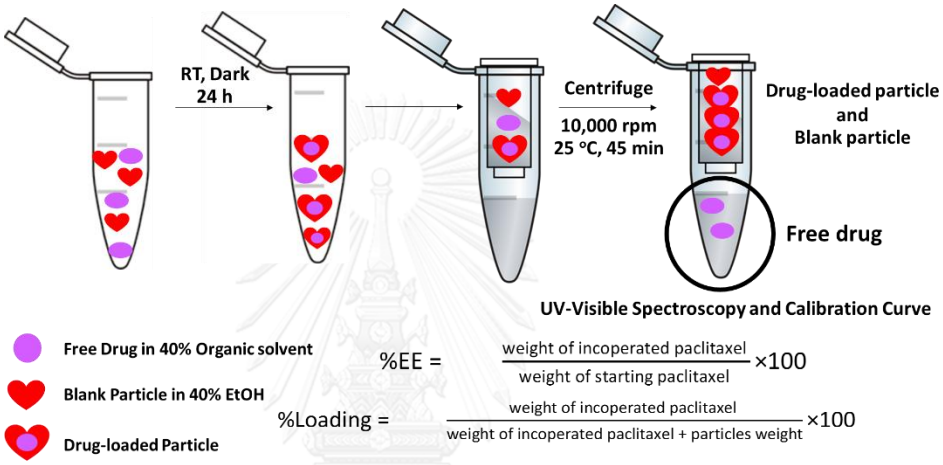

Figure 2.3 Determination of %EE and %loading by the indirect method

2.8 Determination of the Optimum Weight Ratio of P-OTE particle

Varying the weight ratio of drugs and P-OTE particle was carried out as shown in Table 2.1 and Table 2.2. This weight of P-OTE particle was fixed while varying the weight of drugs. Finally, the %EE and %Loading of all preparations were determined.

Table 2.1 Weight Ratio of P-OTE particle to Xanthone

Content	Amount of P-OTE particle (ppm)	Amount of Xanthone (ppm)	Drug to polymer ratio
1	1200	1200	1:1
2	1200	600	1:2
3	1200	400	1:3
4	1200	300	1:4

Table 2.2 Weight Ratio of P-OTE particle to PTX

Content	Amount of P-OTE particle (ppm)	Amount of PTX (ppm)	Drug to polymer ratio
5	1200	1200	1:1
6	1200	600	1:2
7	1200	400	1:3
8	1200	300	1:4

2.9 *In vitro* Anti-cancer Assay

In vitro anticancer properties of products were evaluated [104]. PTX-loaded P-OTE particles, PTX-loaded OTE, Xanthone-loaded P-OTE particles, Xanthone-loaded OTE, free P-OTE particles, free OTE, free PTX, and free xanthone were tested against A549 human lung adenocarcinoma cells. To confirm the anti-cancer activity, the standard EGCG was subjected to the same reaction condition as the OTE. The anti-cancer activity was evaluated by MTT assay.

2.9.1 Cell lines and Culture Conditions

The A549 human lung adenocarcinoma cells was purchased from American Type Culture collection (ATCC, RockVille, MD, USA). The lung cancer A549 cells was treated in RPMI-1640 supplemented with 10% (v/v) fetal bovine serum (FBS), amd 1%

antibiotic (penicillin and streptomycin) in a humidified atmosphere of 5% CO_2 at 37°C until confluent.

2.9.2 Evaluation of Cell Proliferation by MTT Assay

The number of viable A549 cells after samples treatment was evaluated by the MTT (3-[4,5-methylthiazol-2-yl]-2,5-diphenyl-tetrazolium bromide) assay preformed in triplicate. In brief, A549 cells (5×10^3 cells/well) were seeded in a 96-well plate containing 100 µl of the culture medium and allowed to grow in CO_2 incubator for 24 h (37°C, 5% CO_2). After 24 h, additional medium (100 µl) containing samples was added to each well and cells were allowed to grow for 72 h (37°C, 5% CO_2). Then, the wells were replaced with medium containing MTT (0.5 mg/ml) and incubated for 2 hrs. Next, the medium were removed and the pellet (MTT metabolic product) was dissolved completely with 100 µl DMSO. Color developed after the reaction was measured at 550 nm using microplate reader, and substracted with absorbance at 650 nm. The results were reported as percent of viability and the IC_{50} was calculated by nonlinear regression.

$$\% \text{ Cell viability} = \frac{\text{O.D of control-O.D of test compound}}{\text{O.D. of control}} \times 100 \qquad \text{(Eq. 7)}$$

Where O.D is the optical density

CHAPTER III
RESULT AND DISCUSSION

3.1 OTE

Here, dried oolong tea leaves (78 g) were refluxed at 60 °C for 3 h in methanol (500 ml). After 3 hours, the color of the liquid was green whereas the oolong tea leaves changed from green color to yellow color. The mixture was filtered through Whatman No. 1 filter paper, and then aqueous solution was collected. This obtained aqueous solution was extracted with (3:1, v/v) dichloromethane/methanol three times. When dichloromethane was added to the solution, green sticky gum appeared at the bottom of the container and it was removed out of a solution. Then, water was added to the solution and the mixture was incubated for 10 min at room temperature to induce a phase separation between a layer of methanol and dichloromethane. The upper methanol/water phase was collected, and the lower dichloromethane phase was re-extracted with dichloromethane methanol (3:1, v/v). Combined methanol phases were dried below 60 °C under reduced pressure on rotary evaporator to give a crude OTE powder, which presented as a powdery orange colored solid. The yield of OTE was 22.5% regarding the weight of (78 g) oolong tea leaves. The OTE was kept in a refrigerator at -20 °C.

3.2 Determination of the chemical composition of OTE

The extraction process gave us 3.375 g of OTE from 15 g of dry oolong tea leaves. The HPLC analysis of the major compounds in the obtained OTE showed four major peaks (Figure3.3) at retention times 2.6, 17.0, 24.6, 31.6 minutes (Figure 3.3) corresponded to the retention times of the standard gallic acid, caffeine, epigallocatechin-3-gallate (EGCG) and epicatechin-3-gallate (ECG), respectively.

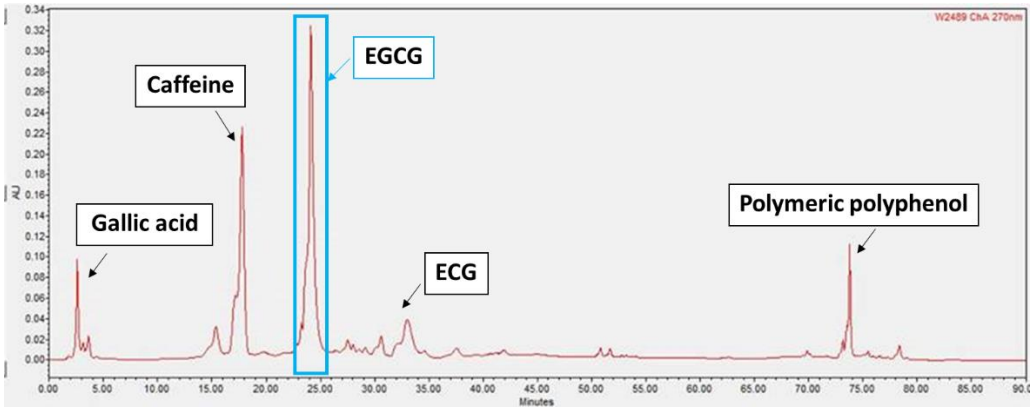

Figure 3.1 HPLC chromatogram of OTE.

To quantify each major components in the OTE, calibration curves of each standard (gallic acid at 30-70 µg/ml, caffeine at 150-800 µg/ml, EGCG at 120-500 µg/ml and ECG 40-120 µg/ml, respectively) were constructed by plotting the peak area versus concentrations. The correlation coefficients for all four standard compounds were close to 1.0, suggesting good linearity for the calibration curves of the four standard compounds. Table 3.1 shows the contents of the four major components in the OTE. EGCG was the major component (46.60% w/w), followed with caffeine at 3.44 % (w/w), and then gallic acid and ECG at 0.42% (w/w) and 0.29% (w/w), respectively. Details of the calculation was given in Appendix (on page 74).

Table 3.1 Contents of the four major components in OTE

Contents	Retention time (min)	Concentration of content (%w/w)
Gallic acid	2.6	0.42
Caffeine	17.0	3.44
Epigallocatechin-3-gallate	24.6	46.60
Epicatechin-3-gallate	31.6	0.29

3.3 Characterization of OTE

OTE was further characterized by nuclear magnetic resonance (NMR), fourier transform infrared spectroscopy (FT-IR), UV-visible spectroscopy and fluorescence spectroscopy.

3.3.1 NMR Analysis of OTE

The sample was subject to ^{1}H analysis using liquid state NMR to examine for chemical shift. ^{1}H NMR spectrum of OTE is shown in Figure 3.2a. Figure 3.2b shows the ^{1}H NMR spectrum of standard EGCG for comparison. The assignment of the proton resonances of standard EGCG in Figure 3.4b is consistent with previously reported data.[1,2] The ^{1}H NMR of standard EGCG (D_2O, δ ppm) shows signals at 2.8-3 ppm (assigned to C-ring methylene (CH_2)), 5.1 and 5.6 ppm (C-ring methane and methylene (CH)), 6–6.1 ppm (A-ring CH), 6.5 ppm (B-ring CH), and 6.9 ppm (D-ring CH), respectively.

All resonance peaks of EGCG appeared in the ^{1}H spectrum of the OTE. The peaks did not show any significant shift in their resonance positions. This data agree well with the HPLC analysis which indicates EGCG as the main component of OTE. Small peaks observed at approximately 1.85-2.0 ppm in the ^{1}H spectrum of OTE (not observed for the standard EGCG) may represent. The epimerization products of EGCG as it was reported previousely that at high temperatures, EGCG could epimerize to GCG (gallocatechin gallate) at C-2 position [105, 106].

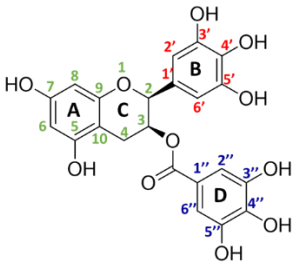

Proton	EGCG (ppm)
H6	5.96
H8	5.85
H3	5.36
H2	4.88
H4	2.88
H4'	2.72
H2', H6'	6.45
H2", H6"	6.84

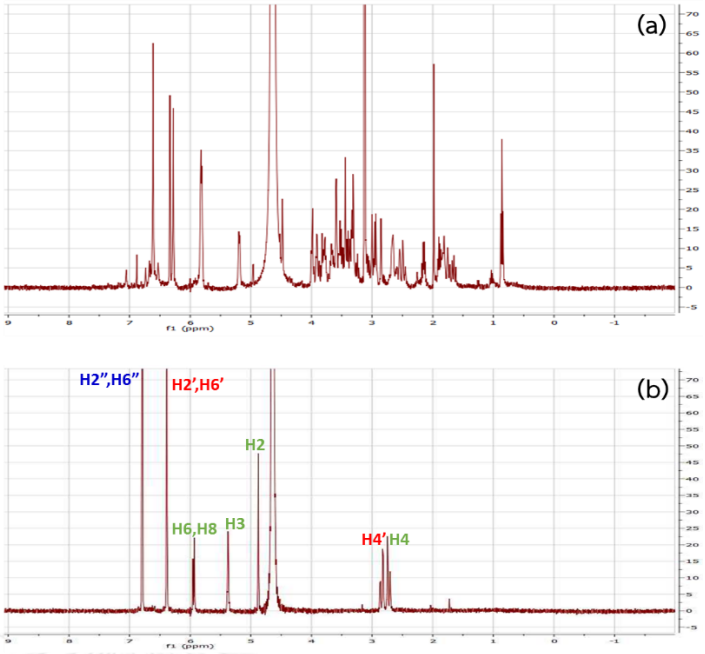

Figure 3.2 Proton NMR spectrum obtained with liquid state NMR using D_2O as solvent. (a) OTE, and (b) EGCG standard

3.3.2 FT-IR Spectrum of OTE

OTE (Figure 3.3) shows the following characteristic pecks: 3222 cm^{-1}, 2913 cm^{-1}, 1730 cm^{-1}, 1687 cm^{-1}, 1335 cm^{-1}, 1024 cm^{-1}, 1007 cm^{-1} and 816 cm^{-1} respectively. The 3222 cm^{-1} and 2913 cm^{-1} peaks correspond to O-H of the phenolic group (phenol stretching vibration). The IR band at 1730 cm^{-1} is characteristic of the C=O stretching mode of the carboxylic group. The peak having the value of 1687 cm^{-1} represents the C=C (C=C symmetric stretching vibration), 1335 cm^{-1} peak corresponds to the O-H phenolic group (O-H bending), the 1024 cm^{-1} corresponds to the C-H bending vibration of the aromatic group, the 1007 cm^{-1} peak corresponds to the ketone group, while 816 peak corresponds to the in-plane deformation vibration of alkene group.

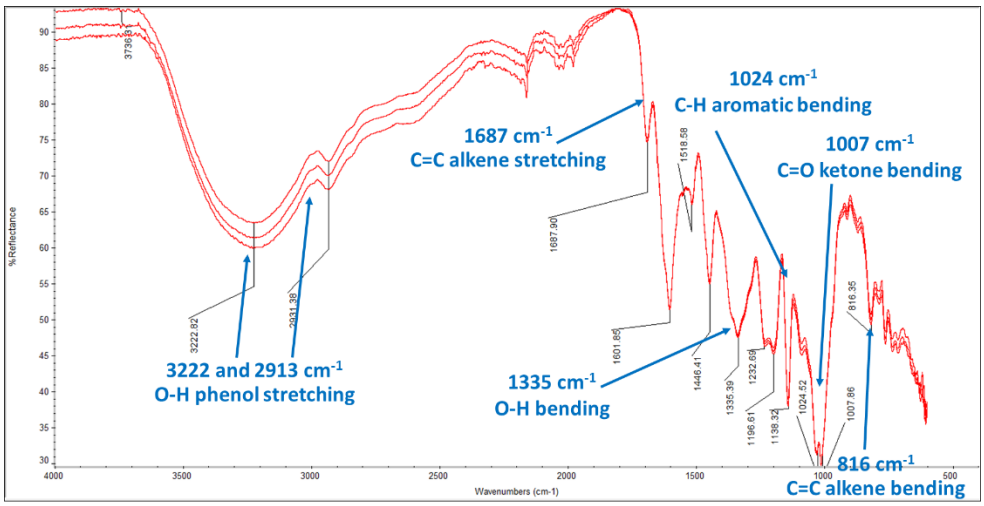

Figure 3.3 FT-IR spectrum of of OTE

3.3.3 UV-Visible and Fluorescence Spectroscopy Analysis of OTE

Light absorption at 200-800 nm of OTE in water was acquired using UV-visible spectrometer (Figure 3.4). The spectrum shows that aqueous solution of OTE absorbs light between 210 nm to 300 nm with maximum wavelenght at 273 nm. When excited at UV_{max}= 273 nm, the solution fluorescence at λ_{max} of 438 and 535 nm (Figure 3.5).

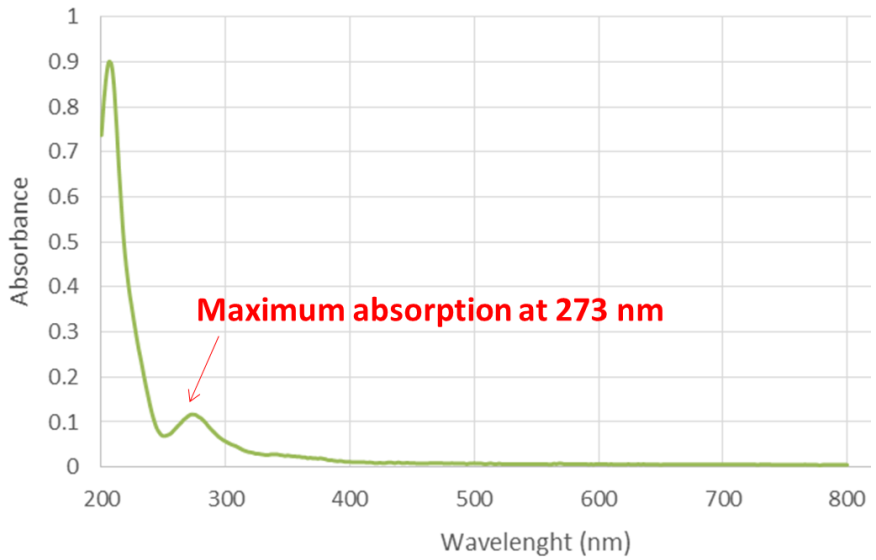

Figure 3.4 UV aborption spectrum of OTE

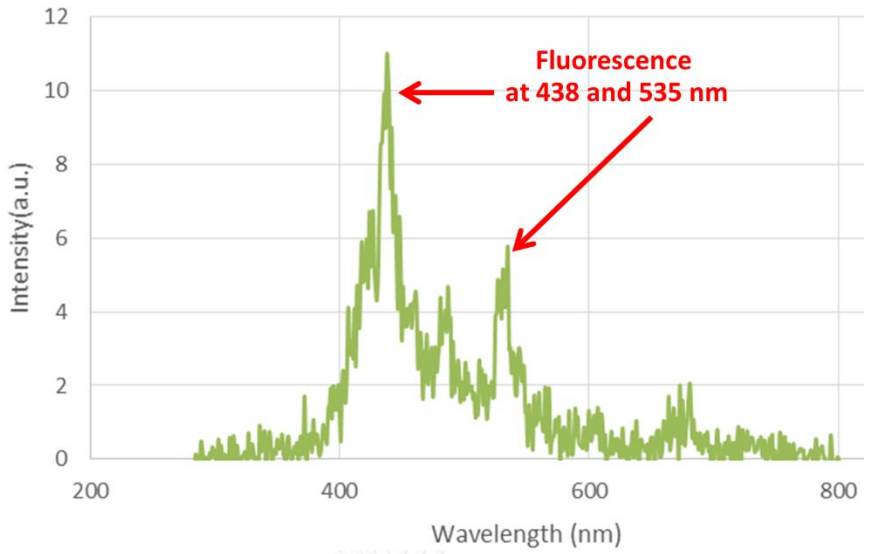

Figure 3.5 Fluorescense spectrum of OTE with the excitation wavelenght at 274 nm

3.4 Synthesis of Polymerized Oolong Tea Extract (P-OTE) particle by Enzymatic Template Polymerization

Mixing OTE (0.54 g) with PEG (0.0342 g), HRP (10 mg), hydrogen peroxide (8% aq. solution, 3.4 mL) in aqueous methanol medium (12.5 mL of methanol and 12.5 mL of 0.1 M phosphate buffer, pH 7) for 24 h caused the change from true solution to turbid suspension with some insoluble non-dispersible yellow gum. The yellow gram was removed and the solution was further purified by dialysis (using membrane cut off 50,000 Da) against water to rid off methanol and small molecules. During dialysis, methanol was slowly displaced with water and fine particles were observed. The obtained brown colored particles dispersed well in water. Finally, the slightly brownish powder could be obtained by freeze drying the suspension. The obtained product was kept in refrigerator at -20 °C. The yield of the product was 26.5% regarding the weight of the starting (0.54 g) OTE. The product was named P-OTE (Polymerized Oolong Tea Extract) particle. The obtained product was characterized for its chemical and physical properties as follows:

3.4.1 Solubility and pH Stability of P-OTE particle

The solubility of P-OTE particle in various solvents (hexane, dichloromethane (CH_2Cl_2), ethyl acetate (EtOAc), acetone, methanol, water, dimethylformamide (DMF), and dimethyl sulfoxide (DMSO)) is shown in Fig 3.6. P-OTE particle is completely soluble in DMSO and DMF. Although it is insoluble in water, the material disperses well in water. The P-OTE particle is partly soluble in methanol and acetone. The material is insoluble in EtOAc, CH_2Cl_2 and hexane.

When the P-OTE particle was tested in water of pH values of 1, 4, 7, and 9, the material showed good dispersion in acidic water, no precipitation was observed if the suspension was not centrifuged. Suspensions of the P-OTE particle in water at pH 7 and 9 are not as well dispersed, some precipitation could be observed when the suspension was left for 30 min. However, redispersion can be done easily by shaking. The reason for this may be the charge on the surface of the P-OTE particles is affected by pH of the medium. Acidic pH seems to make stable suspension, thus indicating probably higher surface charge.

Table 3.2 Solubility tests of the P-OTE particle (+ means soluble and – means insoluble)

Solvent	Hexane	CH_2Cl_2	EtOAc	Acetone	MeOH	H_2O	DMF	DMSO
P-OTE particle	-	-	-	+	+	-	+	+

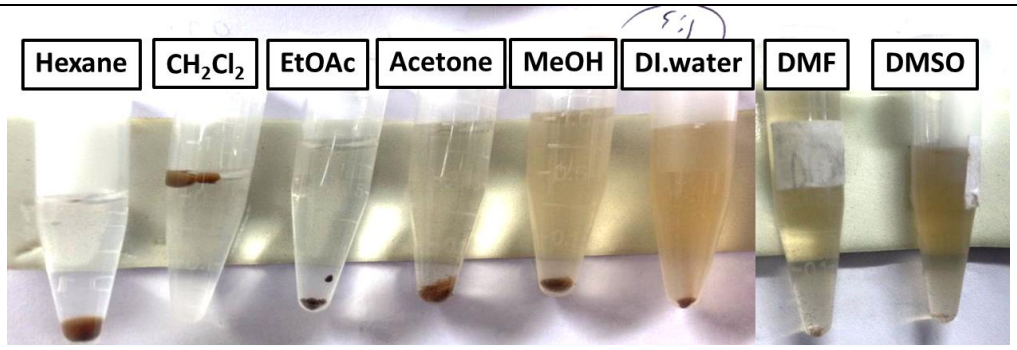

Figure 3.6 Solubility of P-OTE particle in various solvents

3.4.2 Determination of Free EGCG in the P-OTE particle by HPLC Analysis

Figure 3.7 shows the HPLC chromatograms of OTE and P-OTE particle. Peaks at 2.6 min (gallic acid), 17.0 min (caffeine), 24.6 min (EGCG), and 31.6 min (ECG), were observed in the chromatogram of OTE whereas the chromatograms of P-OTE particle displays only peaks of galiic acid and caffeine and shows neither EGCG nor ECG peaks. This implies that all EGCG and EGC in the OTE underwent some changes during the preparation process of the P-OTE particle.

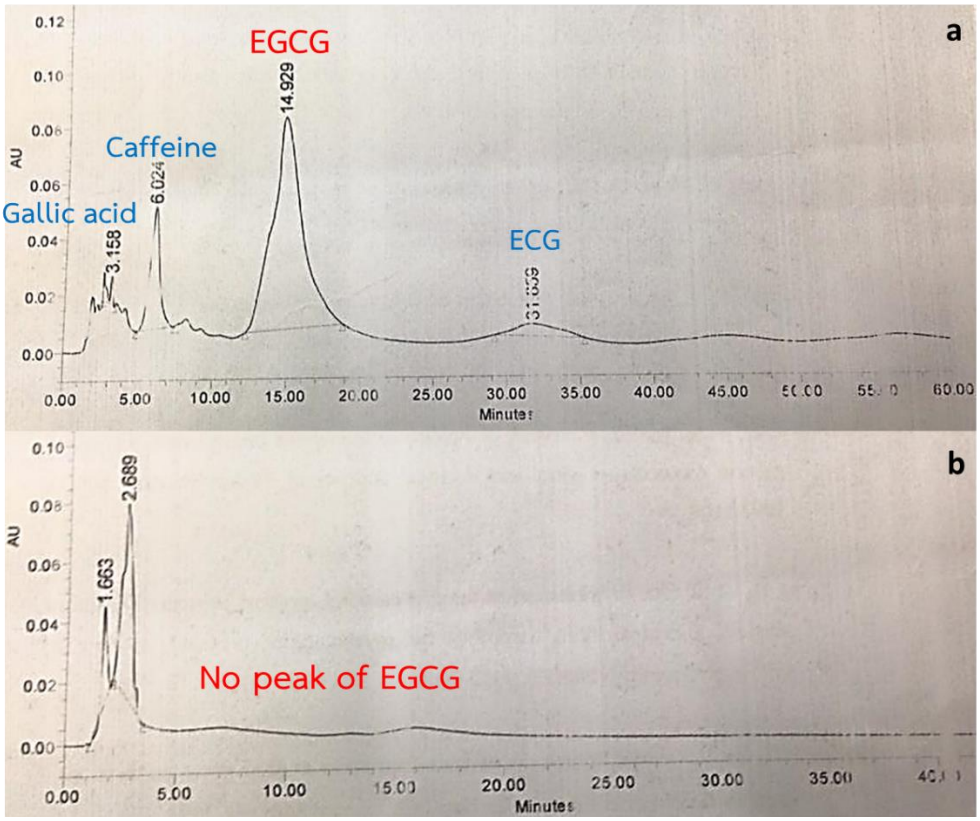

Figure 3.7 HPLC chromatogram of (a) OTE, and (b) P-OTE particle

3.4.3 Mass Spectrometric Analysis of P-OTE particle

The mass spectrum of OTE extract displays ions at 381 [EGCG-77, EGCG-aromatic ring]$^+$, 382 [EGCG+H$^+$-77]$^+$, 497 [EGCG+K$^+$]$^+$, 955 [EGCG Dimer+ K$^+$]$^+$ (Figure 3.11). Interestingly, the mass spectrum of P-OTE particle shows peaks at 1580. These

high m/e peaks indicate a presence of high molecular weight species in the P-OTE sample. The increment of 955 corresponds well to EGCG unit. It is likely that the P-OTE particle is a polymerized product of OTE. We speculate that polymerization of EGCG in the OTE occurred

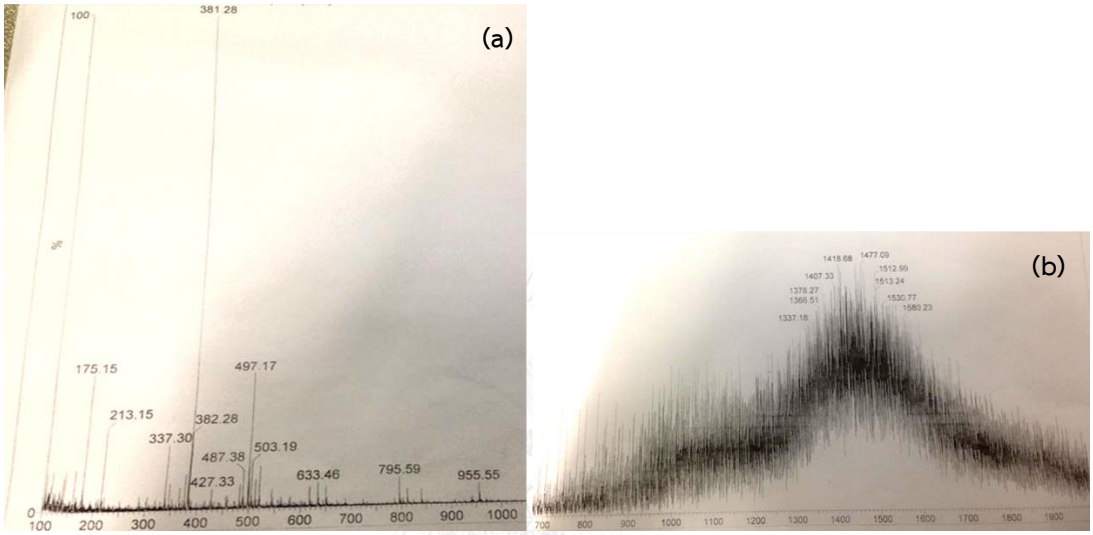

Figure 3.8 Positive charge ESI mass spectrum of OTE (a), and P-OTE particle (b). The solvent was methanol

3.4.4 Gel Permeation Chromatographic Analysis of P-OTE particle

GPC was used to elucidate the molecular weight characteristic of P-OTE particle. The number average molar mass (M_n) and the weight average molar mass (M_w) obtained from GPC are shown in Table 3.3. M_n and M_w of standard OTE extract are 400 and 700, respectively. The polydispersity index (PDI), as a measure of the distribution of molecular mass in a given polymer sample and calculated as M_w/M_n, is 1.75. P-OTE particles show the M_n of 41,000, the M_w of 55,000, and the PDI of 1.34. These data indicate high-molecular-mass polymers in the P-OTE particle. This result suggests that the P-OTE sample contains polymerized polyphenol. The result here agrees well with the mass spectral analysis. It should be noted here that because of the limitation of

mass range of 2000 in the mass spectrometer, higher molecular weight species could not be observed.

To confirm the polymerization of EGCG in the P-OTE particle, the standard EGCG was subjected to the polymerization under the same reaction condition as the OTE. M_n and M_w values of the product also indicated polymerization (Table 3.3).

Table 3.3 M_n and M_w of samples in GPC analysis

Content	M_n(Da)	M_w(Da)
OTE	400	700
P-OTE particle	400 and 41,000	700 and 55,000
EGCG	400	700
P-EGCG particle	400 and 42,000	800 and 55,000

3.4.5 Elemental Analysis (EA) of P-OTE particle

The elemental compositions of OTE and P-OTE particle are given in Table 3.4. Changes in elemental composition could be detected. Reduction of carbon percentage is observed in the polymerized product. This can indicate more of the hydroxyl functionality in the structure of the product as compared to the starting material.

Table 3.4 Elemental analysis of OTE and P-OTE particle

Sample	%C	%H	%O	%N
OTE	8.22	1	5.90	0
P-OTE particle	6.52	1	4.84	0

3.4.6 NMR Analysis of P-OTE particle

P-OTE particle was subjected to ^{1}H analysis using liquid state NMR to examine for potential structural change in OTE extract after polymerization. DMSO-d6 was used as a solvent and the material dissolved well. Figure 3.9 illustrates that ^{1}H spectrum of P-OTE particle appeared to contain substructure of the free EGCG resonances, indicating some preservation of the EGCG sub-structure in the P-OTE product. P-OTE particle showed some broad signals at approximately 8.7-9.5 ppm, which was not observed for the original OTE and free EGCG. These broad peaks can be attributed to the phenolic protons because these peaks shifted to around 7 ppm when the pH of the solution was changed to more acidic (adding TFA into the solution and subjecting to 1H NMR analysis again). The peaks of P-OTE particle were compared to that of the OTE, two double-doublets corresponding to methylene of H-4α and H-4β at 3.02 and 2.88 ppm, a singlet-like at 5.07 ppm which corresponds to methine proton H-2, and the two spin systems corresponding H-8 protons of the A-ring at 6.3 ppm, observed for the OTE spectrum, could not be observed in the P-OTE spectrum. This information suggests that polymerization reaction probably affects H-4α, H-4β or H-2 of EGCG structure. The broadening of resonance peaks observed in the P-OTE spectrum also implies polymerized structure of the material.

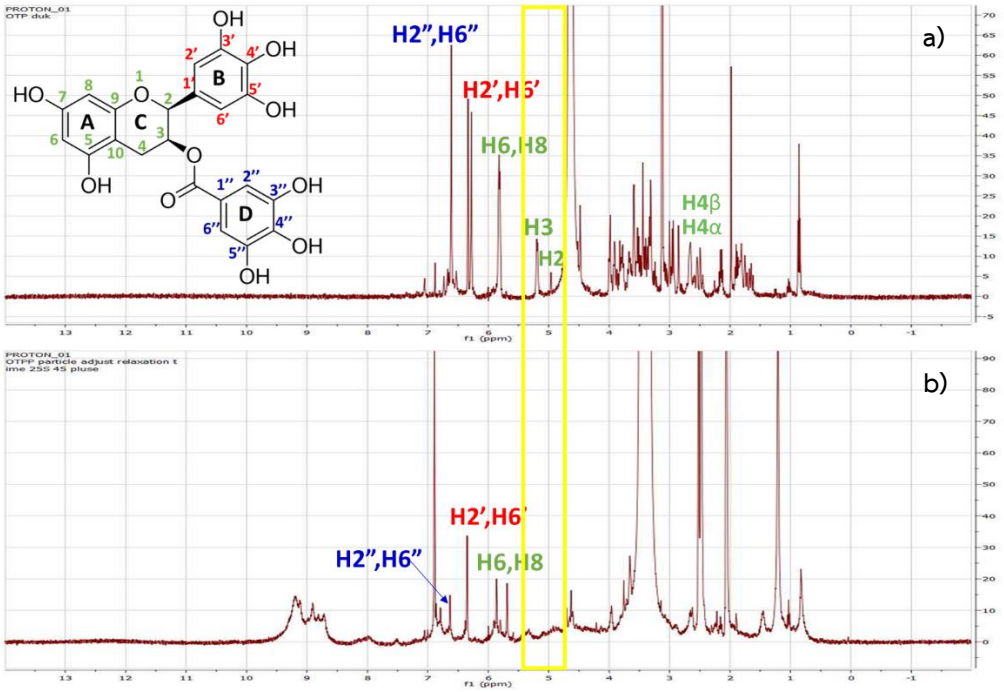

Figure 3.9 Proton NMR spectrum of P-OTE particle (b) obtained with liquid state NMR using DMSO as solvent compared with OTE (a) using D_2O

3.4.7 FT-IR Spectrum of P-OTE particle

Figure 3.10 shows the FTIR spectrum of the P-OTE particle powder sample, revealing the following characteristic pecks: 3351 cm^{-1}, 2883 cm^{-1}, 1703 cm^{-1}, 1606 cm^{-1}, 1462 cm^{-1}, 1339 cm^{-1}, 1142 cm^{-1}, 1093 cm^{-1}, 1006 cm^{-1}, 959 cm^{-1}, and 838 cm^{-1} respectively. The 3351 cm^{-1} peck is specific to O-H stretching vibration. The 2883 cm^{-1} peak is specific to C-H stretching vibration. The peak at 1703 cm^{-1} peak represents the C=O ester stretching vibration; the peck at 1606 cm^{-1} corresponds to C=C aromatic stretching vibration; The 1462 cm^{-1} peck corresponds to C-C aromatic stretching vibration; The 1339 cm^{-1} peck corresponds to O–H bending vibration; The 1241 cm^{-1} peak corresponds to C-O phenol stretching vibration; The 1142.85 cm^{-1} and 1093.05 cm^{-1} correspond to C-OH phenolic group bending vibration; The 1006.53 cm^{-1} peak corresponds to C-O-C ether stretching vibration; The 959.36 cm^{-1} and 838.78 cm^{-1} peak corresponds to C-H out of plane bending of the aromatic group.

The pecks of P-OTE particle were compared to that of the OTE and PEG. After the polymerization of OTE with the PEG, the created peak in 3351 cm^{-1} of P-OTE particle certified to the binding of O-H for phenol group in PEG corresponded to hydrogen bonding. The spectrum of the P-OTE particles is very similar to that of pure PEG but P-OTE particle showed the 1609 cm^{-1} corresponded to C=C aromatic stretching vibration, which was not observed for the original PEG. As the result, the main feature is the presence of all the bands of the PEG in the spectrum of the composite P-OTE particles.

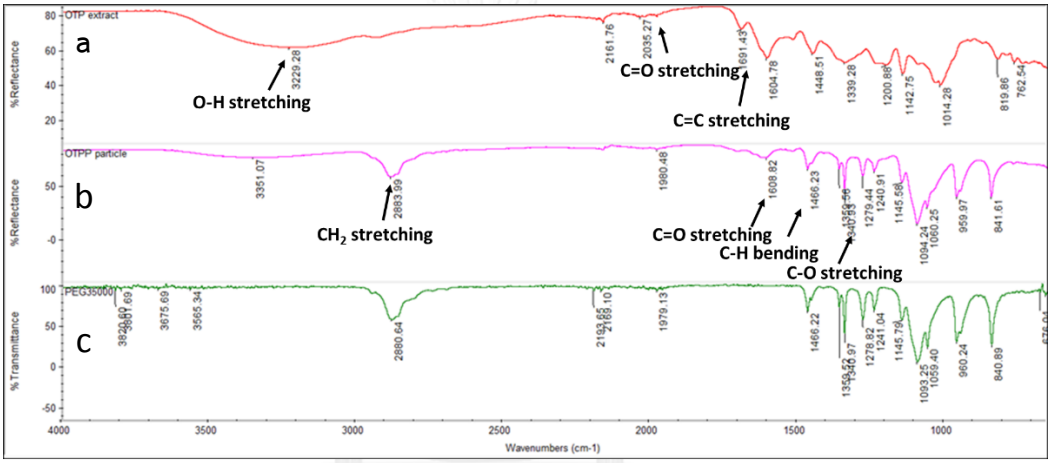

Figure 3.10 FT-IR spectrum of of OTE (a), P-OTE particle (b), and PEG (c)

3.4.8 UV-Visible and Fluorescence Spectroscopy Analysis of P-OTE particle

P-OTE particle (Figure 3.11) possesses UV absorption around 210 nm to 350 nm with no obvious maximum wavelength, whereas the OTE shows a well–defined absorption band with a local maximum at 274 nm, a band that can be attributed to an electronic transition of the n–π^* type, i.e. a transition in which phenol oxygen electrons are largely involved. This information indicated the change in the structure of polyphenol upon polymerization. Fluorescence spectroscopic analysis indicated that when the P-OTE particles were excited at 274 nm, the material strongly emits light around 300-400 nm, whereas, the fluorescence spectrum of the OTE shows very low

fluorescence (Figure 3.12). The increase in fluorescence indicates the more rigid structural change in the polymerized product as compared to the OTE. The rigidity of the structure probably prohibit the non-radiative rotational and vibrational relaxation, thus resulting in the increase in fluorescence.

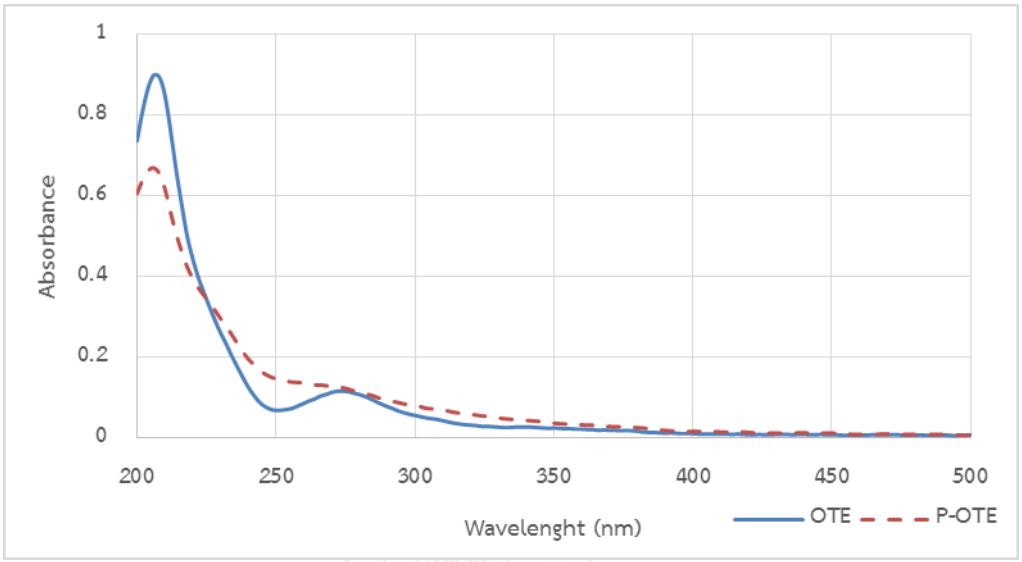

Figure 3.11 UV absorption spectrum of OTE and P-OTE particle

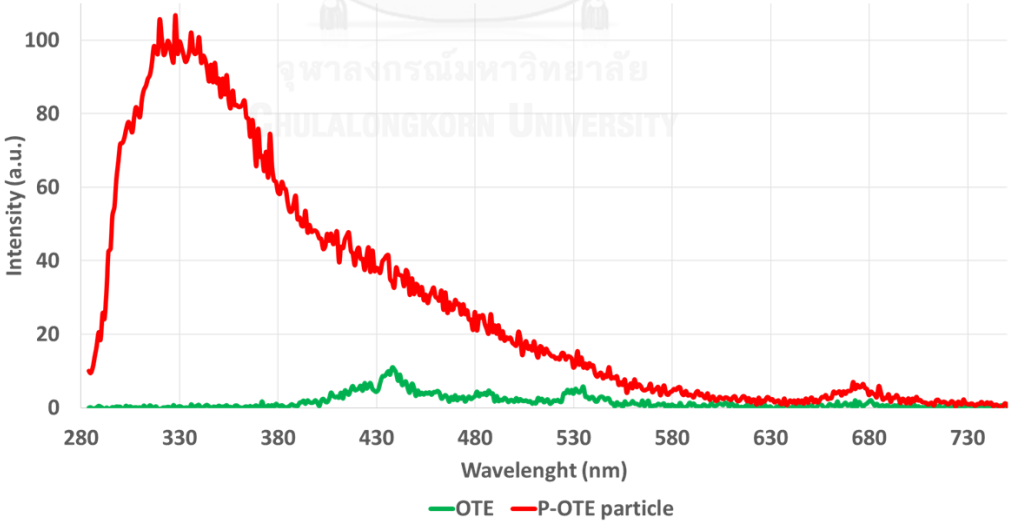

Figure 3.12 Fluorescense spectrum of OTE and P-OTE particle with the excitation wavelenght at 274 nm

3.4.9 Morphological Analysis of P-OTE particle

The morphology and size of the P-OTE particle was characterized through scanning electron microscopy (SEM), transmission electron microscopy (TEM), atomic force microscopy (AFM), dynamic light scattering (DLS) and confocal laser scanning microscopy (CLSM). The energy dispersive X-ray spectrometry (EDS) was used to localize elemental components in the particles.

Figure 3.13 showed the TEM and SEM images of the P-OTE particle. This result revealed spherical particles of approximately 250 ± 40 nm diameter (dry size). The TEM image can be seen as a homogeneous distribution of the main particles with diameter of ~250 nm in the photograph and represented a well-dispersed P-OTE particle. From the SEM image, it was speculated that small P-OTE particles could aggregate into a larger particles.

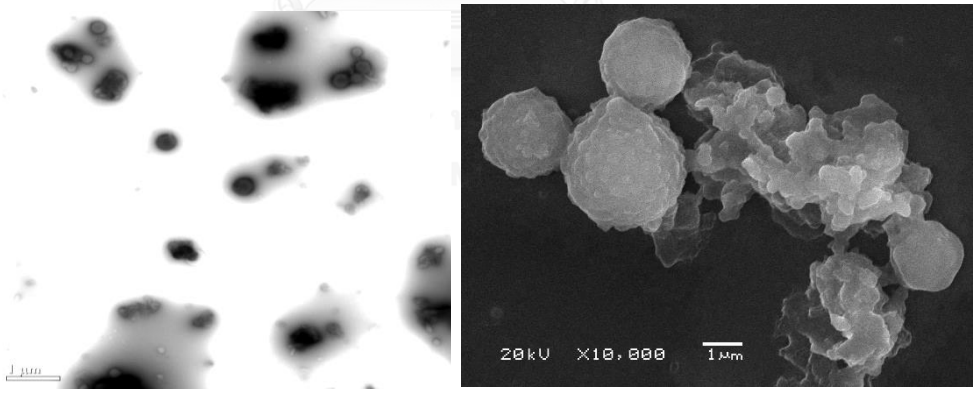

Figure 3.13 TEM (left) and SEM (right) photograph of P-OTE particle

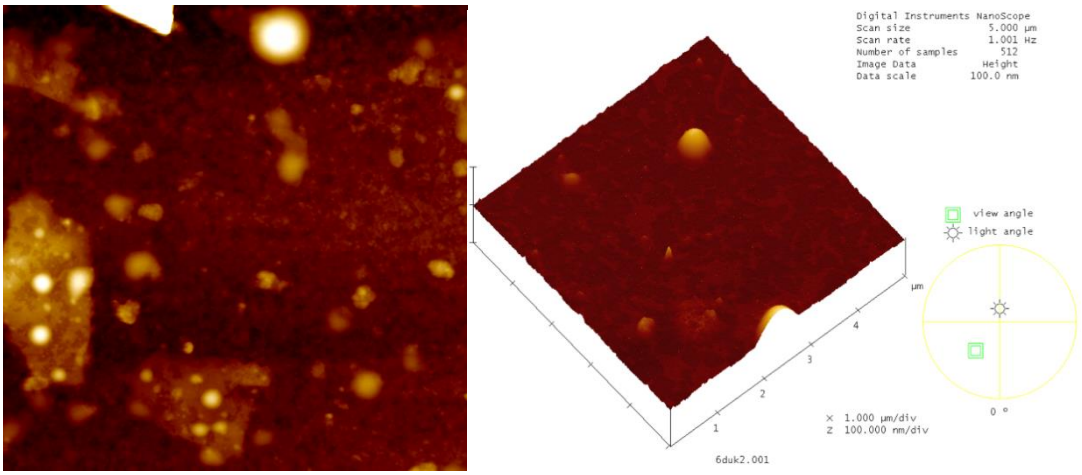

Figure 3.14 AFM photograph of P-OTE particle

As shown in Figure 3.15, the elemental composition of P-OTE particle determined using EDS, it was clear that the P-OTE particle is primarily composed of C and O as expected.

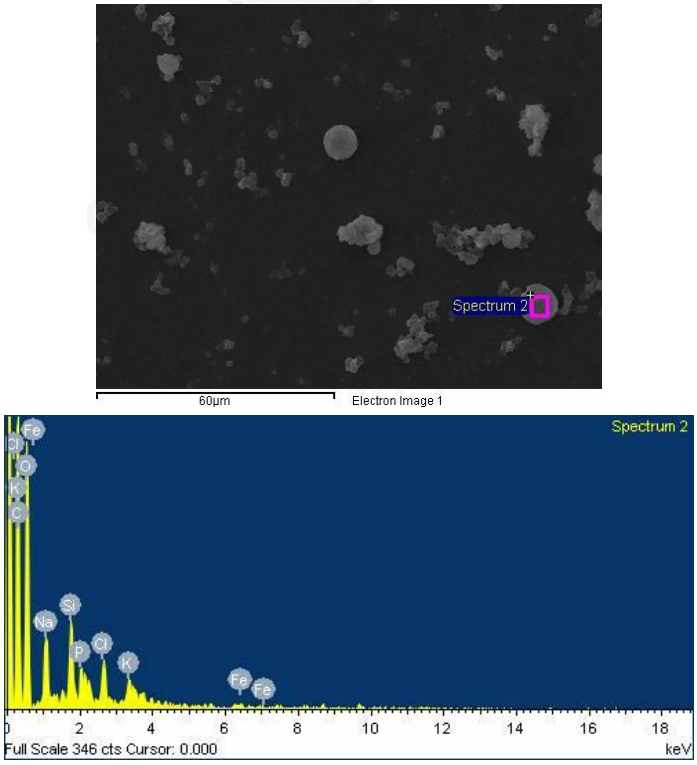

Figure 3.15 SEM (left) and EDX analysis (right) photograph of P-OTE particle

Particle size measurement by DLS indicates presence of structures with dynamic diameter of 250 nm with narrow size distribution. As shown in Figure 3.19b, P-OTE particles obtained possess a negative zeta potential value of −17 to −20 mV, suggesting the fair stability of the P-OTE particles.

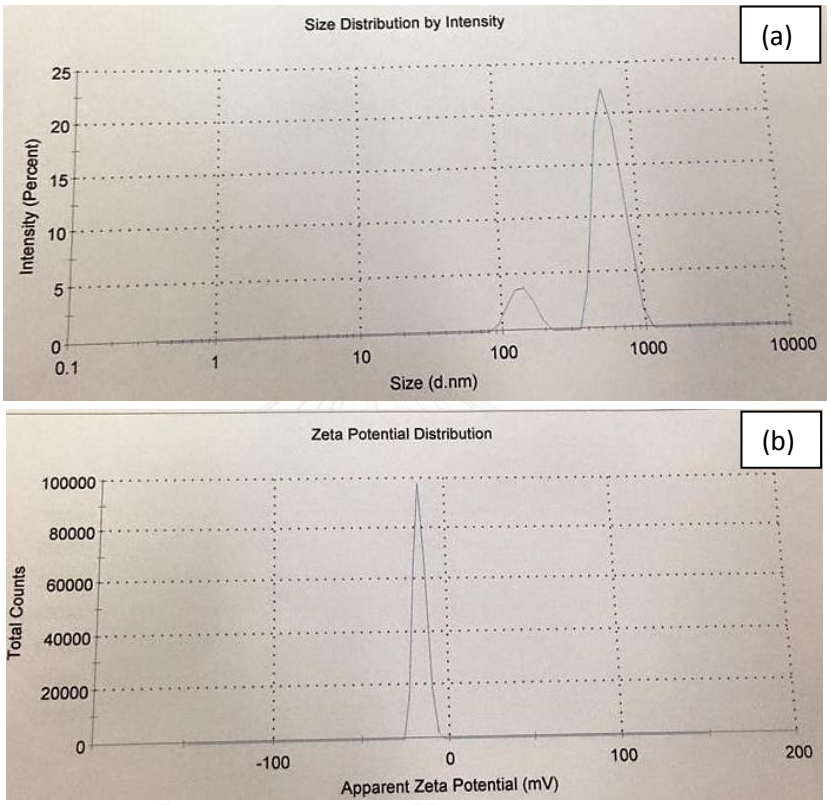

Figure 3.16 Particle size distribution (a) and zeta potential distribution (b) of P-OTE particle

Figure 3.17 shows the CLSF image of P-OTE particles. The particles were observed to be fluorescent and spherical in shape with mean particle sizes within the range of 200-300 nm. Some big aggregated particles were also observed.

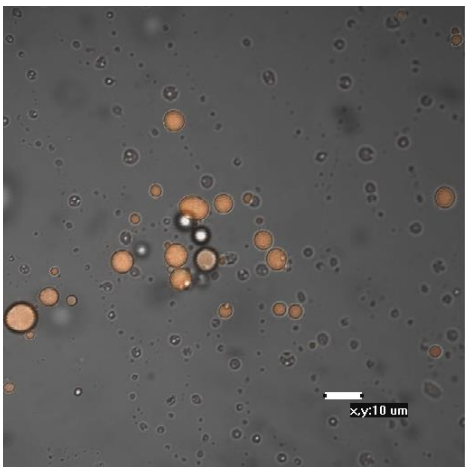

Figure 3.17 CLSF photograph of P-OTE particle

3.5 Thermal Properties of P-OTE particle

The thermal properties of the P-OTE particle were investigated by TGA and DSC analyses.

3.5.1 TG Analysis

Thermal stability of the precursors (OTE and PEG) and product (P-OTE particle) have been analyzed using TGA at the temperature range of 0-600 °C (Figure 3.18).

TG analysis of the standard OTE (Figure 3.18, green line) indicates mass lost from 50 to 500 °C. In the relative DTG graph, this loss is expressed by four endothermic curves at 69.9 °C, 145.2 °C, 207.4 °C, and 286.4. The standard of PEG combustion started at about 388.5 °C and completely combusted at about 418.7 °C (Figure 3.18, blue line). The thermal curve of P-OTE particle (Figure 3.18, red line) shows clearly that the mass losses in two steps, around 50-110°C (accounted for 20% of the total mass lost), and around 405°C (accounted for 60% of the total mass lost). The thermal decomposition patterns of the P-OTE particle and the OTE followed different patterns, indicating different chemical structure. The weight loss of PEG occurs between 300°C and 450°C relating to the thermal degradation of the polymer. This weight loss step is also observed in the TGA of the P-OTE particle, but weight loss during thermolysis of

P-OTE particle occurs over a much broader temperature compared with the sharp signal of PEG.

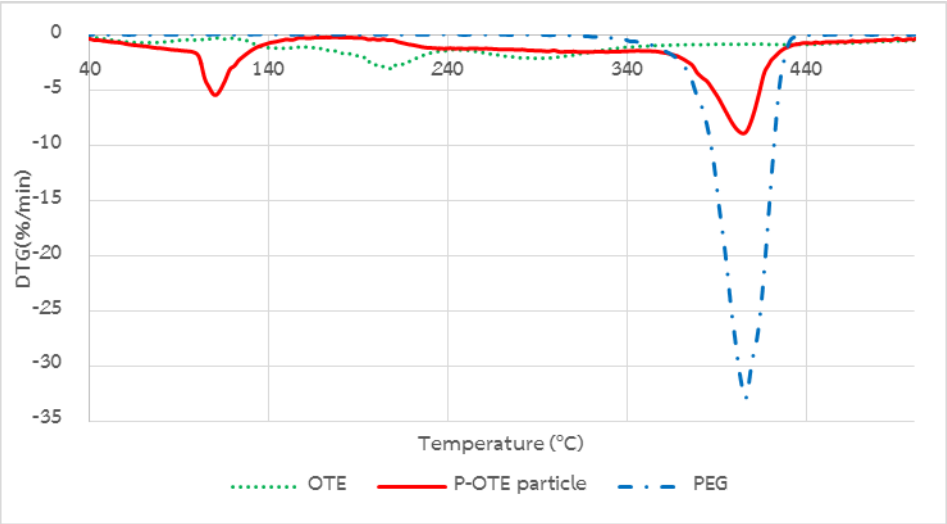

Figure 3.18 TGA thermatogram the exothermic and endothermic peck of OTE (green line), PEG (blue line), and P-OTE particle (red line)

3.5.2 DSC Analysis

The DSC thermatogram of standard OTE, standard PEG, and P-OTE particle are presented in Figure 3.19. All three graphs show one endothermic curve, but with different T_g value. OTE showed an endothermic transition at 128.7 °C, PEG showed endothermic peck at 74.8 °C and P-OTE particle showed endothermic peck at 65.5 °C. The T_g value of P-OTE particle at 65.5 °C is obviously lower than that of standard OTE and PEG. These results indicate different structures of the three materials.

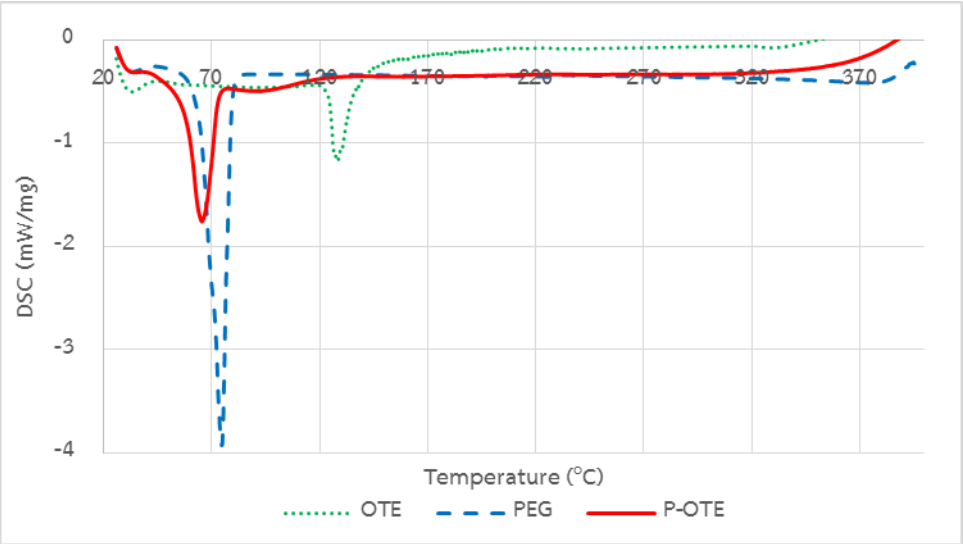

Figure 3.19 DSC thermatogram the exothermic and endothermic pecks of OTE (green line), PEG (blue line), and P-OTE particle (red line)

3.6 Powder XRD Analysis

The XRD patterns of OTE, PEG and P-OTE particle are shown in Figure 3.20. A broad and unresolved peak of OTE in the 2θ region of 10-30° was observed in the diffraction pattern. This indicates the amorphous structure of the OTE. The XRD pattern of PEG showed two broad peaks with highest intensity at 2θ of 19 and 24°, which correspond well to its crystalline properties. P-OTE particle shows similar diffraction pattern to the PEG, but with more amorphous character than PEG. This indicates that the PEG substructure in the P-OTE particle plays an important role in the overall crystallinity of the P-OTE material. It should be noted here that PEG accounts for 21% (w/w) in the P-OTE material.

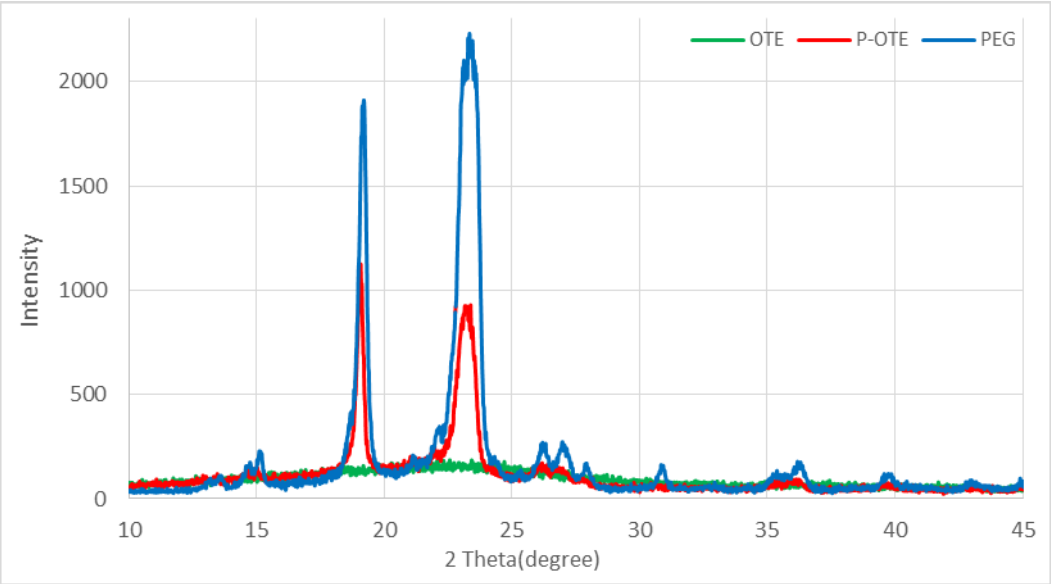

Figure 3.20 X-ray diffraction patterns of standard OTE (green line), PEG (blue line), and P-OTE particle (red line)

3.7 Functional Group on Surface by XPS

The deconvoluted C1s and O1s spectrum were shown in Figure 3.25a. There are five separated peaks in OTE C1s spectra, which are located in 284.6, 285.7, 286.7, 287.9, and 289 eV respectively, corresponding to the C–C or C-H bonds (284.6 eV) [107], C=C in aromatic rings (285.7 eV) [108], epoxy C (C-O, 286.7 eV) [109], carbonyl C (C=O, 287.9 eV) [110], and carboxyl C (-COOH, 289 eV) [111]. These information indicates unsaturation, carbonyl of ketone or aldehyde type and also ester or carboxylic acid functionalities in the OTE. As for O1s spectrum, two peaks exhibited the binding energy at 533.4 and 535.7 eV, corresponding to aromatic C=O positioned [112] and the peak due to water vapor (O_2/H_2O) [113] respectively. The deconvoluted C1s and O1s spectrum were shown in Figure 3.25b. There are five separated peaks in P-OTE particle C1s spectra, which are located in 284.6, 285.1, 286.4, 287.1, and 288.6 eV respectively, corresponding to the C–C or C-H bonds (284.6 eV) [107], C=C in aromatic rings (285.1 eV) [108], epoxy C (C-O, 286.4 eV) [109], carbonyl C (C=O, 287.1 eV) [110], and carboxyl

and/or ester groups (C=O, 288.6 eV) [111]. The XPS O1s spectrum can be curve-fitted into two peak components with binding energy at 531.8 and 534.1 eV, attributable to the carbonyl group (C=O) and carboxyl group (O=C-OH) [114] respectively.

After polymerization, the C=C in aromatic rings (285.7 eV) in P-OTE particle becomes narrower and stronger than that of OTE, indicating that the establishment of the sp^2 bonding network [115]. The intensities of C-O (286.4 eV) and C-O (287.1 eV) in P-OTE particle are much smaller than that of OTE, especially the peak of C=O. It indicates that partial oxygen functionalities from OTE are reduced. It's obvious to find that the peak intensity of carboxyl C in the spectrum of P-OTE particle was much higher than that of OTE. The oxidization of the alcohol group in OTE can produce carboxyl group after polymerization.

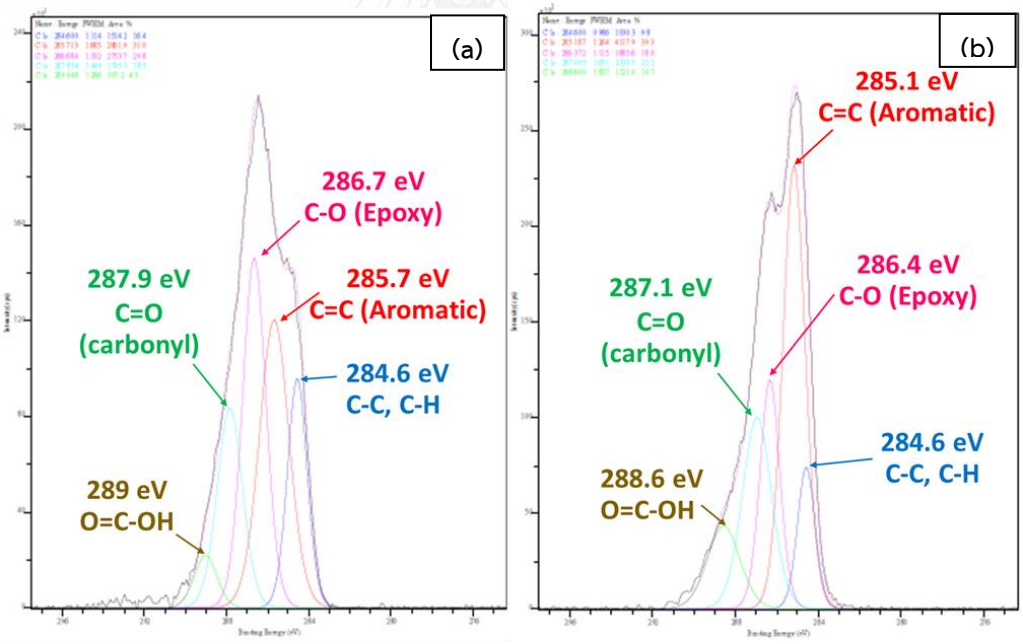

Figure 3.21 C1S XPS spectrum of OTE (a) and P-OTE particle (b)

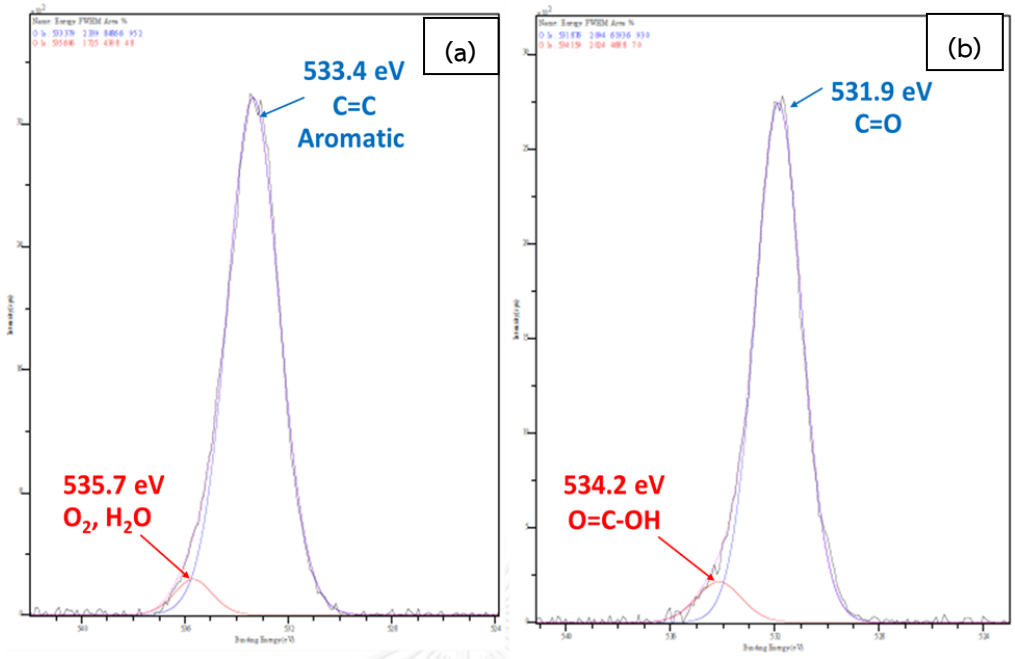

Figure 3.22 O1S XPS spectrum of OTE (a) and P-OTE particle (b)

3.8 Template Polymerization Mechanism of OTE in the presence of PEG

For mechanism of template polymerization of OTE can proceed according to two different mechanisms : type I (zip mechanism) and type II (pick up mechanism). In the case of zip mechanism, OTE which monomer units are connected to PEG template by strong interaction, such as electrostatic interaction, hydrogen bonding or even covalent bonds. In the next step, the polymerization of the aligned monomer proceed along the PEG template and polymerized polyphenol forms a complex on the PEG template. In the pick up mechanism or type II case, monomer at the beginning of the reaction are not associate with PEG template, but an some of polymerized polyphenol which starts outside the PEG template to critical length, complexation with the PEG template occurs, and the propagation proceeds along the PEG template by adding monomer molecules from the surrounding solution. After the polymerization was completed on PEG template, The self assembly of polymerized polyphenol was

occurred from dialysis system. Finally, the P-OTE particle was obtained that suspension in water system. illustrated in Figure 3.23

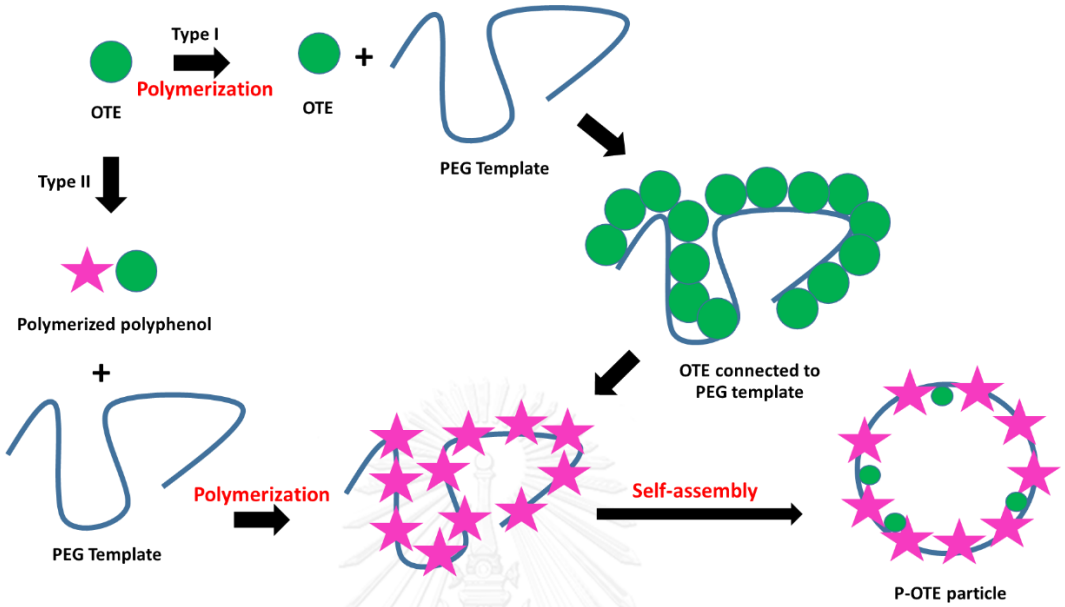

Figure 3.23 Schematic illustration of the two type mechanism on template polymerization

3.9 DPPH Radical Scavenging Activity

Antioxidant activity of the material was determined by DPPH assay [100]. DPPH radical is a stable organic free radical with an absorption band at 517 nm. It loses this absorption when accepting an electron or a free radical species, which results in a visually noticeable discoloration from purple to yellow. This assay can be used with many samples and requires a short period of time and is sensitive enough to detect radical scavenging activity of the ingredients at low concentrations.

Figure 3.24 showed the DPPH scavenging activities in a concentration-dependent manner. OTE exhibites the highest antiradical activity, followed by the P-OTE particle, whereas, as expected, the PEG and HRP showed the lowest antioxidant activity. P-OTE particles show DPPH radical scavenging activity in a dose-dependent

manner. Comparing to OTE, the P-OTE particle appeared to possess a lower antioxidant activity. Comparing to the popular antioxidant BHT, the BHT is more potent in scavenging the radical at low concentration.The strong DPPH scavenging activity of OTE can be attributed in part to the phenolic functionality and probably from catechins present in oolong tea or possibly some other polyphenols. The result implies that OTE possesses higher amount of phenol functionality than P-OTE particle. This may be related to polymerization at the phenolic functionality, further structural determination is needed.

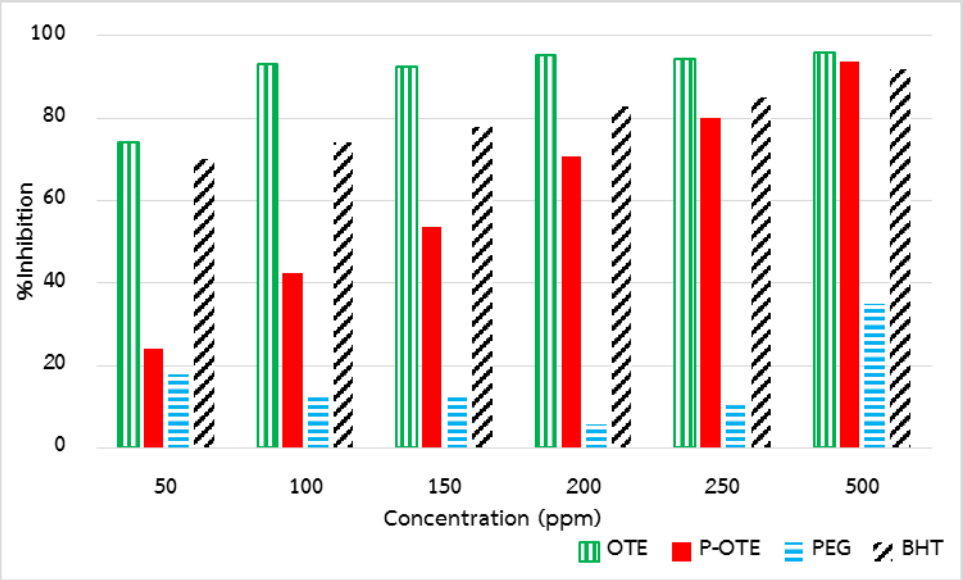

Figure 3.24 DPPH radical scavenging activity of OTE (green column), P-OTE particle (red column), HRP (yellow column), PEG (blue column), and BHT (black column)

3.10 Potentiometric Studies to determine the surface charge of P-OTE particle

The pKa values of the P-OTE solution was determined by potentiometric titration at room temperature (30 °C). P-OTE particles (1 g/l) were dissolved in DMSO: water (3:2) (v/v) and titrated with 80 ml increments of 1 M of NaOH solutions. For the titration performed between acidic and alkaline pH (pH = 2 ⟶ 12), the amount of protons removed at the surface of the P-OTE particles corresponds to the amount of

hydroxide ions. The titration curves showed a very high buffering capacity of the P-OTE particles. The pKa of P-OTE particles were approximately 2.58, which is typical of carboxylic acid dissociation (3-5); being eliminated all the phenolic group presented in the polyphenolic compounds the curve rises quickly in the pH range (7-8) of phenolic association.

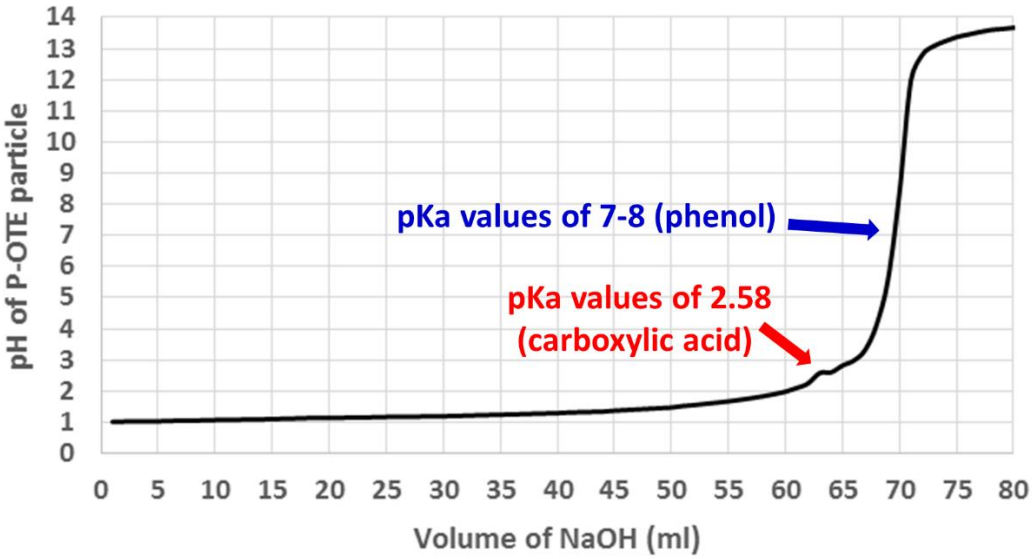

Figure 3.25 Potentiometric Titration Curves for P-OTE particles

Briefly, we have polymerized and characterized the P-OTE particle used for drug entrapment. It was observed that the P-OTE particles were spherical in shape and the size distribution was approximately 250 nm in diameter. The functional group composition of P-OTE particle showed the peck of ester, carboxylic acid, alcohol, and ether. To increase PTX solubility, improve biopharmaceutics effect, and reduce the side effects, P-OTE particle was selected to drug entrapment for PTX encapsulation.

3.11 Determination of Encapsulation Efficiency (%EE) and Loading Capacity (%Loading)

Centrifugation of the mixture of P-OTE particle allowed separation of the unloaded paclitaxel and xanthone from the P-OTE particle. The %EE of the encapsulation process and %Loading of the P-OTE particles were analyzed by indirect method which quantifying the unloaded paclitaxel and xanthone by UV-Visible spectroscopy (Table 3.5).

The process of loaded PTX and xanthone on the P-OTE particle at the drug to carrier ratio of 1:2 gave the percentage of encapsulation efficiency at 74.36 ± 0.82 and 85.38 ± 0.44, for PTX and xanthone, respectively and the loading capacity of the product was 27.10 ± 0.14 and 29.92 ± 0.23 for paclitaxel and xanthone, respectively.

The process of loaded paclitaxel and xanthone on the P-EGCG particle at the drug to carrier ratio of 1:2 gave the percentage of encapsulation efficiency at 73.28 ± 0.31 and 85.94 ± 0.63, for PTX and xanthone, respectively and the loading capacity of the product was 26.81 ± 0.11 and 30.06 ± 0.24 for paclitaxel and xanthone, respectively.

Table 3.5 %EE and %Loading of different batches of P-OTE particle prepared.

Drug to polymer ratio	P-OTE particle			
	Xanthone		PTX	
	%EE	%Loading	%EE	%Loading
1:1	73.90	42.50	63.38	38.80
1:2	85.38	29.92	74.36	27.10
1:3	89.60	23.00	76.76	20.38
1:4	89.82	18.34	77.36	16.21

Table 3.6 %EE and %Loading of different batches of P-EGCG particle prepared.

Drug to polymer ratio	P-EGCG particle			
	Xanthone		PTX	
	%EE	%Loading	%EE	%Loading
1:1	74.47	42.68	62.09	38.30
1:2	85.94	30.06	73.28	26.81
1:3	91.47	23.37	74.72	19.95
1:4	92.22	18.74	76.67	16.08

3.12 Studies of Drug-Polymer Interactions of Xanthone with P-OTE particle

TGA has been used to investigate drug-polymer interactions in particles. Figure 3.26 shows the TGA thermograms for P-OTE particle, pure xanthone, and xanthone-loaded P-OTE particles. The results of P-OTE particle (Figure 3.28, red line) showed a two degradation steps at 110.4 ^{0}C and 404.8 ^{0}C, respectively. Pure xanthone (yellow line) possesses an endothermic peak corresponding to a melting point of 335.8 °C, which indicates its crystalline nature. In the thermogram of xanthone loaded P-OTE particle (red line), the small endothermic peak at 130.6 ^{0}C followed by a broad endothermic peak at 395.6 ^{0}C, were observed. The shift of endothermic melting peaks from the two precursor materials indicates interaction between OTE and xanthone. This implies stability of the complexes. The TGA profile of the xanthon-loaded O-OTE shows a shoulder peak at around 350 ^{0}C corresponding to the melting temperature of xanthone material. Nevertheless, the main peak of the P-OTE at 404.8 ^{0}C has also been shifted to 395.6 ^{0}C upon the xanthone loading. Therefore, it is likely that the P-OTE matrix interacts with the loaded xanthone. However, there probably are some crystalline form of xanthone in the particles. In conclusion, the loaded xanthone in the P-OTE particle was likely to have a good molecular interaction with the P-OTE particle matrix, so that the endothermic characteristic peak at 404.8 ^{0}C shifted to 395.6

^{0}C with some broadening, some xanthone also stays as crystalline form in the particles so that the shoulder peak at 350 ^{0}C can be observed as well.

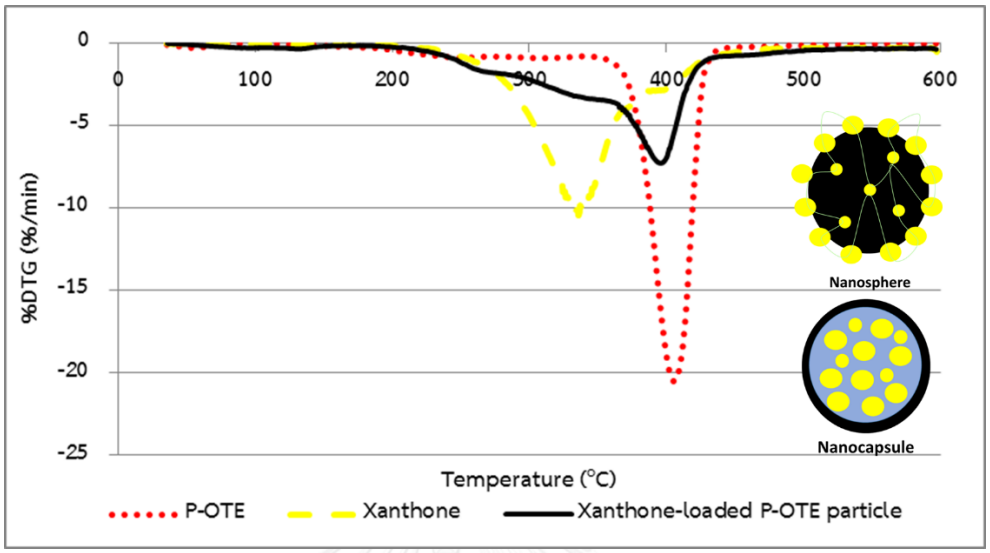

Figure 3.26 TGA thermatogram the exothermic and endothermic peck of a) P-OTE particle (red line) b) xanthone (yellow line), and c) xanthone loaded P-OTE particle (black line)

3.13 *In vitro* Anti-cancer Studies

The results show dose-dependent cytotoxicity with the IC_{50} values of OTE, EGCG, P-OTE particle, P-EGCG particle, xanthone, and PTX are 58, 29, >100, 5, 12, and 0.18 µg/l respectively. Interestingly the P-EGCG particles show low IC_{50} value. The IC_{50} value of P-OTE particle is quite high, indicating not very effective anti-cancer activity from this particle alone.

A549 cell line was used in this study as the main model to determine the anticancer activity of PTX, either free or incorporated in the P-OTE particle and P-EGCG particle. It is shown in Figure 3.27, PTX-loaded P-OTE particle and PTX-loaded P-EGCG particle show significantly higher cytotoxic effect (low viability%) as compared to the free PTX and the two blank particles. More than 50% of cells were killed when the

PTX-loaded P-OTE particle were used at the PTX concentration of <0.007 μg/l which correspond to the concentration of particles of <0.02 μg/l. This indicates effective anti-cancer action even at the very low dose of paclitaxel. In facts, at the P-EGCG particle concentration of 5 μg/l and no PTX, more than 50% cancer cells could be killed. However, the use of P-OTE particle and xanthone produced no benefitial action on the anti-cancer activity of xanthone, i.e., approximately same concentration of xanthone was needed to kill the cancer cells even when the drug was loaded into either the P-EGCG or P-OTE particles.

Table 3.7 Summarized IC_{50} value of the samples in A549 lung cancer cells

Content	IC_{50} (μg/l) of A549 Lung Cancer Cells			
	Unencapsulated		Encapsulated	
	Polymer	Drug	Polymer	Drug
OTE	-	58	-	-
EGCG	-	29	-	-
P-OTE particle	>100	-	-	-
EGCG particle	5	-	-	-
Xanthone	-	12	-	-
PTX	-	0.18	-	-
Xanthone mixed OTE	-	52 (OTE) and 13.67 (Xanthone)	-	-
Xanthone mixed EGCG	-	7 (EGCG) and 2.6 (Xanthone)	-	-

Content	IC_{50} (μg/l) of A549 Lung Cancer Cells			
	Unencapsulated		Encapsulated	
	Polymer	Drug	Polymer	Drug
Xanthone-loaded P-OTE particle	-	-	35 (P-OTE particle)	14.95 (Xanthone)
Xanthone-loaded EGCG particle	-	-	3.5 (EGCG particle)	1.5 (Xanthone)
PTX mixed OTE	-	<0.02 (OTE) and <0.007 (PTX)	-	-
PTX mixed EGCG	-	<0.02 (EGCG) and <0.007 (PTX)	-	-
PTX-loaded P-OTE particle	-	-	<0.02 (P-OTE particle)	<0.007 (PTX)
PTX-loaded EGCG particle	-	-	<0.02 (EGCG particle)	<0.007 (PTX)

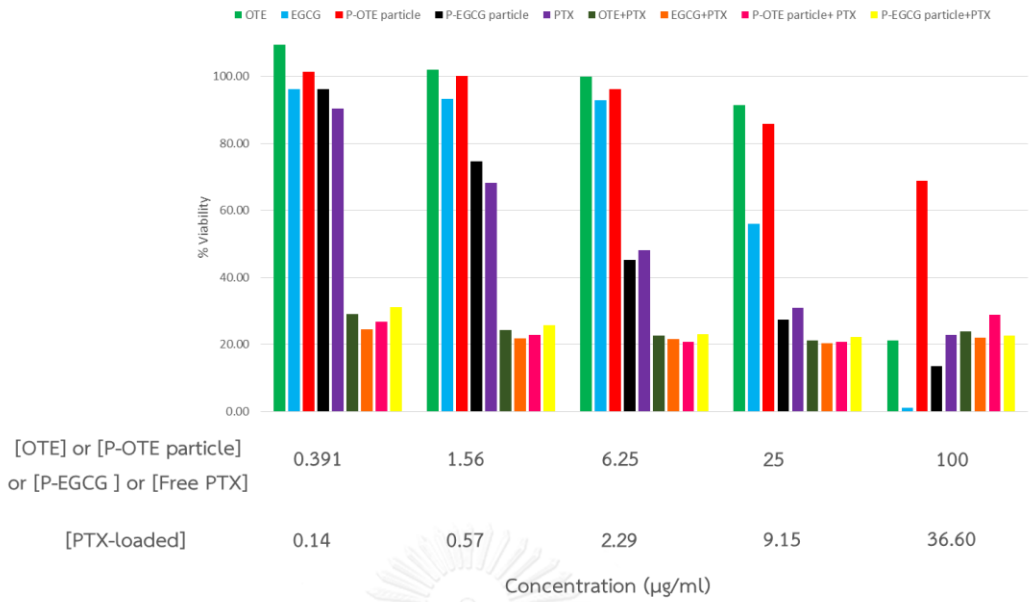

Figure 3.27 Cell viability of A549 cell with OTE (green column), EGCG (blue column), P-OTE particle (red column), PTX (violet column), OTE + PTX (black column), EGCG + PTX (orange column), P-OTE particle+ PTX (pink column), and EGCG + PTX (yellow column)

CHAPTER IV

CONCLUSION

The OTE could be successfully extracted from dried oolong tea leaves. The yield of OTE was 22.5% regarding the weight of oolong tea leaves. The major component in the OTE was EGCG at 24.48% w/w. We have successfully fabricated the P-OTE particles by enzymatic template polymerization of the OTE and the yield of the particle synthesis was 26.5%. The particle dispersed well in water and the dispersion stability increased as pH of water decreased. The particle completely soluble in DMSO and DMF. The particle exhibited spherical morphology and particle size around 250 ± 40 nm. The particle possessed UV absorption around 210 nm to 350 nm and strongly emitted light around 300-400 nm when excited at 274 nm. The addition of PEG played an important role in the crystallinity of the particles, which PEG accounts for 21% (w/w) in the particles. The functional group of P-OTE particle consisted of phenol, carboxylic acid, ester, ether, and aromatic. The particle have 2 pKa values of 2.58 (carboxylic acid) and 7-8 (phenol). The particle showed DPPH radical scavenging activity in a dose-dependent manner. Loading of PTX and xanthone on the P-OTE particles at the drug to carrier ratio of 1:2 gave high encapsulation efficiency of 74.36 ± 0.82% at the loading capacity of 27.10 ± 0.14 for PTX, and gave high encapsulation efficiency of 85.38 ± 0.44 at the drug loading capacity of 29.92 ± 0.23 for xanthone, respectively. The drug incorporation into particle nanospheres was both the crystalline and the amorphous form of xanthone in the P-OTE particle. The *in vitro* cytotoxicity also showed that PTX-loaded particles were more cytotoxic to A549 cancer cell line than the free PTX and the blank particles. However, the xanthone-loaded particles produced no beneficial action on the anti-cancer activity to xanthone, i.e., no increase anticancer activity was observed for the xanthone-loaded P-OTE as compared to the blank P-OTE particles. High encapsulation efficiency, small particle size, good water, and improved anticancer

activity make P-OTE particle as a potential drug delivery system for further development for *in vivo* studies.

REFERENCES

[1] Siegel, R., Naishadham, D., and Jemal, A. Cancer statistics, 2012. CA: A Cancer Journal For Clinicians 62(1) (2012): 10-29.

[2] Wood, C.G. Multimodal Approaches in the Management of Locally Advanced and Metastatic Renal Cell Carcinoma: Combining Surgery and Systemic Therapies to Improve Patient Outcome. Clinical Cancer Research 13(2) (2007): 697s-702s.

[3] Randhawa, M.A. and Alghamdi, M.S. Anticancer activity of Nigella sativa (black seed)—a review. The American Journal of Chinese Medicine 39(06) (2011): 1075-1091.

[4] Nevozhay, D., Kańska, U., Budzyńska, R., and Boratyński, J. [Current status of research on conjugates and related drug delivery systems in the treatment of cancer and other diseases]. Postepy higieny i medycyny doswiadczalnej (Online) 61 (2006): 350-360.

[5] Kullmann, F., et al. Cetuximab plus gemcitabine/oxaliplatin (GEMOXCET) in first-line metastatic pancreatic cancer: a multicentre phase II study. British Journal of Cancer 100(7) (2009): 1032-1036.

[6] Wang, Z., et al. Pancreatic cancer: understanding and overcoming chemoresistance. Nature Reviews Gastroenterology And Hepatology 8(1) (2011): 27-33.

[7] Wani, M.C., Taylor, H.L., Wall, M.E., Coggon, P., and McPhail, A.T. Plant antitumor agents. VI. Isolation and structure of taxol, a novel antileukemic and antitumor agent from Taxus brevifolia. Journal of The American Chemical Society 93(9) (1971): 2325-2327.

[8] Wall, M.E. and Wani, M.C. Camptothecin and taxol: discovery to clinic—thirteenth Bruce F. Cain Memorial Award Lecture. Cancer Research 55(4) (1995): 753-760.

[9] Rowinsky, E.K., Cazenave, L.A., and Donehower, R.C. Taxol: a novel investigational antimicrotubule agent. Journal of The National Cancer Institute 82(15) (1990): 1247-1259.

[10] Gelderblom, H., Verweij, J., Nooter, K., and Sparreboom, A. Cremophor EL: the drawbacks and advantages of vehicle selection for drug formulation. European Journal of Cancer 37(13) (2001): 1590-1598.

[11] Aquilina, J.W., Lipsky, J.J., and Bostwick, D.G. Androgen deprivation as a strategy for prostate cancer chemoprevention. Journal of The National Cancer Institute 89(10) (1997): 689-696.

[12] Suksamrarn, S., Suwannapoch, N., Ratananukul, P., Aroonlerk, N., and Suksamrarn, A. Xanthones from the Green Fruit Hulls of Garcinia m angostana. Journal of Natural Products 65(5) (2002): 761-763.

[13] Chairungsrilerd, N., Takeuchi, K., Ohizumi, Y., Nozoe, S., and Ohta, T. Mangostanol, a prenyl xanthone from Garcinia mangostana. Phytochemistry 43(5) (1996): 1099-1102.

[14] Oloff, S., Mailman, R.B., and Tropsha, A. Application of validated QSAR models of D1 dopaminergic antagonists for database mining. Journal of Medicinal Chemistry 48(23) (2005): 7322-7332.

[15] Santana, L., Uriarte, E., González-Díaz, H., Zagotto, G., Soto-Otero, R., and Méndez-Álvarez, E. A QSAR model for in silico screening of MAO-A inhibitors. Prediction, synthesis, and biological assay of novel coumarins. Journal of Medicinal Chemistry 49(3) (2006): 1149-1156.

[16] Meneses-Marcel, A., et al. A linear discrimination analysis based virtual screening of trichomonacidal lead-like compounds: outcomes of in silico studies supported by experimental results. Bioorganic & Medicinal Chemistry Letters 15(17) (2005): 3838-3843.

[17] Alam, S. and Khan, F. QSAR and docking studies on xanthone derivatives for anticancer activity targeting DNA topoisomerase IIα. Drug Design, Development and Therapy 8 (2014): 183.

[18] Jung, H.-A., Su, B.-N., Keller, W.J., Mehta, R.G., and Kinghorn, A.D. Antioxidant xanthones from the pericarp of Garcinia mangostana (Mangosteen). Journal of Agricultural and Food Chemistry 54(6) (2006): 2077-2082.

[19] Cheng, J.-H., Huang, A.-M., Hour, T.-C., Yang, S.-C., Pu, Y.-S., and Lin, C.-N. Antioxidant xanthone derivatives induce cell cycle arrest and apoptosis and enhance cell death induced by cisplatin in NTUB1 cells associated with ROS. European Journal of Medicinal Chemistry 46(4) (2011): 1222-1231.

[20] Li, L., et al. Pharmacokinetics of α-mangostin in rats after intravenous and oral application. Molecular Nutrition & Food Research 55(S1) (2011): S67-S74.

[21] Suri, S.S., Fenniri, H., and Singh, B. Nanotechnology-based drug delivery systems. Journal of Occupational Medicine and Toxicology 2(1) (2007): 1.

[22] Aumelas, A., Serrero, A., Durand, A., Dellacherie, E., and Leonard, M. Nanoparticles of hydrophobically modified dextrans as potential drug carrier systems. Colloids and Surfaces B: Biointerfaces 59(1) (2007): 74-80.

[23] Duncan, R. The dawning era of polymer therapeutics. Nature Reviews Drug Discovery 2(5) (2003): 347-360.

[24] Green, J.J., Chiu, E., Leshchiner, E.S., Shi, J., Langer, R., and Anderson, D.G. Electrostatic ligand coatings of nanoparticles enable ligand-specific gene delivery to human primary cells. Nano Letters 7(4) (2007): 874-879.

[25] Rivera, E. Liposomal anthracyclines in metastatic breast cancer: Clinical Update. The oncologist 8(Supplement 2) (2003): 3-9.

[26] Yong, K.-T., et al. Quantum rod bioconjugates as targeted probes for confocal and two-photon fluorescence imaging of cancer cells. Nano Letters 7(3) (2007): 761-765.

[27] Yan, F. and Kopelman, R. The embedding of meta-tetra (hydroxyphenyl)-chlorin into silica nanoparticle platforms for photodynamic therapy and their singlet oxygen production and pH-dependent optical properties. Photochemistry and Photobiology 78(6) (2003): 587-591.

[28] Martin, F., et al. Acute toxicity of intravenously administered microfabricated silicon dioxide drug delivery particles in mice. Drugs in R & D 6(2) (2005): 71-81.

[29] Peng, J., et al. An antisense oligonucleotide carrier based on amino silica nanoparticles for antisense inhibition of cancer cells. Nanomedicine: Nanotechnology, Biology and Medicine 2(2) (2006): 113-120.

[30] Oyewumi, M.O. and Mumper, R.J. Engineering tumor-targeted gadolinium hexanedione nanoparticles for potential application in neutron capture therapy. Bioconjugate Chemistry 13(6) (2002): 1328-1335.

[31] Davis, M.E. and Shin, D.M. Nanoparticle therapeutics: an emerging treatment modality for cancer. Nature Reviews Drug Discovery 7(9) (2008): 771-782.

[32] Zhang, L., Pornpattananangkul, D., Hu, C.-M., and Huang, C.-M. Development of nanoparticles for antimicrobial drug delivery. Current Medicinal Chemistry 17(6) (2010): 585-594.

[33] Matsumura, Y. and Maeda, H. A new concept for macromolecular therapeutics in cancer chemotherapy: mechanism of tumoritropic accumulation of proteins and the antitumor agent smancs. Cancer Research 46(12 Part 1) (1986): 6387-6392.

[34] Wilczewska, A.Z., Niemirowicz, K., Markiewicz, K.H., and Car, H. Nanoparticles as drug delivery systems. Pharmacological Reports 64(5) (2012): 1020-1037.

[35] Newman, D.J. and Cragg, G.M. Natural products as sources of new drugs over the 30 years from 1981 to 2010. Journal of Natural Products 75(3) (2012): 311-335.

[36] Lin, J.K. and Lin-Shiau, S.Y. Mechanisms of hypolipidemic and anti-obesity effects of tea and tea polyphenols. Molecular Nutrition & Food Research 50(2) (2006): 211-217.

[37] Kavanagh, K.T., et al. Green tea extracts decrease carcinogen-induced mammary tumor burden in rats and rate of breast cancer cell proliferation in culture. Journal of Cellular Biochemistry 82(3) (2001): 387-398.

[38] Sueoka, N., et al. A New Function of Green Tea: Prevention of Lifestyle-related Diseases. Annals of the New York Academy of Sciences 928(1) (2001): 274-280.

[39] Lecumberri, E., Dupertuis, Y.M., Miralbell, R., and Pichard, C. Green tea polyphenol epigallocatechin-3-gallate (EGCG) as adjuvant in cancer therapy. Clinical nutrition 32(6) (2013): 894-903.

[40] Osada, K., Takahashi, M., Hoshina, S., Nakamura, M., Nakamura, S., and Sugano, M. Tea catechins inhibit cholesterol oxidation accompanying oxidation of low density lipoprotein in vitro. Comparative Biochemistry and Physiology Part C: Toxicology & Pharmacology 128(2) (2001): 153-164.

[41] Albini, A., Tosetti, F., Benelli, R., and Noonan, D.M. Tumor inflammatory angiogenesis and its chemoprevention. Cancer Research 65(23) (2005): 10637-10641.

[42] Sartippour, M., Shao, Z., and Heber, D. Green tea inhibits vascular endothelial growth factor (VEGF) induction in human breast cancer cells.(Abstracts). Alternative Medicine Review 7(5) (2002): 429-430.

[43] Weber, J.M., Ruzindana-Umunyana, A., Imbeault, L., and Sircar, S. Inhibition of adenovirus infection and adenain by green tea catechins. Antiviral Research 58(2) (2003): 167-173.

[44] Weinreb, O., Mandel, S., Amit, T., and Youdim, M.B. Neurological mechanisms of green tea polyphenols in Alzheimer's and Parkinson's diseases. The Journal of Nutritional Biochemistry 15(9) (2004): 506-516.

[45] Haqqi, T.M., et al. Prevention of collagen-induced arthritis in mice by a polyphenolic fraction from green tea. Proceedings of the National Academy of Sciences 96(8) (1999): 4524-4529.

[46] Raederstorff, D.G., Schlachter, M.F., Elste, V., and Weber, P. Effect of EGCG on lipid absorption and plasma lipid levels in rats. The Journal of Nutritional Biochemistry 14(6) (2003): 326-332.

[47] Kumar, N., Shibata, D., Helm, J., Coppola, D., and Malafa, M. Green tea polyphenols in the prevention of colon cancer. Front Biosci 12(2) (2007): 309-2.

[48] Mak, J.C. Potential role of green tea catechins in various disease therapies: progress and promise. Clinical and Experimental Pharmacology and Physiology 39(3) (2012): 265-273.

[49] Gupta, S., Saha, B., and Giri, A.K. Comparative antimutagenic and anticlastogenic effects of green tea and black tea: a review. Mutation Research/Reviews in Mutation Research 512(1) (2002): 37-65.

[50] Łuczaj, W. and Skrzydlewska, E. Antioxidative properties of black tea. Preventive Medicine 40(6) (2005): 910-918.

[51] Alcazar, A., et al. Differentiation of green, white, black, Oolong, and Pu-erh teas according to their free amino acids content. Journal of Agricultural and Food Chemistry 55(15) (2007): 5960-5965.

[52] Chen, Y.L., et al. Production, quality, and biological effects of oolong tea (Camellia sinensis). Food Reviews International 27(1) (2010): 1-15.

[53] da Silva Pinto, M. Tea: A new perspective on health benefits. Food Research International 53(2) (2013): 558-567.

[54] Khan, N. and Mukhtar, H. Tea polyphenols for health promotion. Life Sciences 81(7) (2007): 519-533.

[55] McKay, D.L. and Blumberg, J.B. The role of tea in human health: an update. Journal of the American College of Nutrition 21(1) (2002): 1-13.

[56] Wu, A.H. and Yu, M.C. Tea, hormone-related cancers and endogenous hormone levels. Molecular Nutrition & Food Research 50(2) (2006): 160-169.

[57] Harborne, J.B. and Williams, C.A. Advances in flavonoid research since 1992. Phytochemistry 55(6) (2000): 481-504.

[58] Tachibana, H., Koga, K., Fujimura, Y., and Yamada, K. A receptor for green tea polyphenol EGCG. Nature Structural & Molecular Biology 11(4) (2004).

[59] Babich, H., Zuckerbraun, H., and Weinerman, S. In vitro cytotoxicity of (–)-catechin gallate, a minor polyphenol in green tea. Toxicology Letters 171(3) (2007): 171-180.

[60] Miyata, Y., et al. Theflavins and Theasinensin A Derived from Fermented Tea Have Antihyperglycemic and Hypotriacylglycerolemic Effects in KK-Ay Mice

and Sprague–Dawley Rats. Journal of Agricultural and Food Chemistry 61(39) (2013): 9366-9372.

[61] 佐野満昭, et al. Effect of tea (Camellia sinensis L.) on lipid peroxidation in rat liver and kidney: a comparison of green and black tea feeding. Biological and Pharmaceutical Bulletin 18(7) (1995): 1006-1008.

[62] Jung, Y., et al. EGCG, a major component of green tea, inhibits tumour growth by inhibiting VEGF induction in human colon carcinoma cells. British Journal of Cancer 84(6) (2001): 844.

[63] Subramanian, N., Venkatesh, P., Ganguli, S., and Sinkar, V.P. Role of polyphenol oxidase and peroxidase in the generation of black tea theaflavins. Journal of Agricultural and Food Chemistry 47(7) (1999): 2571-2578.

[64] Vu, H.A., et al. Green tea epigallocatechin gallate exhibits anticancer effect in human pancreatic carcinoma cells via the inhibition of both focal adhesion kinase and insulin-like growth factor-I receptor. BioMed Research International 2010 (2011).

[65] Wang, H., Bian, S., and Yang, C.S. Green tea polyphenol EGCG suppresses lung cancer cell growth through upregulating miR-210 expression caused by stabilizing HIF-1α. Carcinogenesis (2011): bgr218.

[66] Du, G.-J., et al. Epigallocatechin Gallate (EGCG) is the most effective cancer chemopreventive polyphenol in green tea. Nutrients 4(11) (2012): 1679-1691.

[67] Yen, G.-C. and Chen, H.-Y. Comparison of antimutagenic effect of various tea extracts (green, oolong, pouchong, and black tea). Journal of Food Protection® 57(1) (1994): 54-58.

[68] Matsumoto, N., Kohri, T., Okushio, K., and Hara, Y. Inhibitory effects of tea catechins, black tea extract and oolong tea extract on hepatocarcinogenesis in rat. Japanese Journal of Cancer Research 87(10) (1996): 1034-1038.

[69] Yam, T., Shah, S., and Hamilton-Miller, J. Microbiological activity of whole and fractionated crude extracts of tea (Camellia sinensis), and of tea components. FEMS Microbiology Letters 152(1) (1997): 169-174.

[70] Zhang, G., Miura, Y., and Yagasaki, K. Effects of green, oolong and black teas and related components on proliferation and invasion of hepatoma cells. in Animal Cell Technology: Basic & Applied Aspects, pp. 135-139: Springer, 1999.

[71] Higdon, J.V. and Frei, B. Tea catechins and polyphenols: health effects, metabolism, and antioxidant functions. (2003).

[72] Sasaki, H., et al. Antibacterial activity of polyphenol components in oolong tea extract against Streptococcus mutans. Caries Research 38(1) (2003): 2-8.

[73] Tsai, P.H., Kan, N.B., Ho, S.C., Liu, C.C., and Lin, C.C. Effects of Oolong Tea Supplementation on Lipid Peroxidation of Athletes at Rest and Post-exhaustive Exercise. Journal of Food Science 70(9) (2005): S581-S585.

[74] Hsu, T., et al. Polyphenol-enriched oolong tea increases fecal lipid excretion. European Journal of Clinical Nutrition 60(11) (2006): 1330-1336.

[75] Dvořáková, M., Paduchova, Z., Muchova, J., Duračková, Z., and Collins, A. How does pycnogenol® influence oxidative damage to DNA and its repair ability in elderly people? Prague Med Rep 111(4) (2010): 263-271.

[76] Tu, Y.-Y., Tang, A.-B., and Watanabe, N. The theaflavin monomers inhibit the cancer cells growth in vitro. Acta Biochimica et Biophysica Sinica 36(7) (2004): 508-512.

[77] Kundu, T., Dey, S., Roy, M., Siddiqi, M., and Bhattacharya, R. Induction of apoptosis in human leukemia cells by black tea and its polyphenol theaflavin. Cancer Letters 230(1) (2005): 111-121.

[78] John, K.M., Thiruvengadam, M., Enkhtaivan, G., and Kim, D.H. Variation in major phenolic compounds and quality potential of CTC black tea elicited by Saccharomyces cercevisiae and its correlation with antioxidant potential. Industrial Crops and Products 55 (2014): 289-294.

[79] Ju, J., Lu, G., Lambert, J.D., and Yang, C.S. Inhibition of carcinogenesis by tea constituents. in Seminars in Cancer Biology, pp. 395-402: Elsevier, 2007.

[80] Korir, M., Wachira, F., Wanyoko, J., Ngure, R., and Khalid, R. The fortification of tea with sweeteners and milk and its effect on in vitro antioxidant potential

of tea product and glutathione levels in an animal model. Food Chemistry 145 (2014): 145-153.

[81] Sajilata, M., Bajaj, P.R., and Singhal, R. Tea polyphenols as nutraceuticals. Comprehensive Reviews in Food Science and Food Safety 7(3) (2008): 229-254.

[82] Pan, M.-H., Liang, Y.-C., Lin-Shiau, S.-Y., Zhu, N.-Q., Ho, C.-T., and Lin, J.-K. Induction of apoptosis by the oolong tea polyphenol theasinensin A through cytochrome c release and activation of caspase-9 and caspase-3 in human U937 cells. Journal of Agricultural and Food Chemistry 48(12) (2000): 6337-6346.

[83] Koňariková, K., Ježovičová, M., Keresteš, J., Gbelcová, H., Ďuračková, Z., and Žitňanová, I. Anticancer effect of black tea extract in human cancer cell lines. Springerplus 4(1) (2015): 1.

[84] Chen, Z., Wang, C., Chen, J., and Li, X. Biocompatible, functional spheres based on oxidative coupling assembly of green tea polyphenols. Journal of the American Chemical Society 135(11) (2013): 4179-4182.

[85] Chung, J.E., et al. Self-assembled micellar nanocomplexes comprising green tea catechin derivatives and protein drugs for cancer therapy. Nature Nanotechnology 9(11) (2014): 907-912.

[86] Ghioureliotis, M. and Nicell, J.A. Assessment of soluble products of peroxidase-catalyzed polymerization of aqueous phenol. Enzyme and Microbial Technology 25(3) (1999): 185-193.

[87] Mita, N., Tawaki, S.i., Uyama, H., and Kobayashi, S. Laccase-Catalyzed Oxidative Polymerization of Phenols. Macromolecular Bioscience 3(5) (2003): 253-257.

[88] Oguchi, T., Tawaki, S.i., Uyama, H., and Kobayashi, S. Soluble polyphenol. Macromolecular Rapid Communications 20(7) (1999): 401-403.

[89] Hsuanyu, Y. and Dunford, H.B. Oxidation of clozapine and ascorbate by myeloperoxidase. Archives of Biochemistry and Biophysics 368(2) (1999): 413-420.

[90] Oliver, S., Vittorio, O., Cirillo, G., and Boyer, C. Enhancing the therapeutic effects of polyphenols with macromolecules. Polymer Chemistry 7(8) (2016): 1529-1544.

[91] Dordick, J.S., Marletta, M.A., and Klibanov, A.M. Polymerization of phenols catalyzed by peroxidase in nonaqueous media. Biotechnology and Bioengineering 30(1) (1987): 31-36.

[92] Mita, N., Tawaki, S.-i., Uyama, H., and Kobayashi, S. Molecular Weight Control of Polyphenols by Enzymatic Copolymerization of Phenols. Polym J 33(4) (2001): 374-376.

[93] Kurisawa, M., Chung, J.E., Kim, Y.J., Uyama, H., and Kobayashi, S. Amplification of antioxidant activity and xanthine oxidase inhibition of catechin by enzymatic polymerization. Biomacromolecules 4(3) (2003): 469-471.

[94] Walde, P. and Guo, Z. Enzyme-catalyzed chemical structure-controlling template polymerization. Soft Matter 7(2) (2011): 316-331.

[95] Tan, Y.Y. and Challa, G. Template polymerization by free radical mechanisms. in Makromolekulare Chemie. Macromolecular Symposia, pp. 215-233: Wiley Online Library, 1987.

[96] Bruno, F.F., Nagarajan, R., Kumar, J., and Samuelson, L.A. Novel enzymatic polyethylene oxide-polyphenol system for ionic conductivity. Journal of Macromolecular Science, Part A 39(10) (2002): 1061-1068.

[97] Kim, Y.-J., Uyama, H., and Kobayashi, S. Regioselective synthesis of poly (phenylene) as a complex with poly (ethylene glycol) by template polymerization of phenol in water. Macromolecules 36(14) (2003): 5058-5060.

[98] Kobayashi, S., Uyama, H., Ushiwata, T., Uchiyama, T., Sugihara, J., and Kurioka, H. Enzymatic oxidative polymerization of bisphenol-a to a new class of soluble polyphenol. Macromolecular Chemistry and Physics 199(5) (1998): 777-782.

[99] Kim, Y.-J., Uyama, H., and Kobayashi, S. Enzymatic Template Polymerization of Phenol in the Presence of Water-soluble Polymers in an Aqueous Medium. Polym J 36(12) (2004): 992-998.

[100] CHEN, C.W. and HO, C.T. Antioxidant properties of polyphenols extracted from green and black teas. Journal of Food Lipids 2(1) (1995): 35-46.

[101] Aydin, R. and Pulat, M. 5-Fluorouracil encapsulated chitosan nanoparticles for pH-stimulated drug delivery: evaluation of controlled release kinetics. Journal of Nanomaterials 2012 (2012): 42.

[102] Nagarwal, R.C., Nath Singh, P., Kant, S., Maiti, P., and Pandit, J.K. Chitosan nanoparticles of 5-fluorouracil for ophthalmic delivery: characterization, in-vitro and in-vivo study. Chemical and Pharmaceutical Bulletin 59(2) (2011): 272-278.

[103] Papadimitriou, S., Bikiaris, D., Avgoustakis, K., Karavas, E., and Georgarakis, M. Chitosan nanoparticles loaded with dorzolamide and pramipexole. Carbohydrate Polymers 73(1) (2008): 44-54.

[104] Lirdprapamongkol, K., et al. Vanillin suppresses metastatic potential of human cancer cells through PI3K inhibition and decreases angiogenesis in vivo. Journal of Agricultural and Food Chemistry 57(8) (2009): 3055-3063.

[105] Ikeda, I., et al. Heat-epimerized tea catechins rich in gallocatechin gallate and catechin gallate are more effective to inhibit cholesterol absorption than tea catechins rich in epigallocatechin gallate and epicatechin gallate. Journal of Agricultural and Food Chemistry 51(25) (2003): 7303-7307.

[106] Seto, R., Nakamura, H., Nanjo, F., and Hara, Y. Preparation of epimers of tea catechins by heat treatment. Bioscience, Biotechnology, and Biochemistry 61(9) (1997): 1434-1439.

[107] Cheng, C.-H., Lehmann, J., Thies, J.E., Burton, S.D., and Engelhard, M.H. Oxidation of black carbon by biotic and abiotic processes. Organic Geochemistry 37(11) (2006): 1477-1488.

[108] Obata, S., Tanaka, H., and Saiki, K. Electrical and spectroscopic investigations on the reduction mechanism of graphene oxide. Carbon 55 (2013): 126-132.

[109] Qu, D., et al. Formation mechanism and optimization of highly luminescent N-doped graphene quantum dots. Scientific Reports 4 (2014).

[110] Ding, H., Yu, S.-B., Wei, J.-S., and Xiong, H.-M. Full-color light-emitting carbon dots with a surface-state-controlled luminescence mechanism. ACS nano 10(1) (2015): 484-491.

[111] Chen, W., Hu, C., Yang, Y., Cui, J., and Liu, Y. Rapid Synthesis of Carbon Dots by Hydrothermal Treatment of Lignin. Materials 9(3) (2016): 184.

[112] Brender, P., et al. Characterization of carbon surface chemistry by combined temperature programmed desorption with in situ X-ray photoelectron spectrometry and temperature programmed desorption with mass spectrometry analysis. Analytical Chemistry 84(5) (2012): 2147-2153.

[113] Herman, G.S., Dohnalek, Z., Ruzycki, N., and Diebold, U. Experimental investigation of the interaction of water and methanol with anatase-TiO2 (101). The Journal of Physical Chemistry B 107(12) (2003): 2788-2795.

[114] Boudou, J.-P., Paredes, J., Cuesta, A., Martınez-Alonso, A., and Tascon, J. Oxygen plasma modification of pitch-based isotropic carbon fibres. Carbon 41(1) (2003): 41-56.

[115] Abdullah, M., Zakaria, R., and Zein, S. Green tea polyphenol–reduced graphene oxide: derivatisation, reduction efficiency, reduction mechanism and cytotoxicity. RSC Advances 4(65) (2014): 34510-34518.

APPENDIX

1. Calculation the percent yield of OTE

$$\text{Yield (\%)} = \frac{\text{weight of dried OTE}}{\text{weight of dried oolong tea leaves}} \times 100 \quad \text{(Eq. 1)}$$

$$\text{Yield (\%)} = \frac{17.55}{78} \times 100$$

$$\text{Yield (\%)} = 22.5\ \%$$

2. Determination of the chemical composition of OTE by HPLC

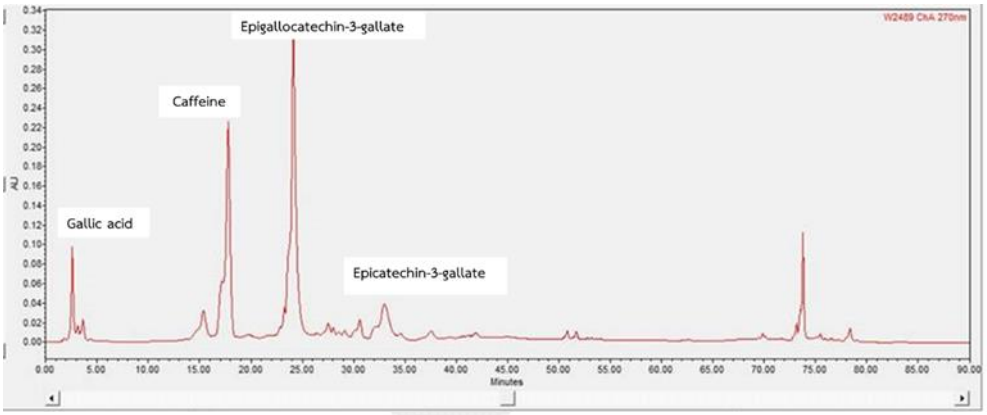

Chemicals	Calibration Curve	R^2	Chemicals amount ($mg_{chemicals}/g_{extract}$)
Gallic acid	y = 0.0081x - 0.0326	0.9991	4.241
Caffeine	y = 2.1254x + 0.0885	0.9990	34.455
EGCG	y = 0.2952x + 0.0115	0.9960	465.924
ECG	y = 0.0006x + 0.0019	0.9932	2.887

3. <u>Calculation the percent yield of P-OTE particle</u>

$$\text{Yield (\%)} = \frac{\text{weight of P-OTE particle}}{\text{weight of OTE}} \times 100 \quad \text{(Eq. 2)}$$

$$\text{Yield (\%)} = \frac{0.1431}{0.5403} \times 100$$

$$\text{Yield (\%)} = 26.5\ \%$$

4. <u>Morphological analysis of P-OTE particle</u>

4.1 TEM of P-OTE particles

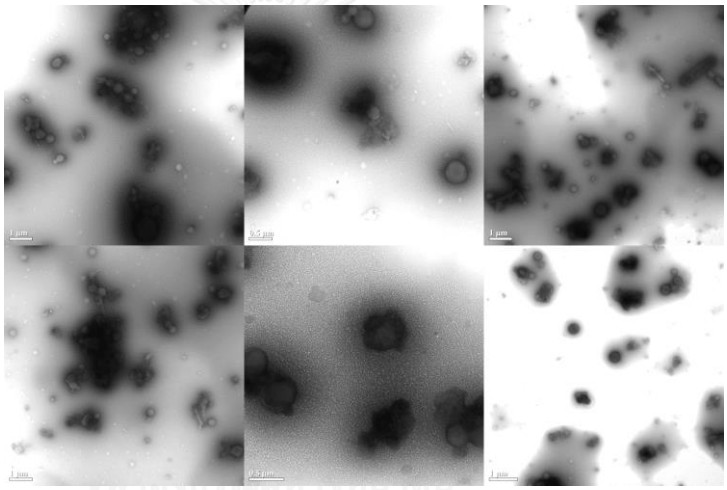

4.2 SEM of P-OTE particles

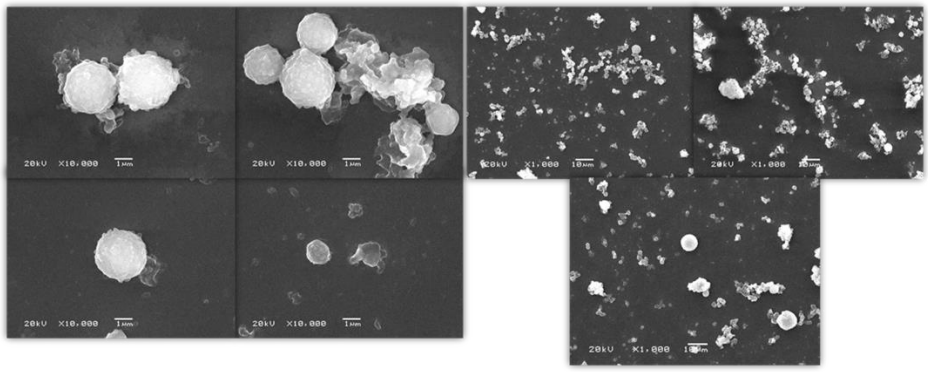

4.3 AFM of P-OTE particles

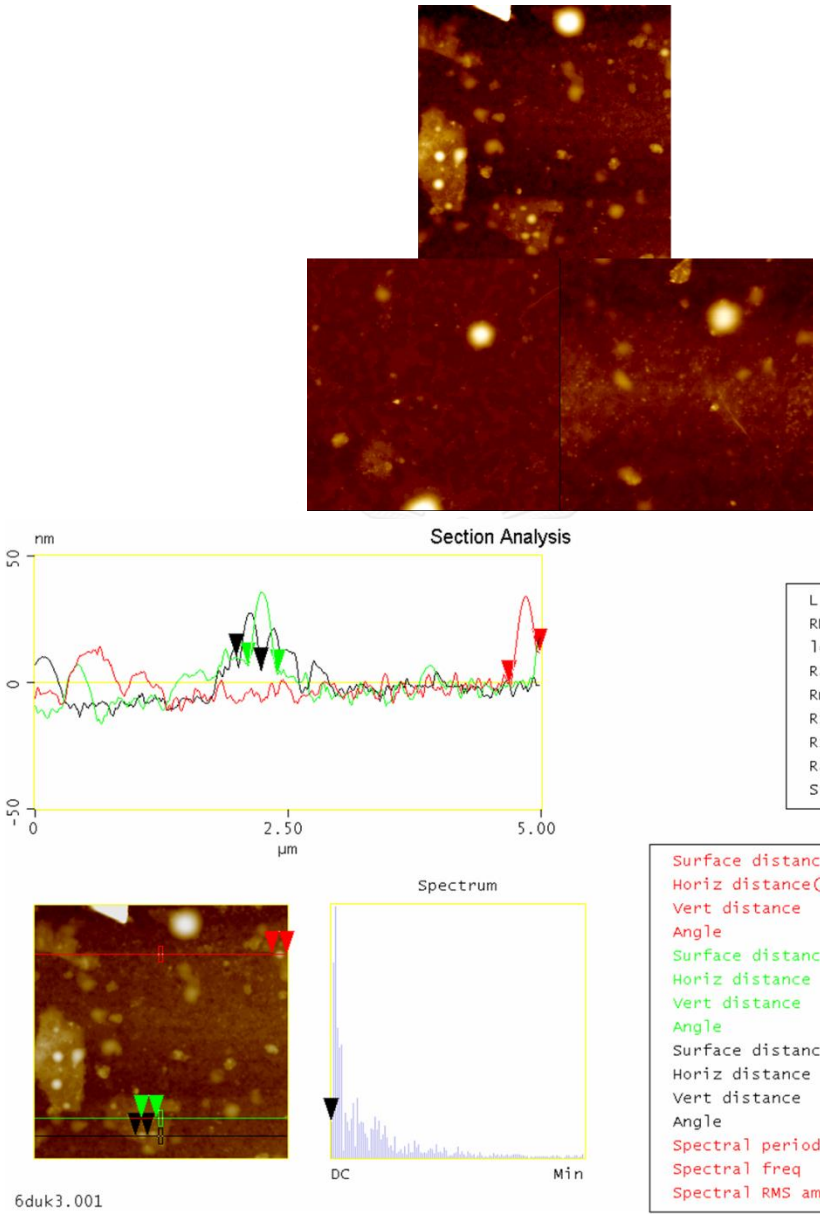

L	244.14 nm
RMS	7.963 nm
lc	DC
Ra(lc)	6.846 nm
Rmax	24.168 nm
Rz	24.125 nm
Rz Cnt	2
Radius	346.27 nm
Sigma	2.998 nm

Surface distance	310.53 nm
Horiz distance(L)	302.73 nm
Vert distance	12.644 nm
Angle	2.392 °
Surface distance	301.34 nm
Horiz distance	292.97 nm
Vert distance	2.469 nm
Angle	0.483 °
Surface distance	250.65 nm
Horiz distance	244.14 nm
Vert distance	5.460 nm
Angle	1.281 °
Spectral period	DC
Spectral freq	0 /µm
Spectral RMS amp	0.708 nm

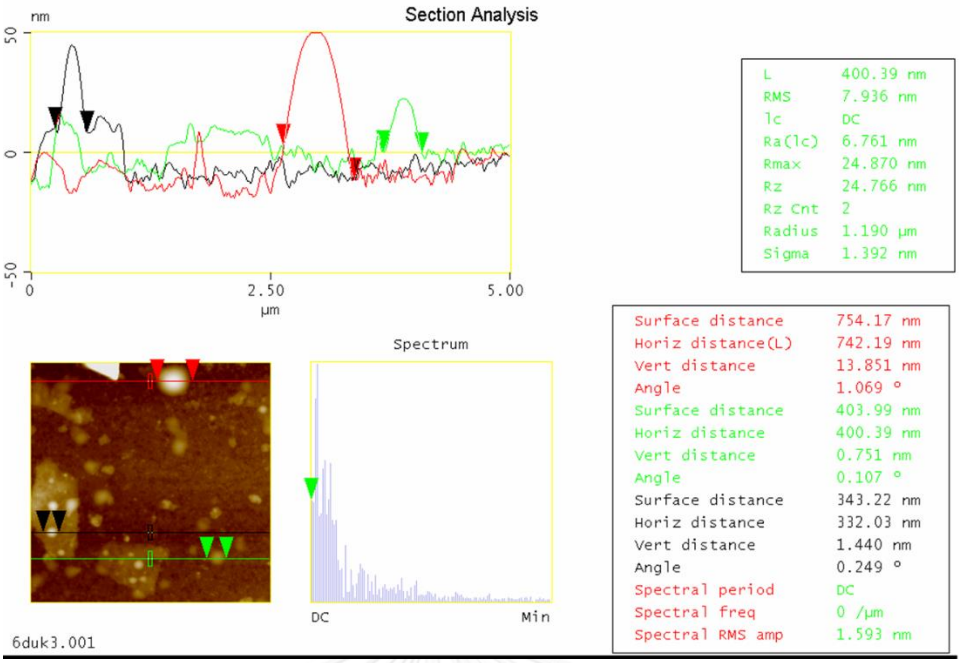

5. Thermal Properties by TGA

5.1 Thermatogram of OTE by TGA

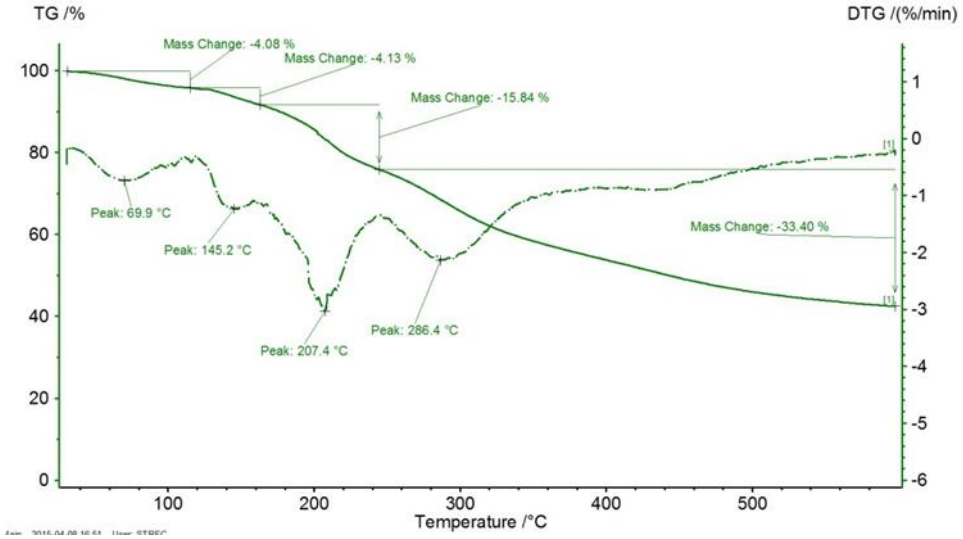

5.2 Thermatogram of HRP by TGA

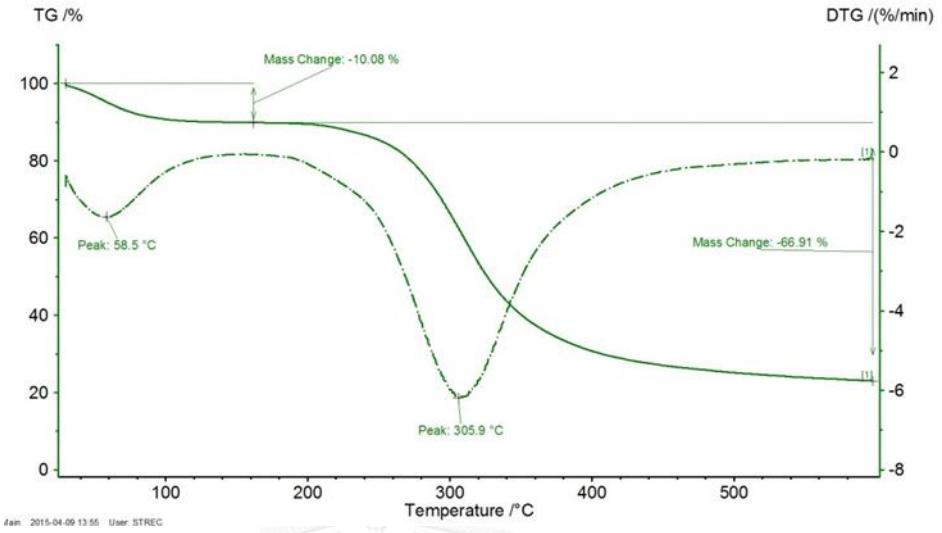

5.3 Thermatogram of PEG by TGA

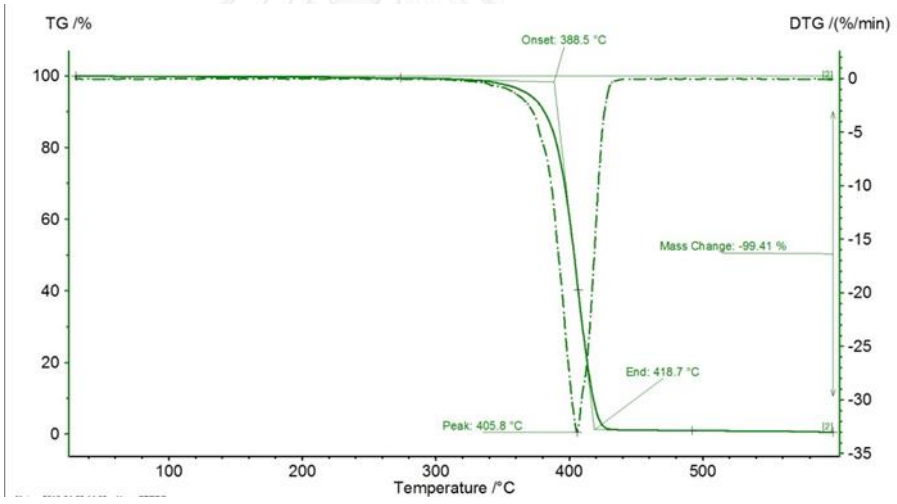

5.4 Thermatogram of P-OTE particle by TGA

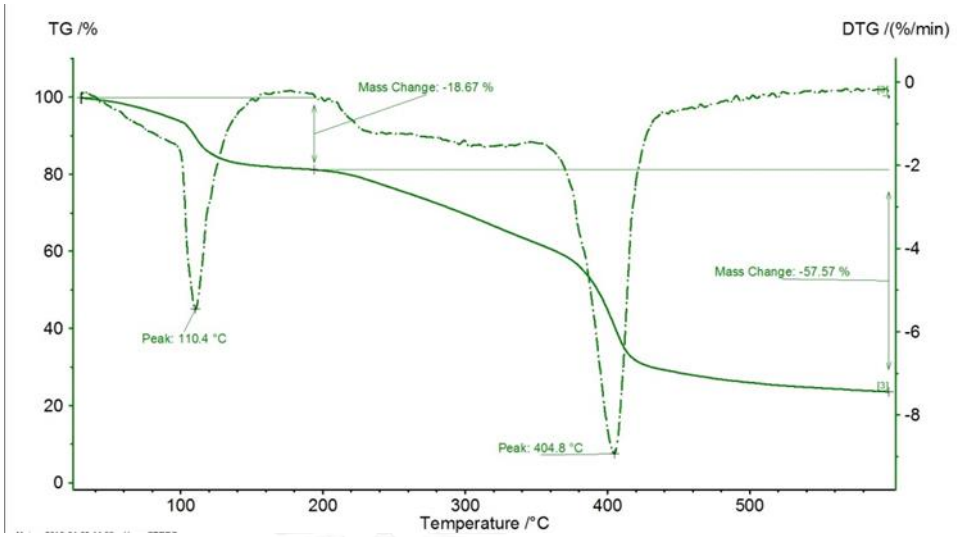

6. Thermal Properties by DSC

6.1 Thermatogram of OTE by DSC

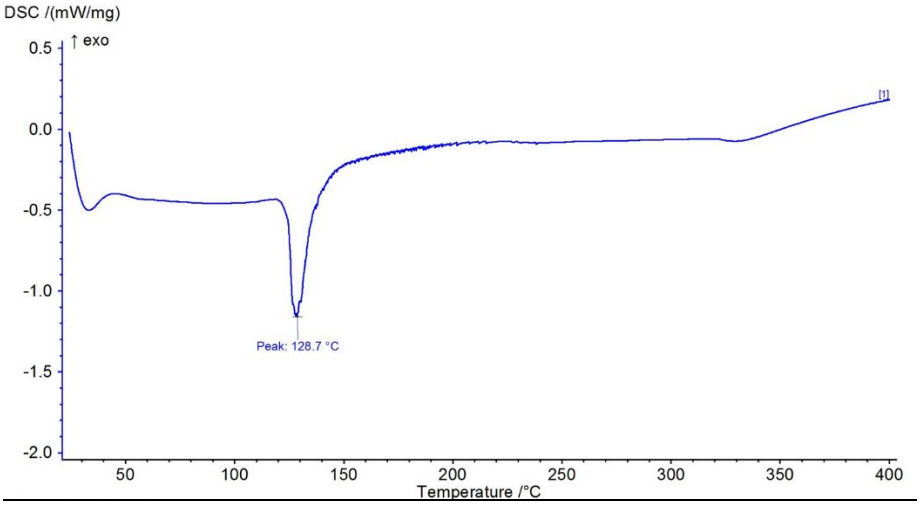

6.2 Thermatogram of HRP by DSC

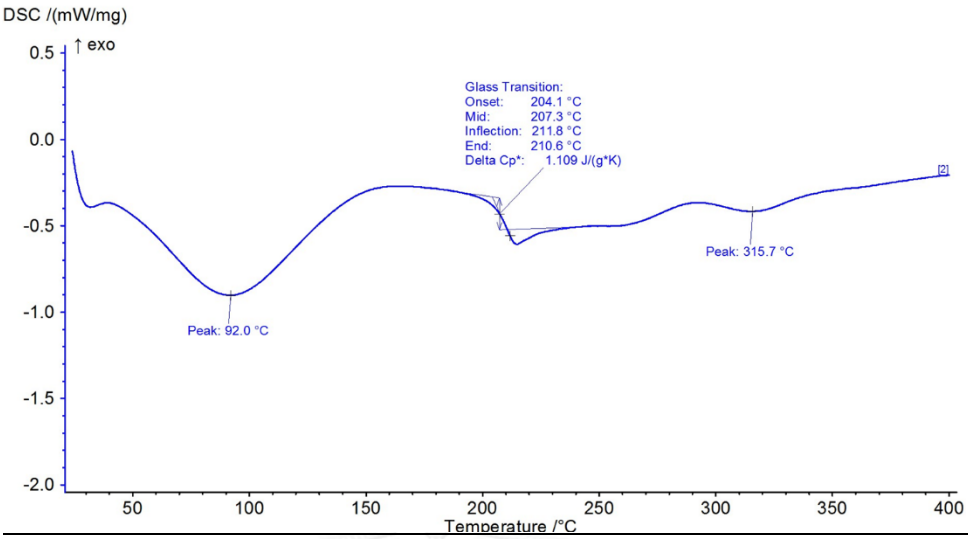

6.3 Thermatogram of PEG by DSC

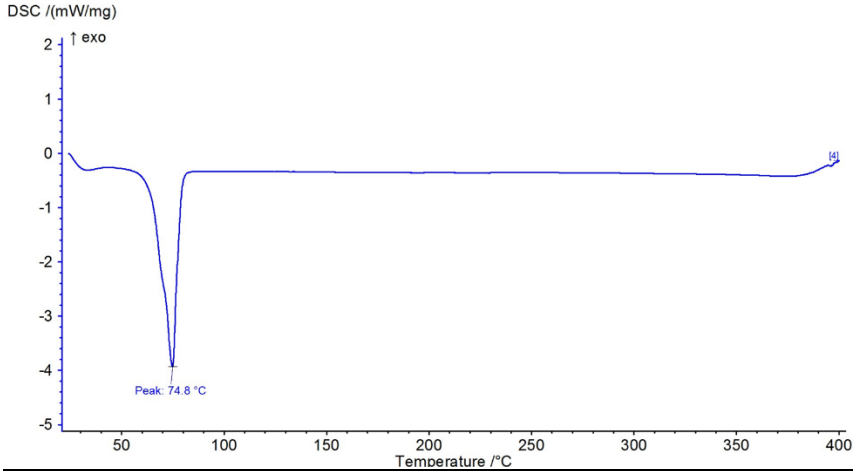

6.4 Thermatogram of P-OTE particle by DSC

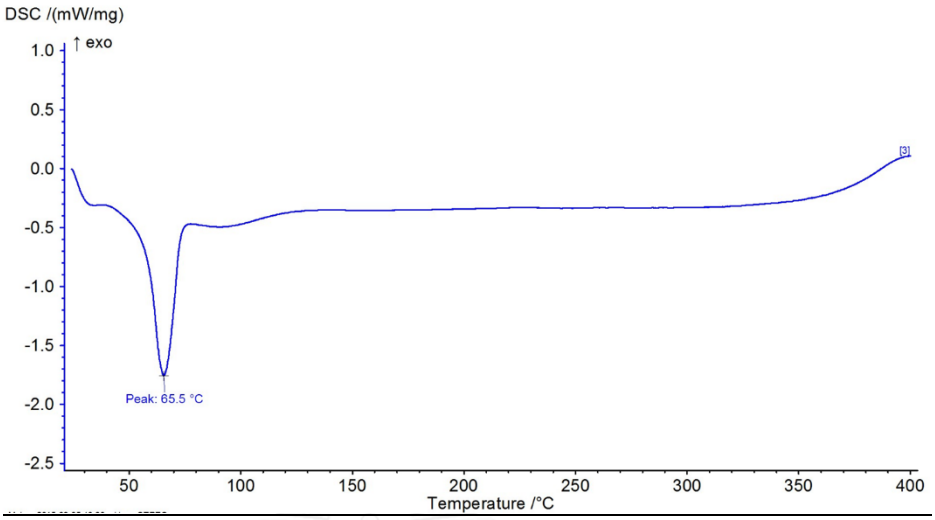

7. Powder XRD analysis

7.1 XRD patterns of OTE

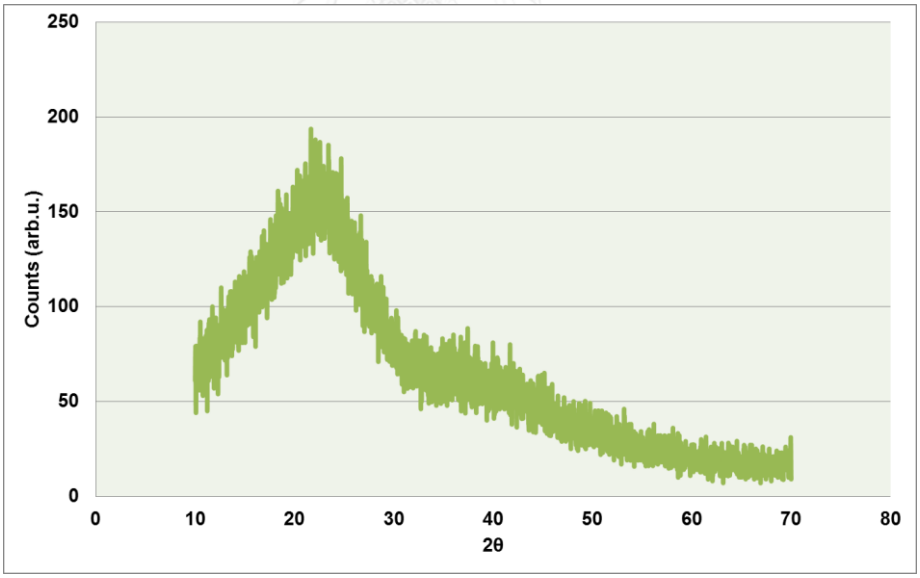

7.2 XRD patterns of HRP

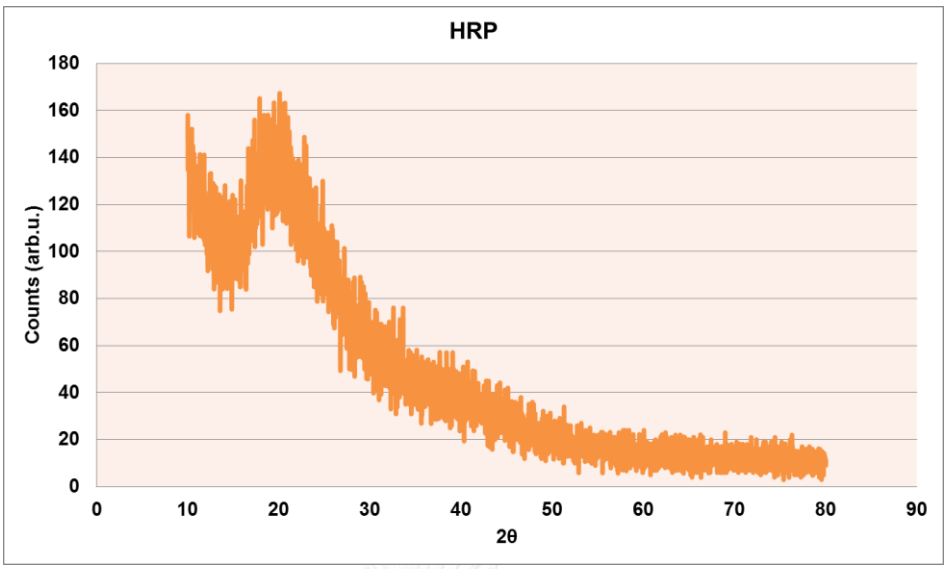

7.3 XRD patterns of PEG

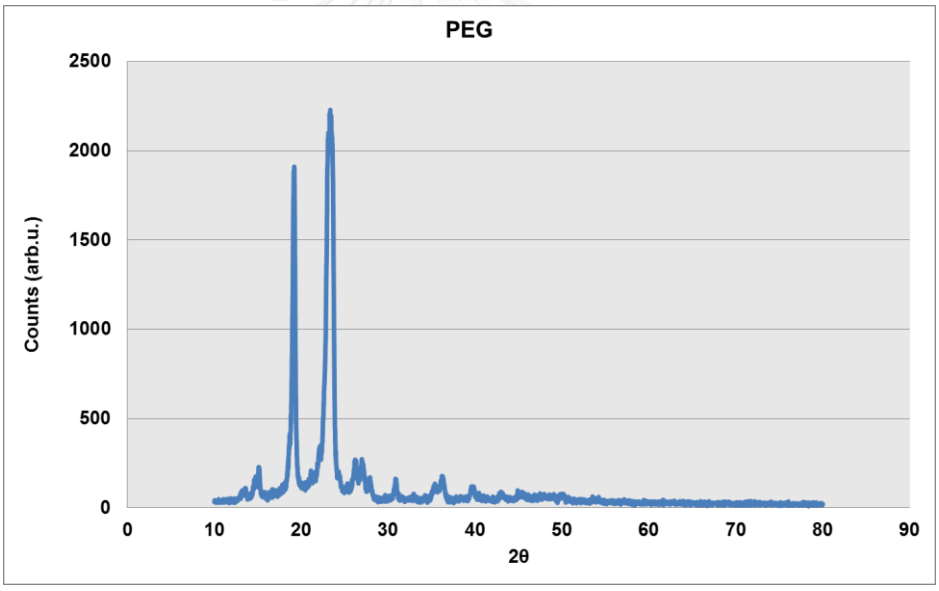

7.4 XRD patterns of P-OTE particle

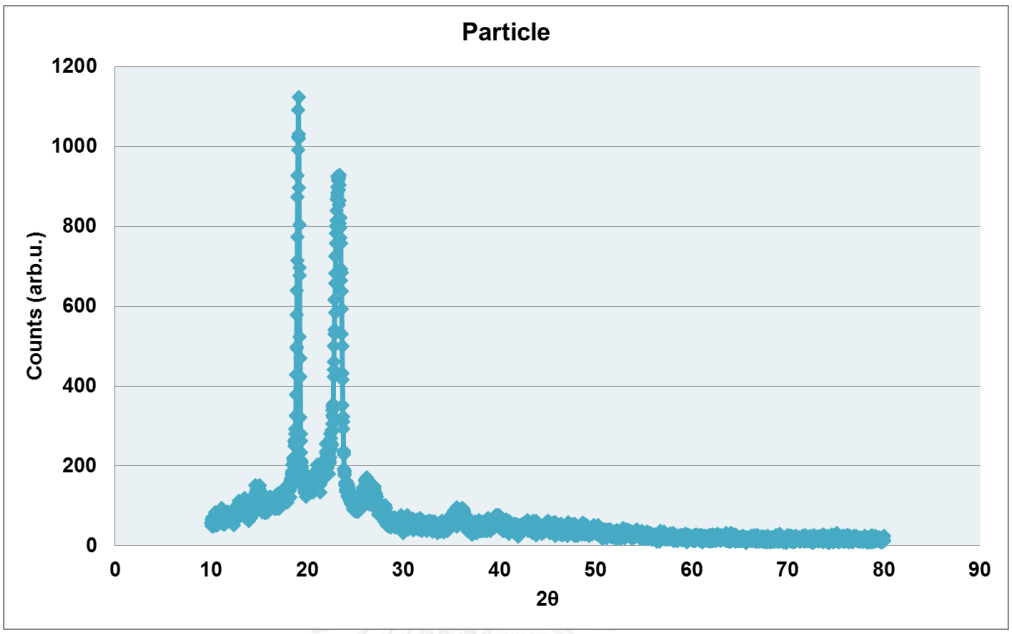

8. DPPH radical scavenging activity

8.1 Standard Calibration Curve of DPPH

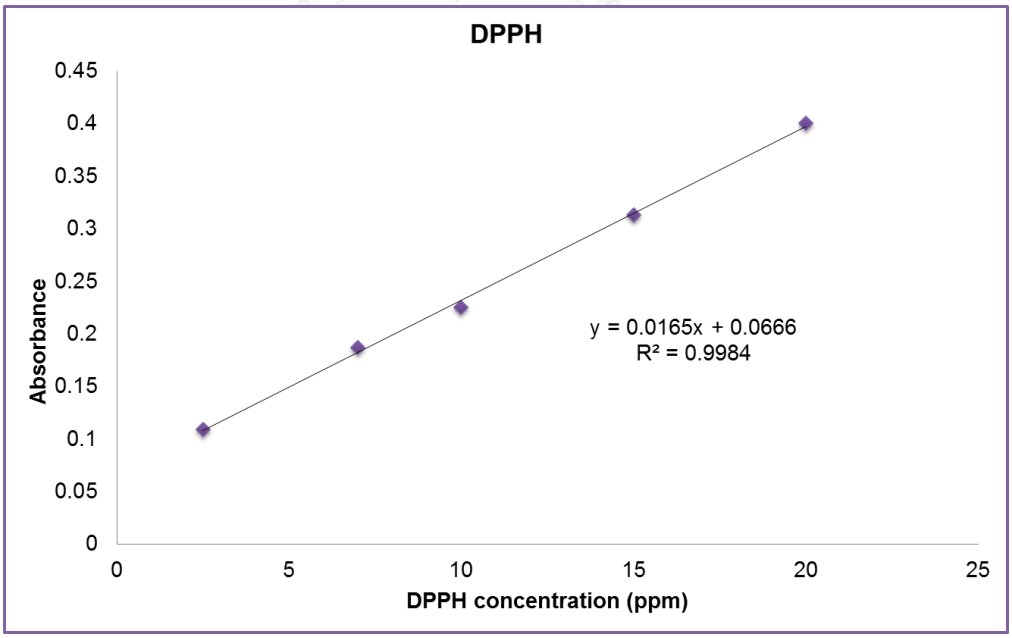

8.2 % Inhibition of BHT standard

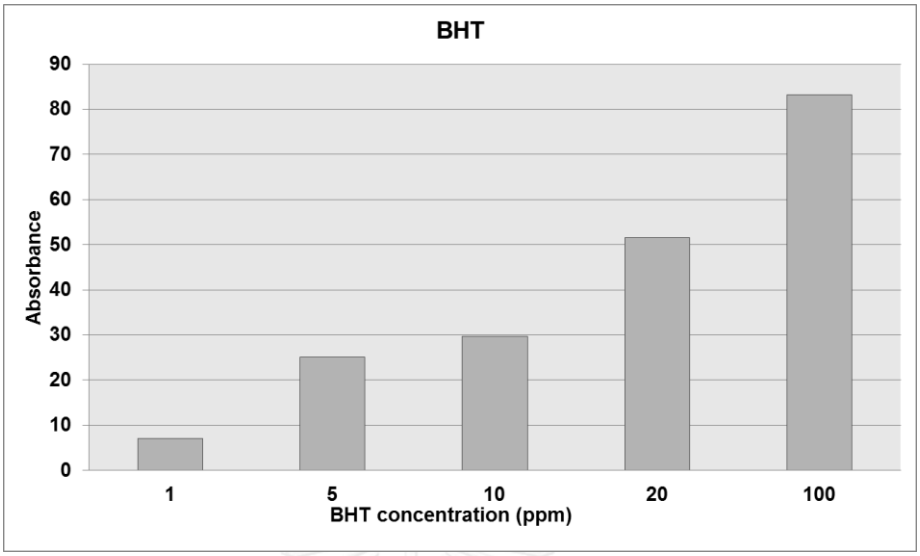

8.3 % Inhibition of OTE, HRP, PEG, and P-OTE particle

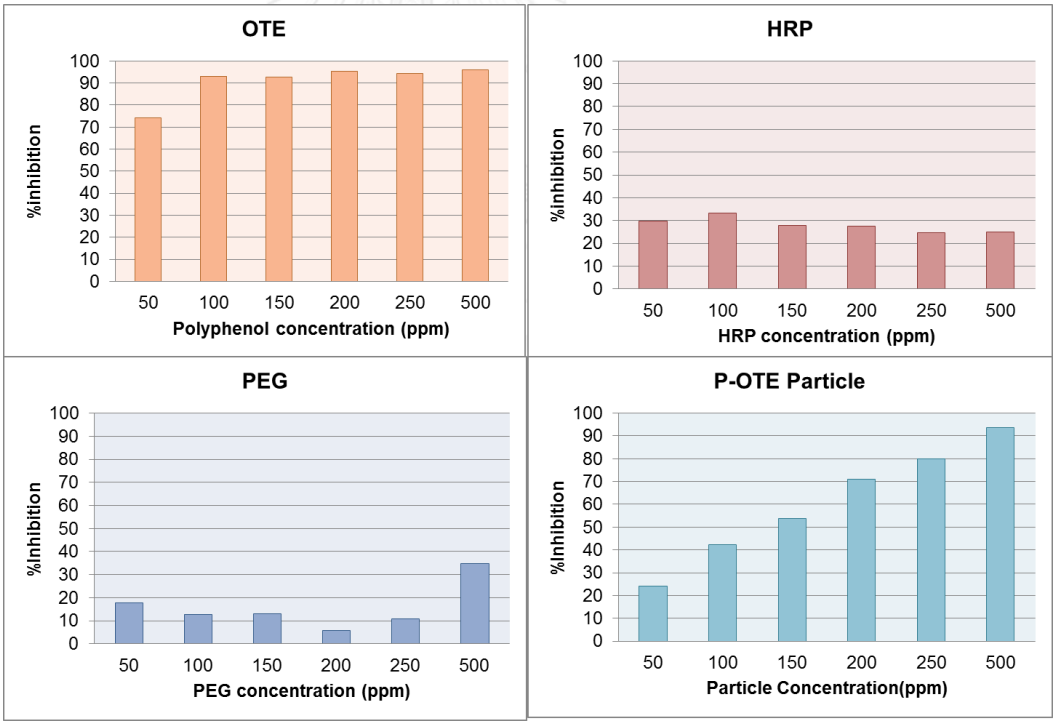

9. Determination of encapsulation efficiency (%EE) and loading capacity (%Loading)

9.1 Standard Calibration Curve of PTX

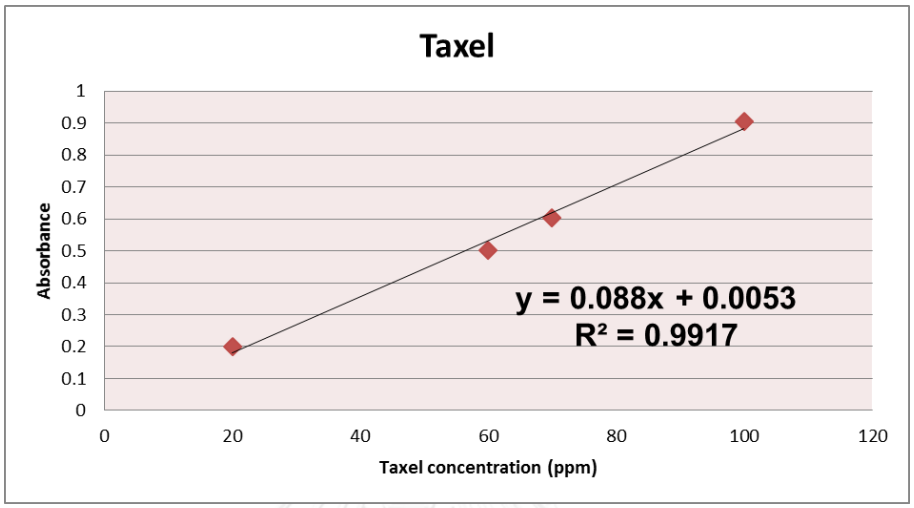

9.2 Standard Calibration Curve of Xanthone

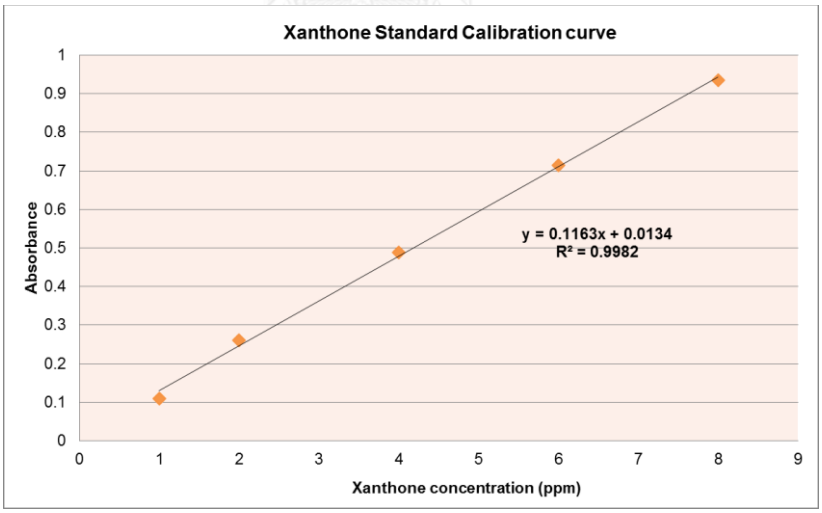

9.3 Calculation of %EE and %Loading of xanthone loaded P-OTE particle

Ratio for encapsulation		Water : 50%Ethanol						
		Absorbance				Calculation X data	Dillution fractor	Non-incooperation of Mangostin on particle
Particle	Mangostin	1	2	3	Average			
1	1	0.46	0.369	0.304	0.37766667	3.13212955	100	313.212955
2	1	1.164	0.749	0.678	0.86366667	7.310977357	12	87.73172829
3	1	0.321	0.411	0.519	0.417	3.47033534	12	41.64402408
4	1	0.313	0.313	0.302	0.30933333	2.544568644	12	30.53482373
10	1	0.301	0.237	0.251	0.263	2.146173689	12	25.75408426

Ratio for encapsution		From stock solution 6000 ppm					Final concentration (ppm)	
Particle	Mangostin	Volume of Particle(ul)	Volume of Mangostin(ul)	H2O (ul)	Ethanol (ul)	Total voloume (ul)	Particle	Mangostin
1	1	200	200	300	300	1000	1200	1200
2	1	200	100	300	400	1000	1200	600
3	1	200	66.7	300	433.3	1000	1200	400.2
4	1	200	50	300	450	1000	1200	300
10	1	200	20	300	480	1000	1200	120

Concentration from standard curve (ppm)			
Non-incooperation of Mangostin on particle	cooperation of Mangostin on particl	%EE	%Loading
313.212955	886.787045	73.9	42.4953302
87.73172829	512.2682717	85.38	29.917524
41.64402408	358.5559759	89.59	23.0056528
30.53482373	269.4651763	89.82	18.3376361
25.75408426	94.24591574	78.54	7.28191718

9.4 Calculation of %EE and %Loading of PTX loaded P-OTE particle

Ratio for encapsulation		Water : 50%Ethanol						
		Absorbance				Calculation X data	Dillution fractor	Non-incooperation of PTX on particle
Particle	PTX	1	2	3	Average			
1	1	0.392	0.391	0.393	0.392	4.394318182	100	439.4318182
2	1	0.1409	0.1442	0.137	0.1407	1.538636364	100	153.8636364
3	1	0.08739	0.088645	0.085422	0.087153	0.930147727	100	93.01477273
4	1	0.06422	0.06514	0.06582	0.06506	0.679090909	100	67.90909091
10	1	0.03741	0.03783	0.03682	0.037353333	0.364242424	100	36.42424242

Ratio for encapsution		From stock solution 6000 ppm					Final concentration (ppm)	
Particle	PTX	Volume of Particle(ul)	Volume of PTX(ul)	H2O (ul)	DMSOl (ul)	Total voloume (ul)	Particle	PTX
1	1	200	200	300	300	1000	1200	1200
2	1	200	100	300	400	1000	1200	600
3	1	200	66.7	300	433.3	1000	1200	400.2
4	1	200	50	300	450	1000	1200	300
10	1	200	20	300	480	1000	1200	120

Concentration from standard curve (ppm)			
Non-incooperation of PTX on particle	Incooperation of PTX on particle	%EE	%Loading
439.43	760.57	63.38	38.7933101
153.86	446.14	74.36	27.1021906
93.01	307.19	76.76	20.3816374
67.91	232.09	77.36	16.2063837
36.42	83.58	69.65	6.51147572

9.5 Calculation of %EE and %Loading of xanthone loaded P-EGCG particle

Ratio for encapsulation		Water : 50%Ethanol						
		Absorbance				Calculation X data	Dillution fractor	Non-incooperation of Mangostin on particle
Particle	Mangostin	1	2	3	Average			
1	1	0.3721	0.3701	0.367	0.36973333	3.063915162	100	306.3915162
2	1	0.1112	0.121	0.1023	0.1115	0.843508169	100	84.35081685
3	1	0.052	0.0531	0.0542	0.0531	0.341358555	100	34.13585555
4	1	0.0402	0.0413	0.0401	0.04053333	0.233304672	100	23.33046718

Ratio for encapsution		From stock solution 6000 ppm					Final concentration (ppm)	
Particle	Mangostin	Volume of Particle(ul)	Volume of Mangostin(ul)	H2O (ul)	Ethanol (ul)	Total voloume (ul)	Particle	Mangostin
1	1	200	200	300	300	1000	1200	1200
2	1	200	100	300	400	1000	1200	600
3	1	200	66.7	300	433.3	1000	1200	400.2
4	1	200	50	300	450	1000	1200	300

Concentration from standard curve (ppm)			
Non-incooperation of Mangostin on particle	Incooperation of Mangostin on particle	%EE	%Loading
306.3915162	893.6084838	74.47	42.6826931
84.35081685	515.6491831	85.94	30.0556307
34.13585555	366.0641445	91.47	23.3747861
23.33046718	276.6695328	92.22	18.7360494

9.6 Calculation of %EE and %Loading of PTX loaded P-EGCG particle

Ratio for encapsulation		Water : 50%Ethanol						
		Absorbance				Calculation X data	Dillution fractor	Non-incooperation of PTX on particle
Particle	PTX	1	2	3	Average			
1	1	0.408	0.403	0.406	0.405666667	4.549621212	100	454.9621212
2	1	0.1467	0.1462	0.1463	0.1464	1.603409091	100	160.3409091
3	1	0.09530	0.09452	0.09321	0.094343333	1.011856061	100	101.1856061
4	1	0.06693	0.06689	0.06687	0.066896667	0.699962121	100	69.99621212

Ratio for encapsution		From stock solution 6000 ppm					Final concentration (ppm)	
Particle	PTX	Volume of Particle(ul)	Volume of PTX(ul)	H2O (ul)	DMSOl (ul)	Total voloume (ul)	Particle	PTX
1	1	200	200	300	300	1000	1200	1200
2	1	200	100	300	400	1000	1200	600
3	1	200	66.7	300	433.3	1000	1200	400.2
4	1	200	50	300	450	1000	1200	300

Concentration from standard curve (ppm)			
Non-incooperation of PTX on particle	Incooperation of PTX on particle	%EE	%Loading
454.9621212	745.0378788	62.09	38.3045434
160.3409091	439.6590909	73.28	26.814055
101.1856061	299.0143939	74.72	19.9473998
69.99621212	230.0037879	76.67	16.0841384

10. Studies of drug-polymer interactions of Xanthone with P-OTE

10.1 Thermatogram of free xanthone

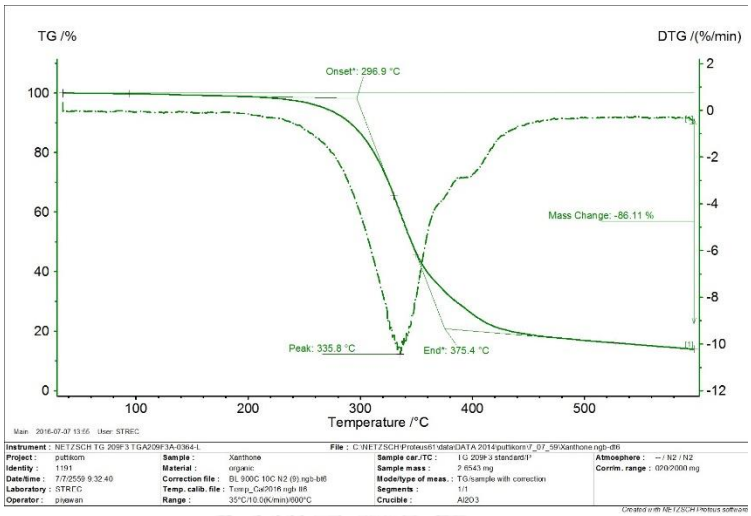

10.2 Thermatogram of xanthone loaded P-OTE particle

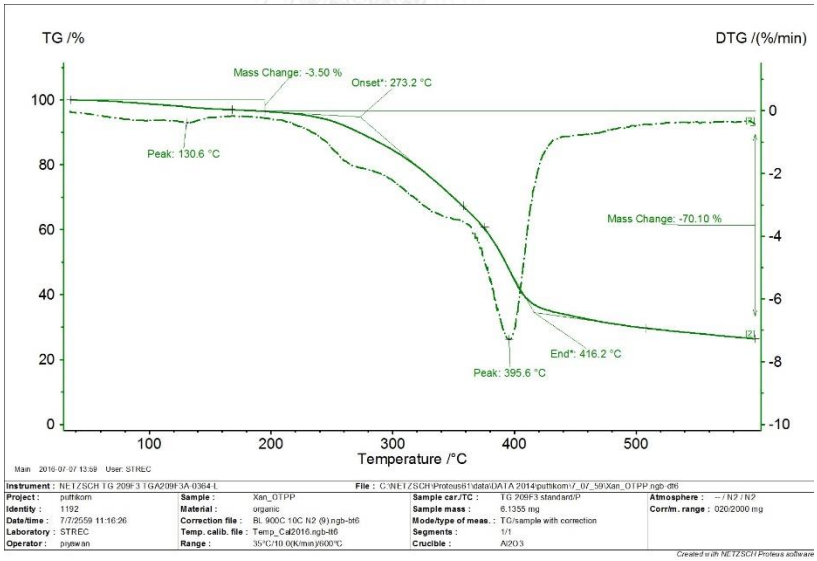

10.3 Thermatogram of xanthone+ OTE

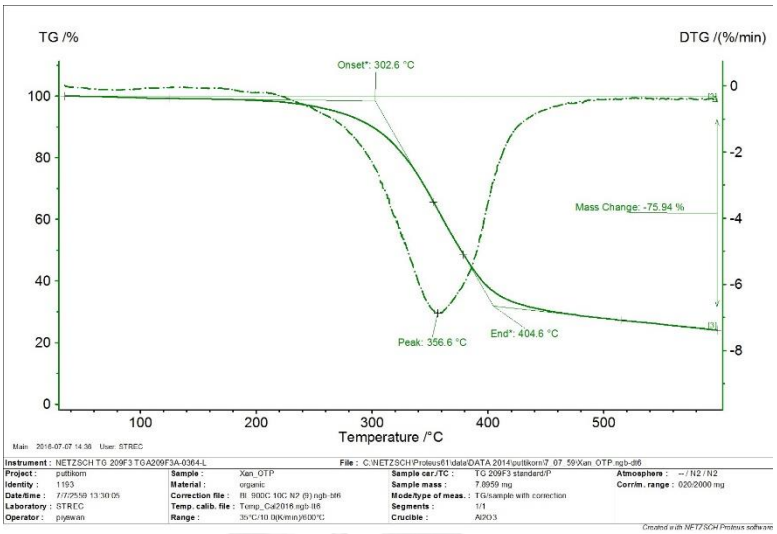

10.4 Thermatogram of OTE+ PEG

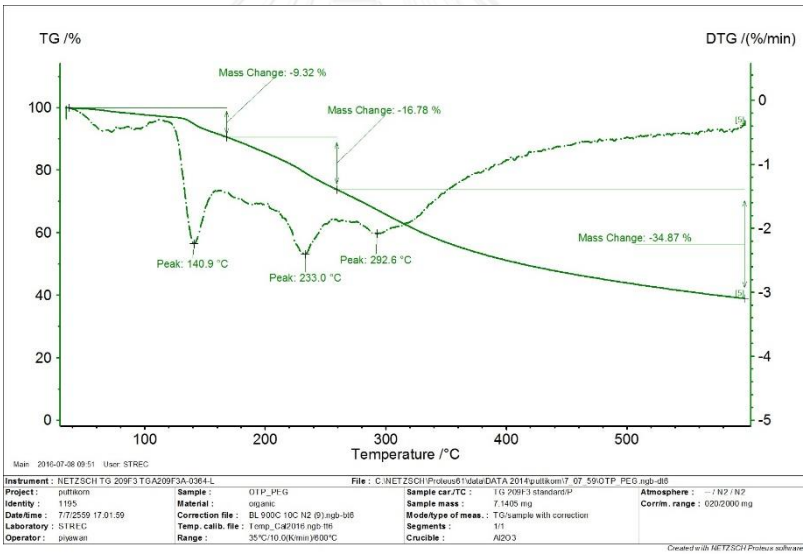

10.5 Thermatogram of xanthone+ PEG

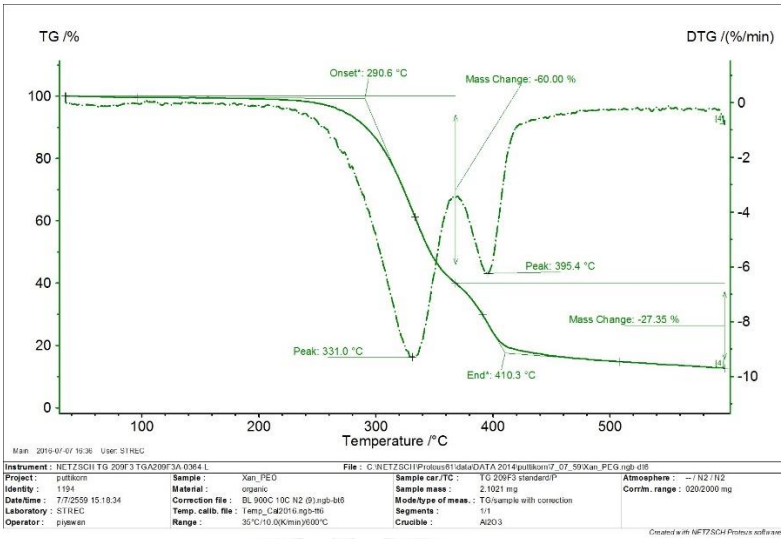

11. <u>In vitro anti-cancer studies</u>

11.1 Cell viability of A549 cell with OTE (green column), P-OTE particle (red column), Xanthone (yellow column), and PTX (violet column)

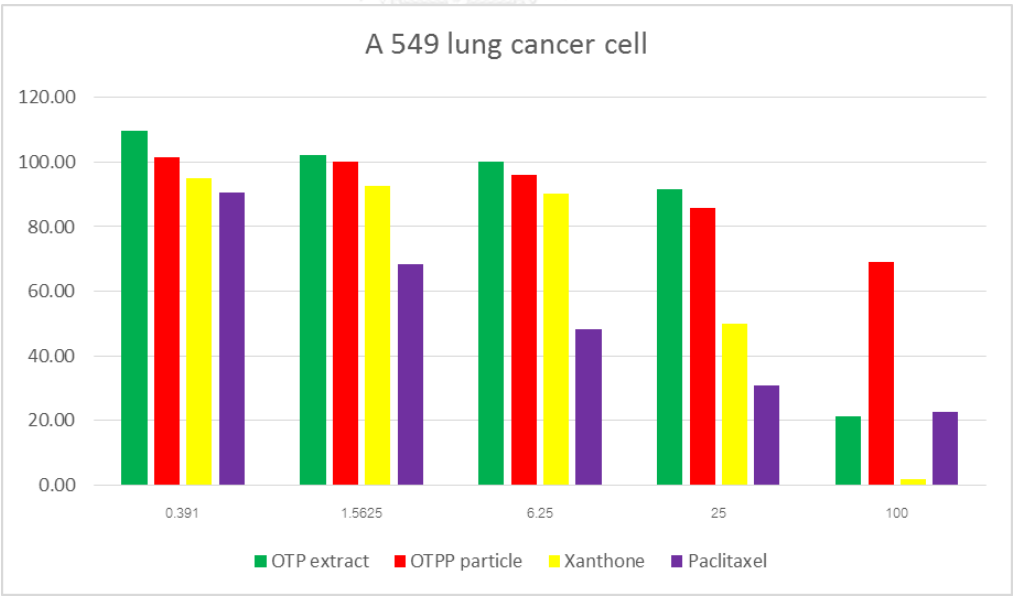

11.2 Cell viability of A549 cell with Free EGCG (green column), P-EGCG particle (brown column), Xanthone (yellow column), and PTX (violet column)

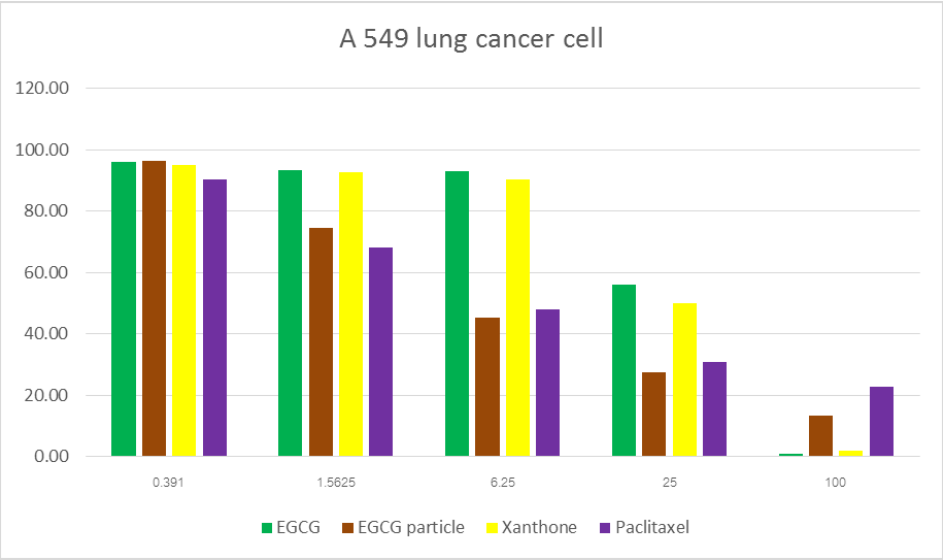

11.3 Cell viability of A549 cell with OTE (green column), EGCG (blue column), P-OTE particle (red column), P-EGCG particle (black column), Xanthone (yellow column), P-OTE particle+ Xanthone (violet column), P-EGCG particle+ Xanthone (yellow column) OTE+ Xanthone (dark green column), EGCG+ Xanthone (orange column)

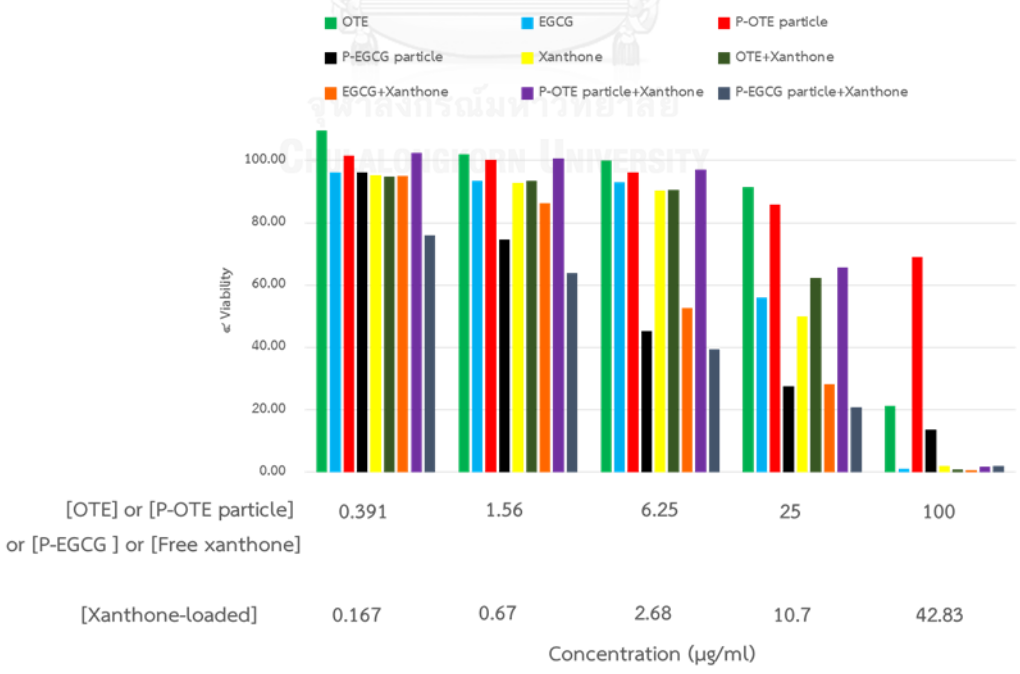

11.4 Cell viability of A549 cell with OTE (green column), EGCG (blue column), P-OTE particle (red column), P-EGCG particle (black column), PTX (violet column), P-OTE particle+ PTX (pink column), P-EGCG particle+ PTX (yellow column), OTE+ PTX (dark green column), EGCG+ PTX (orange column)

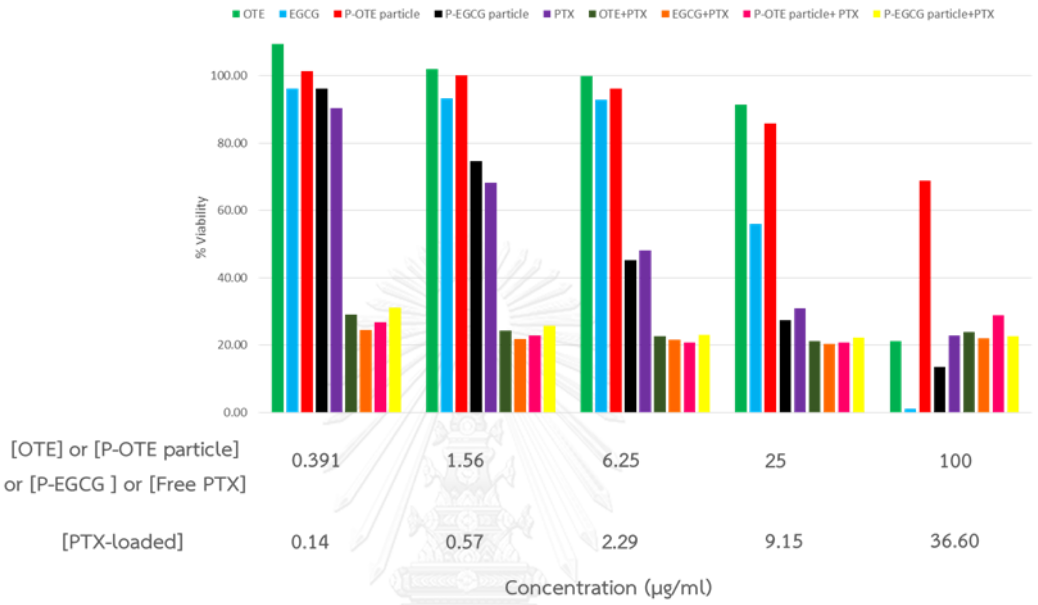

12. Cell viability of A549 cell for calculating of IC50

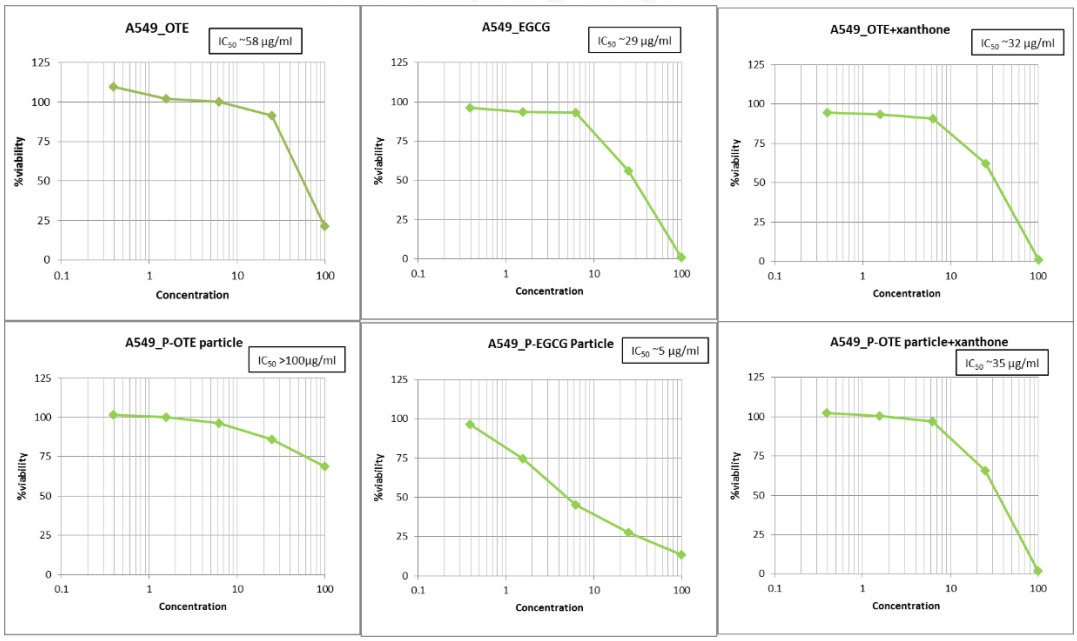

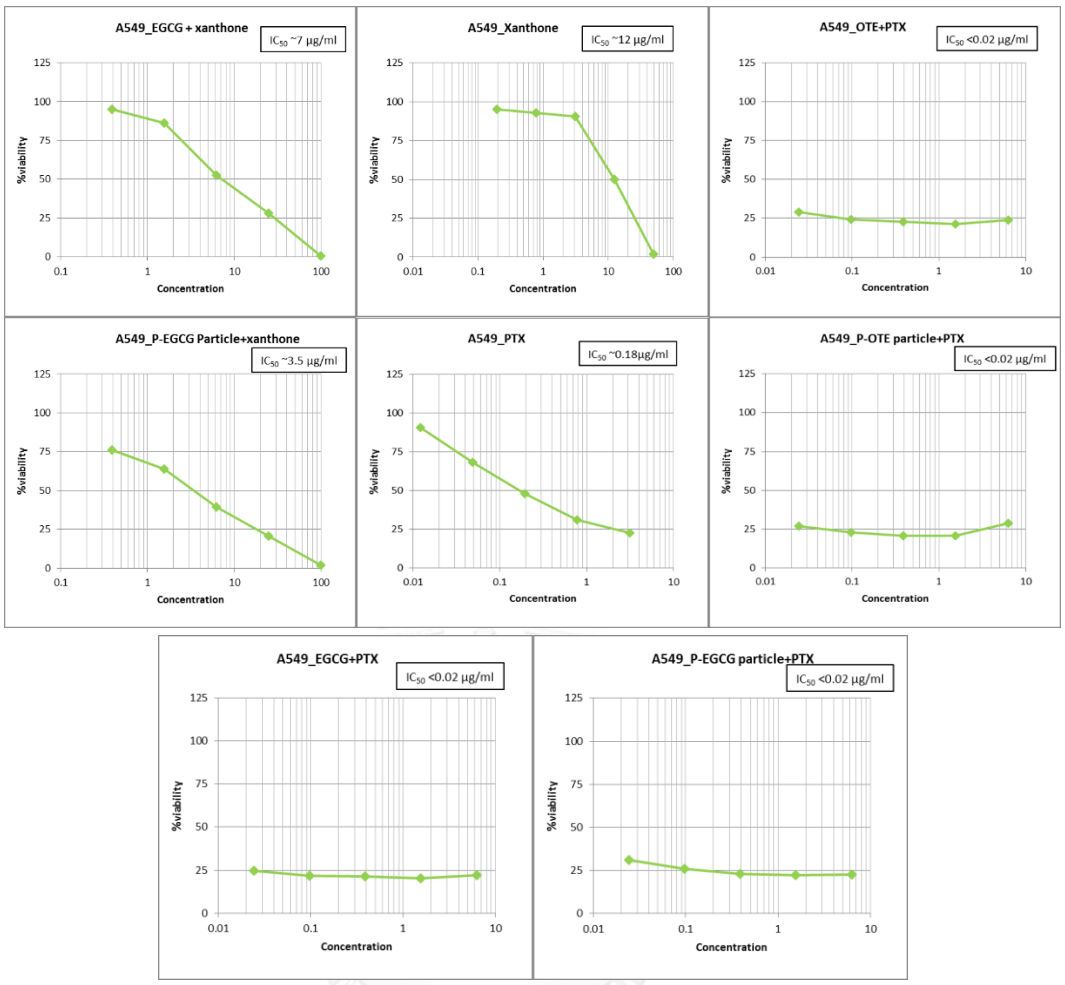

13. ^{1}H-NMR spectrum of P-OTE particle in DMSO after adding a solution of TFA

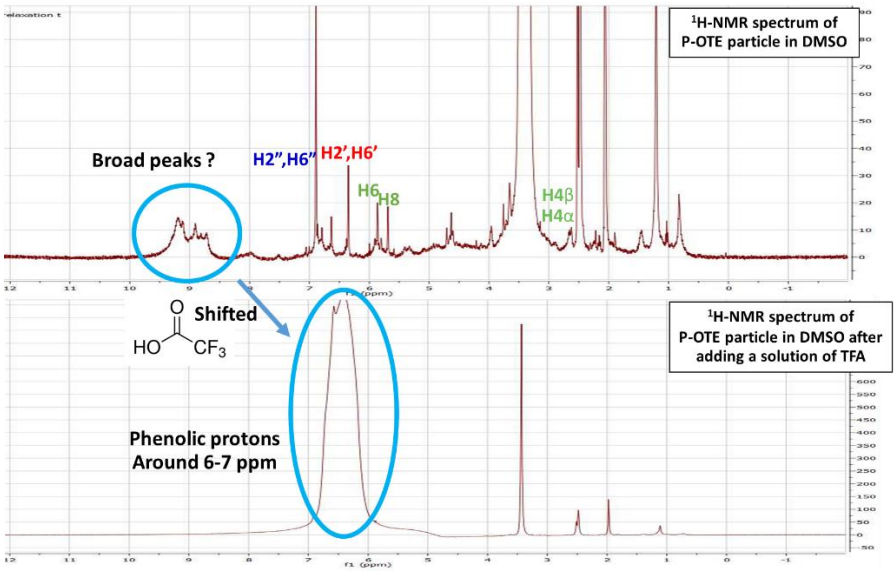

VITA

Mr. Puttikorn Pukfukdee was born on May 14, 1992 in Bangkok Thailand. She graduated with Bachelor's degree of Science, major in Chemistry from Burapha University in 2013 under supervised Assoc. Prof. Dr. Jaray Jaratjaroonphong. He continued his master degree at department of chemistry, Chulalongkorn University under supervised Prof. Dr. Supason Wanichwecharungruang. In the present, He lives with his family, him address is 349/206 Phutthamonthon Sai 2 road, Soi 5, Bangkhae, Bangkok, Thailand.